

Università di Pisa  
Scuola di Dottorato “Leonardo da Vinci”



PhD Programme in  
Land Vehicles and Transport Systems

PhD Dissertation

# Dynamic analysis of vehicle systems

Development of a driving simulator  
Analysis and design of an automatic  
transmission for motor-scooters

Riccardo Bartolozzi

2011



Università di Pisa  
Scuola di Dottorato “Leonardo da Vinci”



PhD Programme in  
Land Vehicles and Transport Systems

PhD Dissertation

# Dynamic analysis of vehicle systems

**Development of a driving simulator  
Analysis and design of an automatic  
transmission for motor-scooters**

Author:

Riccardo Bartolozzi .....

Tutors:

Dott. Ing. Francesco Frenzo .....

Prof. Ing. Massimo Guiggiani .....

SSD ING-IND/14

2011



## **Abstract**

In this work, two researches in the field of dynamic analysis of vehicle systems are presented.

The first part of the thesis deals with the development of a driving simulator. This activity was carried out in the framework of a research project co-funded by the Italian Ministry of Education, Universities and Research (MIUR). It aimed at developing a driving simulator for the analysis of the driving style, in order to identify potentially dangerous conditions coming from a non proper interaction between driver, vehicle and environment, especially those related to low driver's attention. As core part of the driving simulator, a vehicle simulation model, which reproduces the behaviour of the main vehicle systems, was developed. The simulator is made of a fixed driving platform, a single channel visual system and allows to acquire all driver's inputs and vehicle motion signals. The system was involved in experimental campaigns which allowed the development of the driving style analysis techniques and demonstrated the reliability and the capability of the system.

The second part of the thesis treats the dynamic analysis and design of a high efficiency automatic transmission for motor-scooters and was carried out in the framework of the Italian MUSS project funded by the Italian Ministry of Economic Development. Motor-scooters are currently almost always equipped with CVT transmission with rubber belt. This transmission can be very cheap to manufacture, it has good comfort performance but low mechanical efficiency. An alternative automatic transmission was analysed and different architectures were studied. The system is based on a discrete ratio gear box with mechanical control of the gear shift by means of centrifugal clutches and free wheels. A dynamic model of the transmission was developed and its behaviour was investigated by means of results of simulated manoeuvres, highlighting the positive and negative aspects of the system. Finally, a preliminary design was also carried out with reference to an application of the transmission in a hybrid powertrain.



## Sommario

In questo lavoro si presentano due attività di ricerca nell'ambito della simulazione e dell'analisi dinamica di sistemi di veicolo.

Nella prima parte della tesi viene presentato lo sviluppo di un simulatore di guida per applicazioni sulla sicurezza stradale, realizzato nel corso di un progetto co-finanziato dal Ministero dell'Istruzione, dell'Università e della Ricerca (MIUR). Tale progetto ambiva allo sviluppo di un simulatore per l'analisi dello stile di guida, così da poter identificare condizioni potenzialmente pericolose derivanti da una non adeguata interazione guidatore-veicolo-ambiente, con particolare riferimento alle situazioni di basso livello di attenzione del conducente. Come parte principale del simulatore, è stato sviluppato un modello di simulazione di veicolo che riproduce il comportamento dei principali sistemi di un'auto. Il simulatore è a piattaforma fissa con un singolo canale di proiezione frontale e permette l'acquisizione di tutte le azioni del conducente e dei segnali di moto del veicolo. Il sistema è stato utilizzato nel corso di campagne sperimentali che hanno permesso lo sviluppo dei sistemi di analisi dello stile di guida, oltre dimostrare la robustezza e le potenzialità del simulatore stesso.

La seconda parte della tesi riguarda la modellazione e l'analisi di una trasmissione automatica ad alto rendimento per scooter ed è stata svolta nell'ambito del progetto MUSS, finanziato dal Ministero dello Sviluppo Economico. Attualmente gli scooter sono equipaggiati nella quasi totalità con CVT a cinghia di gomma. Questa trasmissione, che ha nei punti di forza l'economia realizzativa e le prestazioni di comfort, ha per contro un rendimento basso. Nel corso del lavoro è stata studiata una trasmissione automatica alternativa e le sue possibili architetture. Il sistema in oggetto si basa su un cambio a gradini con ruote dentate con controllo meccanico della cambiata grazie a frizioni centrifughe e ruote libere. E' stato sviluppato un modello dinamico del sistema e il comportamento del powertrain è stato analizzato sulla base dei risultati di simulazioni, evidenziando gli aspetti di forza e le debolezze. Infine, è stato condotto un dimensionamento preliminare con riferimento ad un'applicazione della trasmissione ad un powertrain ibrido.





# Contents

<b>Introduction</b>	<b>1</b>
<b>I Development of a driving simulator</b>	<b>5</b>
<b>1 Background and aims of the research</b>	<b>7</b>
1.1 Road safety and data about road traffic accidents . . . . .	7
1.2 Monitoring the driver's attention . . . . .	14
1.2.1 Systems based on physiological parameters . . . . .	15
1.2.2 Systems based on behaviour parameters . . . . .	17
1.2.3 Systems based on driver's inputs . . . . .	17
1.2.4 Systems based on vehicle motion conditions . . . . .	18
1.2.5 Considerations on the systems presented . . . . .	19
1.3 Main aim of the research: the development of a driving simulator . . . . .	20
1.4 State of the art of driving simulators . . . . .	22
1.4.1 Employments, structure and classification of driv- ing simulators . . . . .	23
1.4.2 Simulators with monitors and driver's controls . . . . .	25
1.4.3 Simulators with wall screens and driver's controls . . . . .	26
1.4.4 Simulators with vehicle and wall screens . . . . .	26
1.4.5 Simulators with capsule . . . . .	27
1.4.6 Simulators with stereoscopic vision . . . . .	28
<b>2 The driving simulator at DIMNP: architecture and com- ponents</b>	<b>29</b>
2.1 Computers and data flow . . . . .	31
2.2 Driving platform . . . . .	37
2.2.1 Pedals . . . . .	39

2.2.2	Steering system . . . . .	41
2.3	Control desk . . . . .	43
2.4	Visual system . . . . .	45
2.5	Graphical scenario . . . . .	45
<b>3</b>	<b>Simulation model</b>	<b>51</b>
3.1	Input and output blocks . . . . .	52
3.2	Structure of the vehicle model . . . . .	55
3.3	Powertrain and braking system blocks . . . . .	59
3.3.1	Engine . . . . .	60
3.3.2	Clutch . . . . .	61
3.3.3	Transmission . . . . .	63
3.3.4	Clutch and gear control . . . . .	66
3.3.5	Braking system . . . . .	67
3.4	Vehicle dynamics . . . . .	68
3.5	Suspensions . . . . .	73
3.5.1	Suspensions kinematics . . . . .	73
3.5.2	Suspensions stiffness and damping . . . . .	80
3.6	Tire model . . . . .	80
3.6.1	Vertical load . . . . .	82
3.6.2	Rolling radius and deformed radius . . . . .	82
3.6.3	Tire slips . . . . .	82
3.6.4	Tire forces and moments . . . . .	85
3.6.5	Tire model corrections for simulation at very low speed . . . . .	88
3.7	Steering system . . . . .	93
3.8	Parameters and file organization . . . . .	95
<b>4</b>	<b>Real-time driving simulation</b>	<b>97</b>
4.1	Simulation model performances . . . . .	97
4.2	Data acquisition . . . . .	98
4.3	Real-time parameter changing . . . . .	103
4.4	Example of simulated manoeuvres . . . . .	104
4.4.1	Acceleration and braking manoeuvre . . . . .	105
4.4.2	Lane change manoeuvre . . . . .	105
4.4.3	Step steer manoeuvre . . . . .	108
4.4.4	Acceleration and braking manoeuvre with loss of grip	108
4.4.5	Step steer manoeuvre with loss of grip . . . . .	111

---

<b>5</b>	<b>Experimental tests and campaigns</b>	<b>113</b>
5.1	Introduction . . . . .	113
5.2	Driving simulator calibration . . . . .	114
5.2.1	Test protocol . . . . .	116
5.2.2	Results and discussion . . . . .	116
5.3	PRIN experimental campaign . . . . .	119
5.3.1	Test protocol . . . . .	121
5.3.2	Results and discussion . . . . .	122
5.3.3	Reactions to sudden vehicle lateral skid . . . . .	124
 <b>II Analysis and design of an automatic transmission for motor-scooters</b>		<b>127</b>
<b>6</b>	<b>Background of the research and studied transmission</b>	<b>129</b>
6.1	Energy efficiency problems of motor-scooter transmissions	129
6.2	Alternative automatic transmissions . . . . .	132
6.2.1	Electronic controlled continuously variable transmission (ECVT) . . . . .	134
6.2.2	Dual clutch transmission (DCT) . . . . .	135
6.2.3	Zeroshift . . . . .	136
6.2.4	Automated manual transmissions with centrifugal clutches . . . . .	137
6.2.5	Toroidal CVT and NuVinci transmission . . . . .	139
6.2.6	Hydraulic transmission: Honda HFT . . . . .	140
6.2.7	Considerations about the systems presented . . . . .	141
6.3	Layout and characteristics of the studied system . . . . .	142
6.3.1	System working principle . . . . .	142
6.3.2	System architectures . . . . .	144
<b>7</b>	<b>Powertrain simulation model</b>	<b>149</b>
7.1	Equations of the system . . . . .	149
7.1.1	Drive torque . . . . .	153
7.1.2	Drag torque . . . . .	153
7.1.3	Braking torque . . . . .	153
7.1.4	Free wheels . . . . .	155
7.1.5	Centrifugal clutches . . . . .	155
7.2	Model implementation in Simulink . . . . .	157
7.2.1	Open and closed system block . . . . .	160

---

7.2.2	Friction and control block . . . . .	161
<b>8</b>	<b>Applications of the studied transmission</b>	<b>163</b>
8.1	Multi-speed with ICE . . . . .	163
8.1.1	Gear ratios and centrifugal clutch parameters . . .	165
8.1.2	Simulation results . . . . .	169
8.2	Two-speed with electric motor in hybrid powertrain . . . .	176
8.2.1	Modifications to the powertrain model . . . . .	178
8.2.2	Gear ratios and centrifugal clutch parameters . . .	179
8.2.3	Simulation results . . . . .	180
	<b>Conclusions</b>	<b>187</b>
<b>A</b>	<b>Tire constitutive equations of the driving simulator vehicle model</b>	<b>191</b>
	<b>References</b>	<b>197</b>

# Introduction

Modelling and computer simulation play nowadays a fundamental role in automotive engineering, as well as in all other engineering disciplines. The so called *virtual prototyping techniques* are widely employed in universities and industries for research purposes and for product development. Among these techniques, dynamic simulations are carried out to investigate the behaviour of complex mechanisms from the early stages of the conceptual design to the final product. These allow to predict the mechanism working conditions in terms of kinematic characteristics (position, velocity and acceleration of each part) and loads (forces and moments of applied loads and constraints). From the specification definition to the testing phase, dynamic models are used to predict the behaviour of the complete vehicle and its systems, understanding the influence of the design parameters and helping to find the optimal vehicle characteristics. Moreover, this leads to significant time reduction (time-to-market), thus saving energy and costs.

In this work, dynamic analyses of vehicle systems were carried out with reference of two research activities in the field of road safety and environment protection, which are among the main research interests in automotive engineering. Moreover, in some cases, design aspects were studied and some design activity was carried out based on dynamic analyses results. The research activities presented and discussed in the thesis are:

- the development of a driving simulator for road safety purposes;
- the analysis and design of an automatic transmission for motor-scooters.

The development of a driving simulator for safety purposes is the topic of the first part of the thesis, from Chapter 1 to Chapter 5. This activity

was carried out in the framework of a PRIN<sup>1</sup> project funded by the Italian Ministry of Education, Universities and Research (MIUR) and carried out in cooperation between the *Dipartimento di Ingegneria Meccanica, Nucleare e della Produzione* (DIMNP), the *Dipartimento di Ingegneria dell'Informazione* of the *Università di Pisa* and the *Dipartimento di Meccanica e Tecnologie Industriali* of the *Università degli Studi di Firenze*. In 2009 and 2010 some activities on the driving simulator were carried out also in cooperation with the *Dipartimento di Ingegneria Civile (Vie e trasporti)* section) of the *Università di Pisa*.

The main objective of the activity was to develop a driving simulator for the analysis of the driving style in order to identify potentially dangerous conditions, especially those related to driver's drowsiness. The background and the aims of the research are treated in Chapter 1, focusing on road safety and on the state of the art of driving simulators. In Chapter 2, the developed driving simulator at DINMP is described from the hardware point of view, whereas in Chapter 3 the vehicle simulation model is deeply described. Real-time driving simulation is topic of Chapter 4, where typical and extreme manoeuvres, carried out with the driving simulator, are presented. Finally, in Chapter 5 the results of experimental campaigns involving the driving simulator are described.

The second part of the thesis, from Chapter 6 to Chapter 8 treats the analysis, by means of dynamic simulations, and design of a high efficiency automatic transmission for motor-scooters. The study and the development of high efficiency motorcycle transmissions are within the main objectives of the national project MUSS (*Mobilità Urbana Sicura e Sostenibile*, i.e. safe and sustainable urban mobility) funded by the Italian Ministry of Economic Development and carried out mainly in cooperation with the project leader Piaggio & C. S.p.A..

This activity regarded the preliminary study and development of a high efficiency low-cost transmission for motor-scooter applications. The background and the aims of this research are described in Chapter 6, where the state of the art of conventional and innovative transmission solutions is also presented. In Chapter 7 the developed powertrain simulation model is described in details and, finally, in Chapter 8 two application of the studied transmission and the simulation model are presented and discussed. Dynamic simulation results and preliminary design results are

---

<sup>1</sup>from the Italian: *Progetto di Rilevante Interesse Nazionale*, i.e. project of national relevant interest.

both presented in this chapter. The MUSS project is still ongoing at the moment of writing this thesis and further activities will follow the present work.

*Acknowledgements.* I would like to thank the tutors Ing. Francesco Frendo and Prof. Massimo Guiggiani for their fundamental support, their constant helpfulness and for all I have learned from them in these years. Many thanks also go to Antonio Sponziello, whose opinions and support to these researches have been very important in many situations. I thank Armando Cofrancesco and the PRIN project partners for the collaboration in the driving simulator activities. I acknowledge the support of Ing. Onorino di Tanna and Ing. Paolo Capozzella in the works carried out in cooperation with Piaggio & C..

Although the activities carried out in the Formula SAE team of the *Università di Pisa* have not been included in this thesis, I would like to thank all team members of the past three years, especially those I worked with.





Part I

Development of a driving  
simulator



# Chapter 1

## Background and aims of the research

### 1.1 Road safety and data about road traffic accidents

Road traffic accidents represent worldwide one of the main problems for public health. Every day, at every hour, millions of people are on world roads, moving goods or people, working or spending their free time. With different means of transport and on different kind of roads, people from high-income countries, as well as from middle and low-income countries are often exposed to the risk of traffic accidents.

According to the World Health Organization (WHO), road traffic accidents are among the top ten causes of death in the world [65]. In the Global Burden of Disease Project for 2004, the WHO has shown that road traffic accidents caused over 1.27 million deaths that year, being the 9<sup>th</sup> cause of mortality with 2.2% of all world deaths [63, 65]. This result is similar to that of many communicable diseases (see Table 1.1) and makes road traffic accidents being the first cause of death in the category of injuries, before violence, war and any kind of unintentional injury.

People of all ages are exposed to road traffic accidents, but their impact on young people is extremely higher. Road traffic accidents are, in fact, in the top 3 causes of death for people aged between 5 and 44 years and they represent the 1<sup>st</sup> cause of death for people aged between 15 and 29 years [63].

As shown in Figure 1.1, although road traffic accidents are a common

Table 1.1: Top ten causes of death in the world in 2008 (data from the World Health Organization [63, 65]).

Cause	Deaths	
	(mil.)	(%)
Coronary heart disease	7.20	12.2
Stroke and cerebrovascular diseases	5.71	9.7
Lower respiratory infections	4.18	7.1
Chronic obstructive pulmonary disease	3.02	5.1
Diarrhoeal diseases	2.16	3.7
HIV/AIDS	2.04	3.5
Tuberculosis	1.46	2.5
Trachea, bronchus, lung cancers	1.32	2.3
<i>Road traffic accidents</i>	<i>1.27</i>	<i>2.2</i>
Prematurity and low birth weight	1.18	2.0

problem all over the world, there are some differences among the countries depending on their average income. High-income countries (HIC) have reduced the number of deaths in the last years, increasing infrastructure and vehicle safety and improving the enforcement of road safety laws. However, the problem is still very much important because of the extremely increased number of vehicles: 15.6% of the world population owns 52.1% of the world registered vehicles, with an average of one vehicle every two persons. In low-income and middle-income countries, which have 84.4% of the world population, there are just 47.9% of the vehicles, but about 90% of all deaths due to road traffic accidents occur in these countries. In these cases, this number is depending on safety lacks in roads, vehicles, laws and drivers' behaviour.

The same considerations can be done looking at the data for single countries (Table 1.2). The world mean rate of death due to road traffic accidents is about 19 persons every 100 000, but there are huge differences among different countries, mainly, but not only, correlated to the average income. In the table, the Disability-Adjusted Life Year (DALY) is also shown. This index is expressed as the number of years lost due to ill-health, disability or early death and represents a measure of overall disease burden often used by the WHO for analysing and comparing different

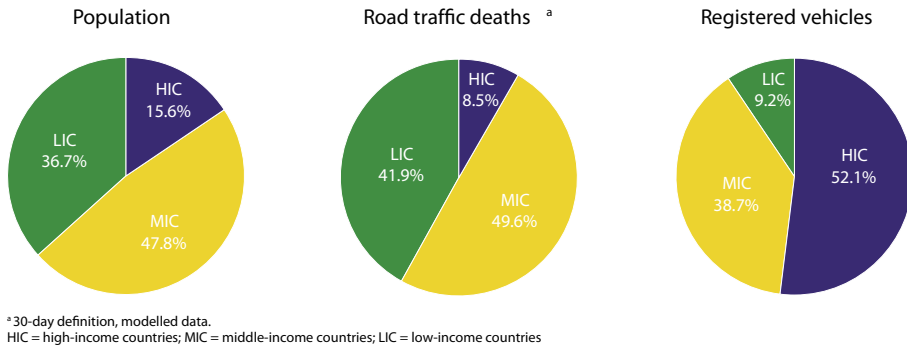


Figure 1.1: Population, road traffic deaths and registered motorized vehicles, by income group (World Health Organization [63]).

causes of death. Once more, these numbers highlight the importance of the road traffic accidents all over the world.

In addition to fatalities, there are between 20 and 50 million injuries per year, many of them being an important cause of disability. It has been estimated that a single person has an overall probability of 1/7 of being injured in his whole life.

Road traffic accidents have also an important impact on the economy of many countries, which in general results very difficult to estimate. In the U.S.A it has been estimated an overall cost for the society of 70 billion dollars per year, considering health costs and damages to vehicles and roads [49]. For many low-income countries, these costs can be between 1 and 3% of their gross national product [63], representing a brake in their development. In proportion, the problem is similar in high-income countries: according to the White Paper of the European Community, the cost for the society of road traffic accidents is about 160 billion euros, which represents 2% of the EU gross national product [11].

In Italy the situation is similar to that of other Mediterranean high-income countries. Detailed official reports on road traffic accidents are available every year from the national institute of statistics (ISTAT) and the national auto-mobile club (ACI). According to the last available report [31], in 2009 there were 590 accidents per day with at least one person injured, with 12 deaths and 842 injuries.

The trends of accidents, deaths and injuries from 2001 to 2009 can be observed in Table 1.3 and Figure 1.2. These show how there is a

Table 1.2: Estimated deaths and disability-adjusted life year (DALY) due to road traffic accidents in various countries in 2004 (data from the World Health Organization [64]).

Country	Deaths		DALY	
	number <sup>a</sup>	rate <sup>b</sup>	number <sup>a</sup>	rate <sup>b</sup>
Italy	7.1	12.1	174	297
Germany	6.0	7.3	161	195
U.K.	3.7	6.2	108	180
U.S.A	45.6	15.4	1252	422
Japan	9.9	7.7	202	158
China	284.8	21.7	8192	624
India	202.3	18.1	6747	606
Indonesia	50.6	22.7	2364	1059
South Africa	18.6	39.1	550	1157
Brazil	40.4	21.9	1249	677

<sup>a</sup> Number of deaths and DALYs are expressed in thousands.

<sup>b</sup> Rates are expressed in deaths (or DALYs) every 100 000 people.

continuous decrease of accidents, although the registered vehicles grew of about 18% in this period (from 42 million to 49.5 million vehicles). With a similar rate, injuries also decreased. The number of deaths shows a higher decreasing rate, as it can be observed in the mortality index.

Even if there is this positive trend, road traffic accidents remain an important problem. In order to overcome it, the European Union fixed in 2001 the objective, for 2010, of a global reduction of 50% of deaths on the road. Almost all EU 27 countries obtained positive results in these years, but this goal seems difficult to reach. Up to 2009, the average EU result is 35.1%, whereas Italy reached a reduction of 40.3% (10<sup>th</sup> country in the ranking) [31].

This reduction trend in the number of accidents depends on improving related to the three main elements which are involved in road safety:

- driver;
- vehicle;

Table 1.3: General statistics about road traffic accidents in Italy (data from ACI [31]).

Year	Accidents	Deaths	Injuries	Mortality index <sup>a</sup>
2001	263 100	7096	373 286	2.7
2002	265 402	6980	378 492	2.6
2003	252 271	6563	356 475	2.6
2004	243 490	6122	343 179	2.5
2005	240 011	5818	334 858	2.4
2006	238 124	5669	332 955	2.4
2007	230 871	5131	325 850	2.2
2008	218 963	4725	310 745	2.2
2009	215 405	4237	307 258	2.0

<sup>a</sup> Number of deaths relative to the number of accidents (in percentage).

- environment (road, infrastructures, etc.).

On one side, road infrastructures have increased their quality and several laws have been redefined and better enforced to improve the drivers' behaviour in the traffic. On the other side, the automotive industry has highly improved the active and passive safety of vehicles. Well known active safety systems such as ABS (Anti locking Braking System) and ESC (Electronic Stability Control) are since some years ago in the standard equipment of almost all new cars and are demonstrated to be responsible for avoiding many accidents. Passive safety has played an important role as well, reducing the damages once accidents occur. The increased passive safety performances of modern systems (such as air-bag) can be understood looking at the decrease of the mortality index of road accidents (Table 1.3).

Further improvements in road safety, which are worldwide as demonstrated absolutely necessary, need to focus at the same time on the three elements introduced (driver, vehicle and environment). In specific, the driver seems to be the critic element, as it can be stated referring to Table 1.4. The driver is responsible for the accidents mainly (93.52%) because his incorrect behaviour (i.e. not following the traffic rules) and, in a minor proportion (3.12%), because of his abnormal psycho-physical

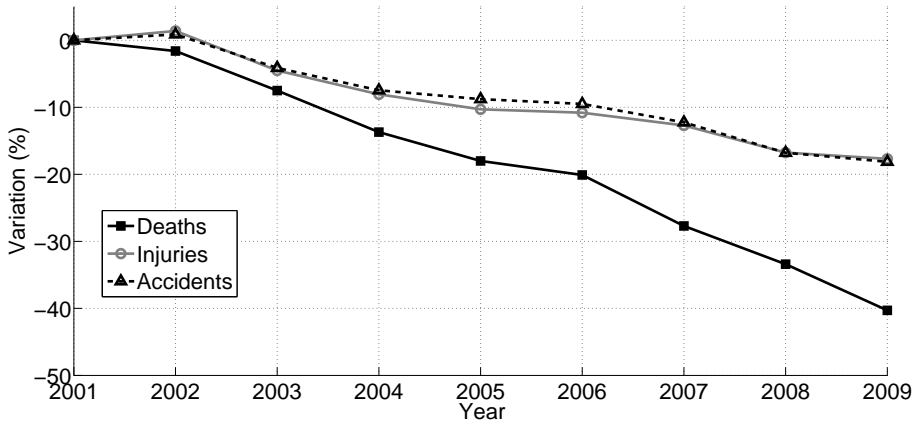


Figure 1.2: Trend of deaths, injuries and accidents in Italy in the period 2001–2009. All values are relative to those of 2001.

conditions (e.g. drowsiness, alcohol, drugs). However, this last cause is correlated to accidents with a higher rate of deaths and injuries [30]. As it is shown in Figure 1.3, during the hours of the night, when there is a higher incidence of the factors related to abnormal psycho-physical conditions, there are less deaths (and less accidents) but the mortality index is very much higher.

Many researchers agree that accidents due to abnormal psycho-physical conditions are underestimated because of the difficulties to directly prove them. Especially the number of accidents due to drowsi-

Table 1.4: Causes of road traffic accidents (Italy 2008, data from ACI [30]).

Cause	Accidents	
	(-)	(%)
Driver incorrect behaviour	259 219	93.05
Driver abnormal psycho-physical conditions	8697	3.12
Defect or failure of the vehicle	1076	0.39
Incorrect pedestrian behaviour	9600	3.45



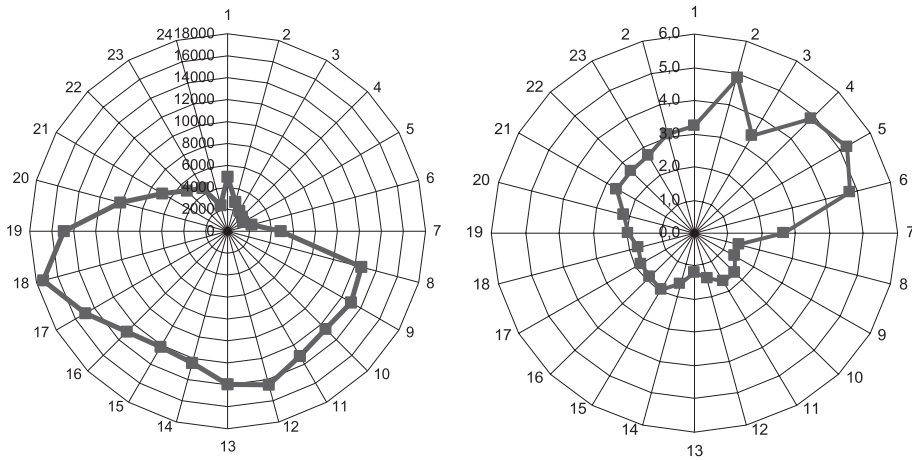


Figure 1.3: Number of deaths in road traffic accidents (left) and mortality index at each hour of the day (right) (Italy 2009, ACI [31]).

ness (or hypovigilance conditions), which are officially just 0.25% of the total accidents in Italy in 2008 [30], appears to be extremely underestimated if compared to the results of some specific studies. In these researches, drowsiness is considered to be within the causes of 22% of all road traffic accidents [15], and of 40% of accidents with deaths [46]. Moreover it has been observed that this kind of accidents is generally more critic, having a percentage of deaths which is triple with respect to other accidents.

For these reasons, current technology development is focused, on one side, on systems which help the driver to avoid incorrect manoeuvres and possibly correct them and, on the other side, on monitoring the driver's attention level to detect abnormal psycho-physical conditions. Among the first category, there are active systems, such as ABS and ESP, most of which are employed in modern vehicles<sup>1</sup>. With these systems, incorrect manoeuvres due to driver's errors are corrected modifying the driver's inputs. This can be done at different levels, from the well established ABS which controls the brake pressure, to automated driving systems, such as the Adaptive Cruise Control or the Frontal Crash Warning [43], which have been recently developed. An other possibility to avoid incorrect

<sup>1</sup>For an extensive review on active safety systems, see [43].

manoeuvres, is to inform the driver about current environment and traffic conditions. Systems which display the traffic signs on-board, or night vision systems, are among the examples of such systems which have been developed in the last years.

In the second category, there are systems which can recognize when the driver's behaviour is not consistent with the driving conditions, monitoring his attention level in several possible ways, and consequently take a countermeasure, such as alerting the driver or limiting the engine power. In the next section, recently developed systems which detect hypovigilance conditions are presented and briefly described.

## 1.2 Monitoring the driver's attention

In the previous section, it was pointed out, the importance of the influence of driver's abnormal psycho-physical conditions and, within them, of hypovigilance conditions on road traffic accidents. For these reasons, diagnosis systems, able to monitor the driver's attention and identify hypovigilance conditions, have been studied and developed in the last years. Some of them have also been launched in the market.

It is worth noting that the objective of such systems is very complex because of the many variables to be taken into account. A low level of driver's attention depends on the interaction of the three main elements of road safety already introduced: driver, vehicle and environment. Abnormal driver's psycho-physical conditions are of course at the basis of driver's hypovigilance, however, they are often associated with factors related to the environment and, in some cases, to the vehicle, which reveal more their effects. Monotonous driving, such as in straight highways, especially during the night, is often an increasing factor for driver's hypovigilance. In these situations, the driver needs to interact rarely or repetitively with the vehicle commands and the environment changes slowly. On the contrary, driving in urban areas, requires a higher level of driver's attention, because of the frequency of the driver's interactions with the vehicle (i.e. steering input, changing gear, braking, etc.) and of the changes in the environment. Distractions, such as the use of mobile phone, are also causes of a low level of driver's attention.

In order to monitor the level of driver's attention, systems based on different information sources have been studied and developed. The systems can be classified in four groups, depending on the source of

information:

- driver's physiological parameters;
- driver's behaviour parameters;
- driver's inputs;
- vehicle motion conditions.

Of course, there are also some systems which combine more than one source of information.

The use of driver's physiological or behaviour parameters represents a direct measure of the driver's condition and it is therefore a reliable way to identify hypovigilance. However, these systems make often use of sensors (such as video cameras or electrodes) which can be felt as intrusive by many drivers. It is fundamental to consider this aspect if a system is developed for industrial production. On the other side, systems based on vehicle motion conditions or driver's inputs can use signals which are nowadays often available on all vehicles, being invisible to the drivers. In this case, the measure is of course indirect and, in turns, it requires the development of complex procedures of signal analysis and driving style identification.

Although these systems are based on different concepts, they share a common architecture, which is shown in Figure 1.4. Dedicated or already on-board sensors measure the quantities on which the system is based, a control unit processes these data and detects driver's hypovigilance conditions and, finally, an alert system alerts the driver (or other countermeasures are taken). Systems based on driver's inputs generally need also to identify the driving style of each driver. The block related to this function is connected with dashed lines in the picture indicating that is not always present.

In the following, a brief description of the four categories of systems and some example are presented.

### 1.2.1 Systems based on physiological parameters

Among all physiological parameters, the electrical brain activity, measured by Electroencephalography (EEG) is considered the most accurate to detect driver's hypovigilance conditions. Many studies have demonstrated the correlation of the amplitude of some parts of the EEG spectrum to

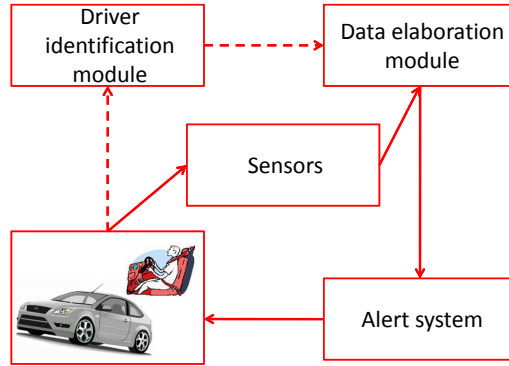


Figure 1.4: Block scheme of a generic system which monitors the driver's attention.

drowsiness conditions [40, 38, 42, 41]. However, accurate measurements are possible only intrusively, using common electrodes for EEG. For this reasons, it is unlikely to foresee commercial applications of such systems in vehicles. Thanks to their high accuracy, they have anyway an important role as test systems in laboratory when developing other systems.

Other systems are based on the electrical cardiac activity, measured by Electrocardiography (ECG) [66] or on the blood pressure. The relationship between these parameters and the driver's conditions varies very much among people. The system has therefore to learn the basic parameters of each driver before working properly. Also in this case, the acquisition sensors are intrusive and, therefore, these systems will be difficultly employed in applications other than test equipments in laboratory.

A less intrusive solution is represented by a sensor-equipped steering wheel, which can measure the cardiac frequency [9] and, in some applications, the hand sweat and the skin temperature.

As found out in the cited studies, in order to correlate these physiological parameters to driver's hypovigilance conditions, systems based on EEG, ECG or other parameters need complex data elaboration which, in turns, requires dedicated and expensive hardware.



Figure 1.5: Example of eye-tracking system for detecting driver's drowsiness.

### 1.2.2 Systems based on behaviour parameters

According to several studies, the percentage of eye closure (PERCLOS) is correlated to driver's drowsiness [32, 52]. Systems based on this concept, need to monitor with a video camera the face of the driver and analyse the image to detect the eyes and their blinking [13, 33, 50]. This task has to be carried out in real-time, processing a lot of data and, therefore, requires high performance components (camera and dedicated hardware). Moreover, because of the use of cameras, these systems are felt as intrusive by many potential costumers. Other systems based on driver's eyes, analyse the eye look direction (Figure 1.5).

An other kind of system is based on the head position, which is strongly correlated to the driver's drowsiness [55]. As for other systems, the normal position of the head has to be acquired by the system in a first phase.

Finally, there are systems which acquire the position of the complete body of the driver by pressure sensors on the seat and by video cameras. The analysis of the driver's posture is very complex and, therefore, in recent year research have been focused on the analysis of the eyes and the head.

### 1.2.3 Systems based on driver's inputs

The systems developed in this category focus mainly on the steering wheel, which is, within the driver's inputs, the most representative of the driving style. While driving even on a straight road, every driver makes little corrections to maintain the vehicle direction. The amplitude and the frequency of these corrections are typical for each driver. However, it has been demonstrated how all drivers increase the amplitude and

decrease the frequency of the corrections on the steering wheel when their attention level is lower. This information could be therefore used for detecting driver's drowsiness [8, 56, 34, 57]. The information of the steering wheel angle is often correlated to other input signals (throttle and braking pedals position) and to vehicle dynamics signals (accelerations, speed, etc.) to avoid false alarms.

This kind of system has the advantage of being completely transparent to the user. Moreover, being the signal of the steering wheel angle already measured on-board and available in the CAN of modern vehicles, as well as the other driver's inputs, such systems result less expensive than others.

Specific algorithms (mainly based on fuzzy logics and neural networks) have to be studied and developed to correlate the driver's inputs information to the driving style. In a first phase the system should learn how the single driver interacts with the vehicle and store this information as the normal driving style. Then, it should be able to detect dangerous conditions when the driver's inputs are different from those of the normal driving style, especially if related to unusual vehicle motion conditions.

#### **1.2.4 Systems based on vehicle motion conditions**

The quantities describing the vehicle dynamics are of course influenced by the driving style and it is expected to find differences between normal and hypovigilance driver's conditions. However, they are also highly dependent on the driving and traffic conditions and on the single driver's style. For these reasons, systems based on vehicle motion conditions need, as those based on the driver's inputs, to learn the normal driving style of each driver before working properly.

As well for the systems based on driver's inputs, they make use of signals, most of which are already on the CAN of modern vehicles. This means they are completely transparent to the driver and need less additional equipment if compared to other systems.

The main challenge for these systems is to properly and effectively identify hypovigilance conditions from signals which are influenced by the driving and traffic conditions. In the literature, the lateral lane position has been considered as a signal highly correlated with the driver's drowsiness, to be used in highways and extra-urban roads [54]. This system needs of course cameras to detect the lateral vehicle position in the lane.

Table 1.5: Comparison of solutions for monitoring the driver's attention.

Type	Signals	Effectiveness	Feasibility
Physiological	EEG, ECG, etc.	Very good	Bad
Behaviour	PERCLOS, etc.	Good	Sufficient
Driver's inputs	Steer. wheel, etc.	Good	Very good
Vehicle motion	Lat. lane pos., etc.	Sufficient	Good

Other signals, such as the longitudinal velocity and the lateral acceleration, are not enough to identify the drive's conditions, but are often used in addition to other information (i.e. lateral lane position or driver's inputs).

### 1.2.5 Considerations on the systems presented

The different solutions for monitoring the driver's attention can be easily compared in Table 1.5, where all considerations already made are summarised. As already pointed out, systems based on physiological or behaviour parameters have in general high effectiveness, measuring directly driver's parameters. However, being these systems intrusive, their possibility of being employed in commercial vehicles is very low at the moment. On the other side, systems based on driver's inputs or vehicle motion conditions use less direct measures, which therefore need advanced post-processing, but represent solutions completely transparent to the driver.

It is also worth noting that, in order to detect dangerous driver's hypovigilance, systems based on driver's inputs and vehicle motion conditions have to store information about the normal driving style, defining a so called *user profile*.

Among all available driver's input and vehicle dynamics signals, the steering wheel seems to be the quantity which better correlate with the driving style and hence the driver's conditions. However, because of the complexity of identifying the driving style, in general, these systems need also to combine information of different signals (both inputs and vehicle dynamics quantities) and to use environment and traffic information.

Following this direction, some industrial solutions have been recently

developed, such as the *Attention Assist* by Mercedes [45]. This system uses the steering wheel angle, the way the driver activates the indicators, the positions of the pedals (driver's inputs), the vehicle speed and the lateral and longitudinal accelerations (vehicle motion conditions). Moreover, it takes into account the lateral wind force and the quality of the road surface as environment variables.

### **1.3 Main aim of the research: the development of a driving simulator**

As shown in the previous section, the use of driver's input and vehicle dynamics signals seems to be the best compromise between effectiveness and feasibility, for driver's attention monitoring systems. In order to develop such systems, a driving simulator is needed, which allows to carry out safe and completely monitored test drives in laboratory. With a driving simulator, all driver's input signals (steering wheel angle and pedals position) and all vehicle quantities (velocities, accelerations, engine speed, etc.) are available to be monitored and stored for further analyses. Moreover, additional medical equipments, such as those for EEG or ECG, can be used to monitor also driver's physiological parameters.

The developing of a driver simulator has to face many interesting challenges. First of all, if the target of the simulated drives is the human factor, the actual driving conditions should be reproduced as close as possible. To do so, a driving simulator must reproduce faithfully the interfaces between the driver and the vehicle and also the environment. Only if the driver feels himself like in actual driving conditions, his behaviour and his reactions could be representative of what happens in real vehicles on real roads. This means that the physical interfaces of the vehicle and their behaviour must be close to the real ones: both the input commands (steering wheel, pedals) and the cockpit elements, such as the seat, should be realistic. In addition to this, it is important to closely reproduce the visual and the audio sensations which a driver feels during driving. In some cases, when test drives are performed at high accelerations, it is also required to reproduce the effects of the inertia on the driver body.

From the simulation point of view, the main aspect of a driving simulator is the real-time simulation. Usually, in simulations, the simulation time is different from the real time because there is no need to connect the



simulation environment with the real world. This means that simulation time can be slower or quicker than real time and its rate could be not constant. In driving simulator applications this is, of course, not possible. Simulation time and real time must be the same, so that the simulation environment can be connected with the driver and any real component of the simulator. This means that simulation tasks in each time step must be performed within the time step itself, limiting the complexity of the simulation models in relation with the available hardware.

Simulation models should however reproduce all vehicle subsystems with a different detail depending on the simulator target. In driving simulators, a core part of vehicle dynamics with a tire model is always present and often the elements of the complete powertrain are also modelled (engine, clutch, gearbox and differential). The complete model could be very complex depending on the application, including in some cases also vehicle auxiliary systems, such as the electrical or the cooling system.

As the simulator physical environment, the simulation model must reproduce as faithfully as possible all driving conditions. This means that the simulated vehicle should be able to reproduce unusual manoeuvres, which are rarely simulated outside the field of driving simulators and usually require specific modelling techniques. These manoeuvres include stopping and restart the vehicle, lose of grip, etc..

All these aspects will be further analysed in the following sections, describing the driving simulator at the *Dipartimento di Ingegneria Meccanica, Nucleare e della Produzione* of the *Università di Pisa*, which is the object of this part of the present work. This driving simulator was mainly developed to study the driving style with the aim of developing a diagnosis tool, for detecting driver hypovigilance conditions, based on driver's inputs and vehicle motion signals. This activity was carried out in the framework of a PRIN project funded by the Italian Ministry of Education, Universities and Research [5]. Thanks to the possibility of carrying out safe and completely monitored test drives, the driving simulator can be used for several purposes related to the human factor and it is, in fact, currently used also for other projects involving different university departments. Studies about the driver's behaviour in urban environment are carried out in cooperation with transport engineers of the *Dipartimento di Ingegneria Civile* of the *Università di Pisa*, who are involved also in the development and the customization of the graphical scenario of the simulator. Other examples are: the study of alcohol effects

among people with different genotype (carried out with the biologists of the *Dipartimento di Biologia* of the *Università di Pisa*) and the study of narcolepsy effects on driving (cooperation with the *Dipartimento di Neuroscienze* of the *Università di Pisa*).

The physical description of the driving simulator is the topic of Chapter 2, whereas Chapter 3 treats the simulation model. Before going into details of the developed system, in the next section the state of the art of driving simulators is presented.

## 1.4 State of the art of driving simulators

With the general technology development, driving simulators have reached a very high level of accuracy in reproducing the real driving conditions. Thanks to this, they are now a fundamental instrument for studying the interactions between driver, vehicle and environment, both in academic and industrial fields.

The use of driving simulators has many advantages with respect to test drives on roads. First of all, the safety in laboratory tests is very much higher than in a vehicle which is really moving on roads with traffic. Moreover, from the experimental point of view, driving simulators allow to completely control the test environment, to acquire a big amount of data regarding all vehicle model signals (needing no sensors) and driver's inputs and to save time and money. An other important advantage, is that driving simulators can reply the same environment and traffic conditions for several drivers. On the other side, the simulation of aleatory elements, such as other vehicles motion or pedestrians behaviour, is not simple and requires specific developed software.

The first driving simulators were built in the seventies and were based on flight simulators, which were already in use. At the beginning of the eighties, thanks to the computer technology, Daimler-Benz built the first high-fidelity driving simulator in the automotive industry. With the increase of computational and graphical performances of the computers and, on the same time, with the decrease of their costs, driving simulators have been developed in many academic and industrial institutions. Some example of institutions which currently own a driving simulator are: Ferrari and Dallara in Italy, VTI in Sweden, TNO and the University of Groningen in the Netherlands, Daimler-Benz in Germany, University of Leeds in England, University of Iowa in U.S.A., Triggs in Australia, Toyota

in Japan. A good list of current driving simulator can be found online here: [http://www.inrets.fr/ur/sara/Pg\\_simus\\_e.html](http://www.inrets.fr/ur/sara/Pg_simus_e.html) (in french).

### 1.4.1 Employments, structure and classification of driving simulators

Driving simulators are employed in several fields (for more details on these application see [43]):

- road safety and monitoring of driver;
- studies of people behaviour;
- development of new vehicle subsystems;
- ergonomic studies;
- education;
- rehabilitation;
- training of race and other special drivers.

The structure of a driving simulator, from the hardware and software point of view, can be very different depending on the goals of the simulation activities and on the available budget. However, some subsystems are common to all architectures. Regarding the hardware, driving simulators have the following three main parts [43, 29].

- Driving platform or vehicle, with the driver's input elements, such as steering wheel, pedals and gear lever. These are equipped with sensors which acquire their position. In addition, they are endowed with passive or active feedbacks to produce realistic sensations. The driving platform or vehicle could be optionally moved to reproduce inertial effects and vehicle body inclinations.
- Video system made of monitors, or projection system with flat or shaped screens. This last kind of system can project just the front view or cover a wide angle of visual field, up to 360°. A last possibility is the stereoscopic vision (see Section 1.4.6).

- Audio system with more channels to create a three-dimensional audio effect. The engine noise and the environment noise (aerodynamic noise and other effects) are reproduced by independent systems in high level applications.

From the software point of view, driving simulators are made of the following parts:

- vehicle simulation model (which computes, from the driver's inputs, all vehicle quantities needed by the graphical and audio software, by the feedbacks and the data acquisition);
- software dedicated to the graphical scenario;
- software for the audio system;
- software for managing the simulated drives (external interventions and data acquisition).

Depending on the hardware equipment, driving simulators can be classified following these categories:

- simulators with monitors and driver's controls;
- simulators with wall screens and driver's controls;
- simulators with vehicle and wall screens;
- simulators with capsule;
- simulators with stereoscopic vision.

All these categories have also the possibility of implementing the moving driving platform. This equipment allows the driving simulator to reproduce both the pitch, roll and bump motions and the inertial effects due to linear accelerations. In order to do so, the driving platform needs to have 6 degrees of freedom fully controlled by a motion system driven by the vehicle simulation model. An example of a simulator with such an equipment has been developed at the University of Kookmin in Korea [39].



Figure 1.6: Simulator with driver's inputs and three monitor (left) and one monitor (right).



Figure 1.7: Simulator with driver's inputs, one monitor and moving platform.

### 1.4.2 Simulators with monitors and driver's controls

Driving simulators with monitors and driver's controls represent the most simple configuration. They are made of a driving platform with a seat (just a chair in some basic simulators), the driver's inputs elements (steering wheel, pedals and gear lever if present) and one or three computer monitors (Figure 1.6).

The simulator configuration with one monitor is very close to videogames and sometimes, the differences between the two are not that defined. The three monitor configuration is widely employed for low cost applications, when a wide visual system is required, especially for urban environment simulation.



Figure 1.8: Simulator with cylindrical screen and driver's inputs.



Figure 1.9: Simulators with vehicle and wall screens. On the right, the vehicle is on a moving platform.

Driving simulator with monitors are built, in some cases, as a single compact system (commercial solutions) and are sometimes equipped with the moving platform Figure 1.7.

### 1.4.3 Simulators with wall screens and driver's controls

This driving simulator configuration is very close to the previous one. In this case, the monitors are replaced with wall screens which widen the visual field of the driver. The most employed solutions are: the single flat screen, three flat screens and a cylindrical shaped screen (Figure 1.8). The latter solution has the advantage of avoiding discontinuities in the image projected, but it is more expensive.

### 1.4.4 Simulators with vehicle and wall screens

In order to better reproduce the actual driving environment, some simulators use a real vehicle, or the front part of it, instead of specific developed

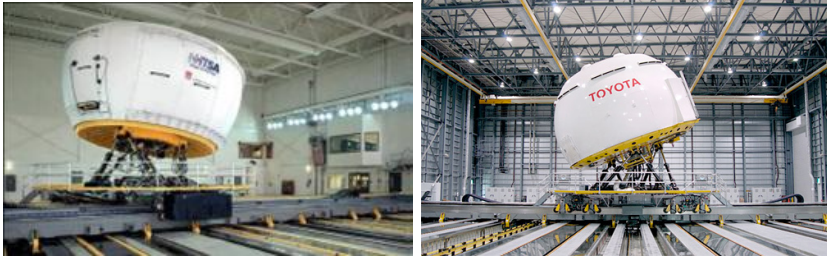


Figure 1.10: Simulators with capsule: NASD (left) and Toyota (right).

driving platforms (Figure 1.9). This solution is quite common being at the same time very realistic and few expensive. Moreover, using a real vehicle, the graphical scenario does not need to reproduce the dashboard and the cockpit.

As in the previous category, different screens can be employed: flat single, three flat or cylindrical. In addition, a rear vision system is often present in this solution. This can be made of a monitor, a wall screen or a monitor replacing the rear-view mirror.

As shown in Figure 1.9, the vehicle can be installed on a moving platform.

### 1.4.5 Simulators with capsule

Among all configurations, the simulators with capsule represent the most complex and expensive solution. A big capsule (of some meters in diameter) is supported by hydraulic pistons whose motion is correlated to the simulated driving conditions as the moving platforms for the other simulator configurations. In some cases (Figure 1.10) the capsule can also be moved longitudinally and laterally on linear runners to reproduce the inertial effects without tilting it.

On the capsule inner walls, the graphical scenario is projected at  $360^\circ$  by several projectors. A real vehicle (or a part of it) is usually installed inside the capsule [59], although there are also solutions with specific designed driving platforms. While the low frequency body movements are reproduced by the capsule motion, the vibrations due to road unevenness are reproduced by actuators on the vehicle wheel hubs.

Such simulators represent the highest technology level in driving simulation and, as already mentioned, require a big budget. Examples of this solution are: the Daimler simulator, the National Advanced Driving



Figure 1.11: Simulator with stereoscopic vision and gloves to reproduce the driver's hands.

Simulator (NADS) developed by the University of Iowa [48] and the Toyota simulator [60].

#### 1.4.6 Simulators with stereoscopic vision

Driving simulators with stereoscopic vision represent a particular category. In these simulators the only hardware needed are the physical interfaces of the driver's input controls. Everything else (vehicle, dashboard, road, etc.) is virtually reproduced using stereoscopic vision glasses. The driver needs to wear special gloves with sensors to reproduce his hands, and their interaction with the input controls, in the graphical environment (Figure 1.11) [61].



## Chapter 2

# The driving simulator at DIMNP: architecture and components

In this work, a driving simulator was developed, starting from an embryonic version available at the beginning of the activities [43, 16]. Although there are still many improving possibilities, the developed DIMNP simulator is now a complete system which allows to carry out experimental driving campaigns, monitoring several signals (as described in Chapter 5) [4, 3]. Driver's input signals (steering wheel angle and pedals positions), together with vehicle model signals (velocities, accelerations, angles, engine speed, etc.) are acquired and stored for analyses.



Figure 2.1: Instrumented driving platform (left) and simulator control desk (right).

The developed system is a fixed base driving simulator with a single channel front visual system, which represents the view of the driver with a three-dimensional scenario. It is worth noting that the choice of a non-moving driving platform is related to the aims the simulator, as well as to the project budget. As already pointed out, the driving simulator was developed to study driver's hypovigilance conditions. These are usually correlated to monotonous highway driving, in which longitudinal and lateral accelerations are very low and can be therefore neglected without losing much simulation realism.

The driving simulator is installed in a specific room with dark walls, which improve the quality of the visualisation of the front view images. In the same room, there are the driving platform and the control desk, where an operator can follow the simulated drive and control it (Figure 2.1).

In short, the simulator is made of:

- the instrumented driver's cabin;
- the control desk;
- the visual system (single front screen and video projector);
- the audio system (2+1);
- four personal computers connected by a local area network (with UDP communication protocol)

These elements are connected to each other as shown in Figure 2.2. The driver interacts with the simulator by means of the typical inputs of an automatic transmission vehicle: the steering wheel, the throttle and brake pedals. At the same time, the driver feels the vehicle motion conditions by means of the front view, the engine noise and the active feedback on the steering wheel. All input elements are installed in a driver's cabin which reproduces the geometry layout of a real car, having a real car seat and, in the last version, also a real car bodywork with front window. The pedals and the steering wheel are endowed with sensors which acquire the driver's inputs during the simulation. The pedals have also passive feedbacks, whereas, on the steering column, a brushless electric motor applies the actual steering torque feedback computed by the vehicle model.

In the next sections the driving simulator is presented in details, focusing on the computers and data flow (Section 2.1), on the driving

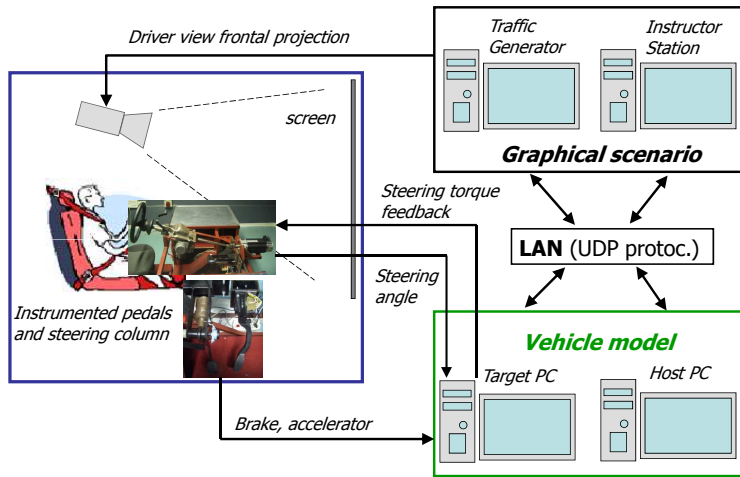


Figure 2.2: Block scheme of the driving simulator architecture.

platform (Section 2.2) and on the control desk (Section 2.3). Finally, the externally developed visual system is also presented: projection system is described in Section 2.4 and the graphic scenario in Section 2.5.

## 2.1 Computers and data flow

During the simulated drives, four computer are involved to carry out all functions of the driving simulator, such as the real-time simulation of the vehicle model, the data acquisition, the generation of the graphical scenario, etc.. The computers, which are connected through a local area network, are arranged following the simulator architecture shown in Figure 2.2 and will be further identified as:

- Target PC;
- Host PC;
- Traffic Generator PC;
- Instructor Station PC.

As shown in Figure 2.2, two of these computers (Target PC and Host PC) are dedicated to the vehicle simulation model and the other

two (Traffic Generator and Instructor Station) to the graphical scenario (Section 2.5). The Host PC and the Instructor Station are the computers used to monitor and control the simulated drive, respectively from the vehicle model and the graphical scenario point of view. These are installed in the control desk, as described in Section 2.3.

As already mentioned, the four computers are connected through a local area network which is based on the User Datagram Protocol (UDP) as communication protocol. Without going into details, UDP was considered as more suitable for this real-time application, rather than the usually employed TCP/IP. The main advantages of UDP are the small dimension of the data packet, the packet-oriented communication (data are ready to use when received) and the complete compatibility with Matlab/Simulink data types (double, int8, int32, uint8, etc.). It is worth noting that, in UDP communication, the sender does not need a confirmation from the receiver. This means that data packets are sent in the network even if the receiver is busy and they can get lost. This guaranties the synchronization of the simulated data communication with the real time, but particular care must be taken to set the proper communication settings between the computers.

The vehicle simulation model (Chapter 3) was built in Matlab/Simulink environment and it is available in the Host PC for modifications of its structure or parameters. In the other computer dedicated to the model, the Target PC, the vehicle model is run during the simulated drives. In order to guarantee the real-time simulation, the model has to be run on a dedicated computer with specific features. For this application, the xPC Target toolbox of Matlab [44] was chosen [43].

Once the model and its parameters are defined, it is compiled, in the Host PC, in C code by the Realtime Workshop Matlab toolbox. To this aim, the toolbox uses an internal compiler whose options are set in the *Simulation parameters* of the Simulink model. In order to be run in Target PC, the model must be compiled with the option *System target file* set to *xpc target.tlc*.

The compiled model is then sent to the Target PC using the xPC Target toolbox which has a user friendly graphical interface shown in Figure 2.3. With the commands of the xPC Target, most of them available in the graphical interface, the real-time simulation of the model in the Target PC is controlled from the Host PC. It is possible to set the communication parameters between the two PCs, to check the communication once the PCs are connected, to load a new model, to start and

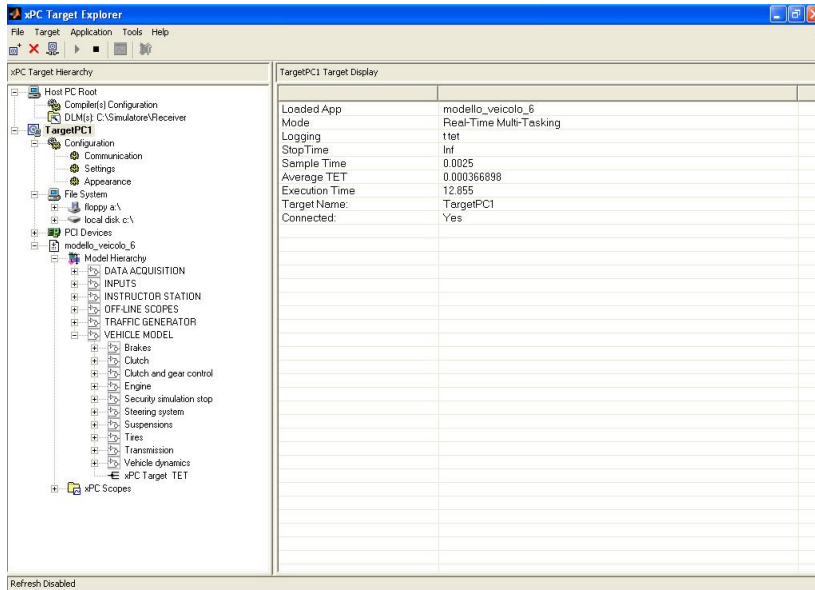


Figure 2.3: xPC Target explorer interface in the Host PC.

stop the simulation, to monitor some output variables and to change model parameters.

The Target PC runs a specific xPC Target kernel which is generated from the Host PC (in the xPC Target Explorer interface) and saved in a removable drive (such as floppy disk or usb stick). It contains the Target PC software together with the information about the communication settings between the two PCs (IP addresses, port numbers, communication protocol, etc.) and must be generated once these settings are determined. This specific xPC Target kernel is then booted by the Target PC instead of any other operating system, which would not guarantee the real-time simulation.

Other options include the possibility of setting Target or Host output graphs (scopes) using, in the Simulink model, the specific xPC Target block called *Scope xPC*. These scopes can be then managed with the xPC Target Explorer interface and allow to see some selected output signals of the model both in the Target PC and in the Host PC. By means of this feature, it was possible, in the first phases of the simulator development, to monitor in real-time the evolution of some fundamental vehicle model quantities, such as the longitudinal velocity, the lateral



Figure 2.4: Target PC screen-shot during a simulated drive.

velocity, the yaw rate and the roll angle (Figure 2.4). A so called *file scope* can also be added to the Simulink model, saving the signals to the hard disk of the Target PC. However, all these functions of signals plotting or data saving were replaced by a self-developed data acquisition software, specifically designed for this driving simulator application. The data acquisition software is a Simulink model running in the Host PC during the simulated drivers and it is described in Section 4.2.

A fundamental aspect in the xPC Target application, is the model equations solver. In order to guarantee the real-time simulation, the solver (to be set in the Simulink model in the Host PC) has to be a fixed time-step solver. Using a fixed time-step solver is, in fact, necessary to synchronise the input signals and the model computed outputs. In the developed vehicle model, the Runge–Kutta solver was chosen (ode4) and a fixed time-step of 2.5 ms was set, i.e. the solver frequency of the model is 400 Hz. As shown in Section 4.1, the value of this parameter is consistent with the present application.

In order to run a real-time simulation, the Target PC requires also a network card chosen from a specific set of supported cards by xPC Target.

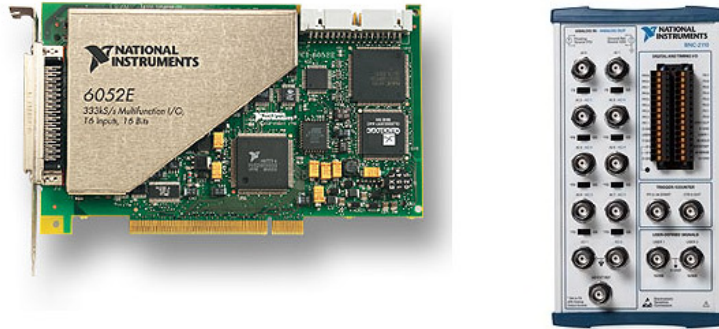


Figure 2.5: National Instrument PCI-6052E acquisition board (left) and connector block (right).

Table 2.1: Frequencies of model solution and data flow.

Model simulation	400 Hz
Data sent to Host PC (acquisition)	100 Hz
Data sent to Traffic Generator PC	100 Hz
Data sent to Instructor Station PC	100 Hz

These cards have an hardware clock which guarantees that inputs and outputs are at fixed time intervals.

During the simulated drive, the vehicle model, running in the Target PC, has to be connected to physical inputs and outputs. To this aim, a National Instrument acquisition board is connected to the Target PC, which is then able to receive the signals of the driver's inputs and send, as outputs, the signal of the steering wheel torque feedback. These analogue signals (see Section 2.2) are acquired with the PCI-6052E acquisition board, a 333kS/s, 16 bit, 16-analogue-input multifunction DAQ from National Instrument (Figure 2.5). This board, supported by the xPC Target, has a specific Simulink block to be put in the model, in which all communication settings (channel numbers, voltage and sample time) can be set (Figure 2.6).

The Target PC communicates, of course, also with the other computers of the driving simulator, sending all model output signals to the Host PC,

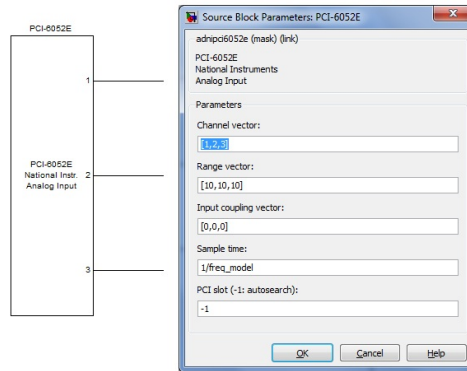


Figure 2.6: Specific block in Simulink for the National Instrument PCI-6052E acquisition board.

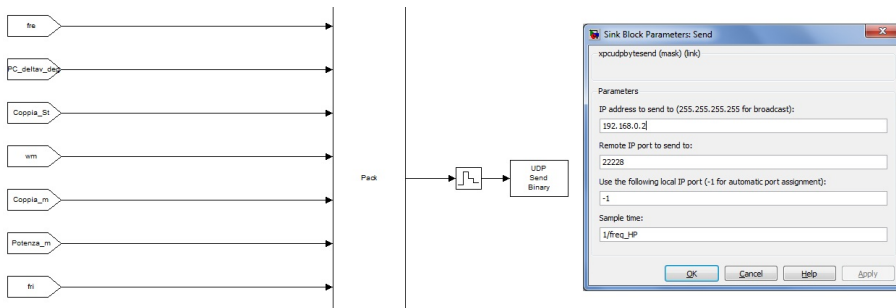


Figure 2.7: Specific block in Simulink for sending data via UDP.

for data acquisition, and some signals to the Traffic Generator and the Instructor Station, for the graphical scenario. These communications are implemented in the Simulink model using the specific xPC Target block for UDP data send. This block, shown in Figure 2.7 allows to set the IP address of the receiving computer, the port number and the sample time. Before this block, a *zero-order hold* block is used to keep the signal constant when the sending frequency is different from the model solution frequency. A *pack* block is also used, which packs all the signals to be sent in a single channel defining the number of bytes for each signal. The working frequencies of these communications are shown in Table 2.1.

In the model, also blocks for UDP data receive are implemented, which allow to send signals from the Host PC to the Target PC during the



simulated drivers. This feature is used to modify in real time some model parameters or to force some variable, making an external intervention in the simulation (see Section 4.3).

As already written, the Traffic Generator PC and the Instructor Station PC are dedicated to the graphical scenario. The former generates the driver front view, manages the other vehicles and pedestrians in the graphical environment and reproduces the sounds (engine noise). The latter is used to control some graphical scenario parameters, such as the weather and the daylight, from the control desk. Both of them need to correctly display the vehicle in the graphical environment and thus receive from the Target PC the position and orientation of the car body with respect to a fixed reference. These signals are described in Section 2.5. Finally, the graphical software is also used to obtain the distance of the vehicle center of mass to the lane centreline; this signal is sent by the Traffic Generator to the Host PC and acquired together with all other signals.

## 2.2 Driving platform

The driving platform of the DIMNP driving simulator reproduces the vehicle–driver interface of a small/medium size car with automatic transmission; i.e. the driver physically interacts with the throttle and brake pedals and the steering wheel, whereas there is no gear lever and no clutch pedal. The driving platform, shown in Figure 2.8, is made of the driver’s seat and a tubular space frame on which all other elements are fixed. Just recently, the front part of a bodywork of a Fiat Panda, with a plastic front window and the two doors, was added to the structure. It is planned to develop the driver’s cabin including a physical dashboard (which is currently virtually reproduced in the graphical scenario) and digital rear mirrors using small flat screens. It is worth noting that the more the simulator reproduces the real driver’s cabin of actual cars, the more the driver would behave naturally feeling himself in real driving conditions.

The driving platform was designed to reproduce the geometrical layout of a real car. The dimensions of the Fiat Idea (commercial car of small/medium size) were considered as a reference. In addition to this, the SAE J1100-JUN84 (1984) norm was taken into account for ergonomic design [43].



Figure 2.8: Driving platform of the driving simulator.

A driver's seat of Fiat Idea is employed, as well as Fiat Idea pedals and steering system. In order to allow different sized drivers to properly interact with simulator (at least from 5<sup>th</sup> to 95<sup>th</sup> percentile), the setting possibilities of the original seat and the steering wheel were kept. The seat allows the typical settings of other car seats of similar vehicles. The steering wheel position is also tunable and allows to change the inclination angle and distance from the driver's seat.

The main structure of the driving platform is made of welded square tubes measuring 30 mm, 2 mm thick. Covered wooden panels are used as floor for the driver's feet, for comfortably supporting the driver's left foot (which is not used, having no clutch pedal) and for protection. This structure, which was designed before this work (see [43] for details) supports the pedals sub-structure, the steering system with the electric motor for the torque feedback (and its converter), the connector block of the acquisition board, a DC power generator and the Target PC.



Figure 2.9: Driving simulator throttle and brake pedals.

In the following, the main driver's interfaces, i.e. the pedals and the steering system, are described in more detail.

### 2.2.1 Pedals

The throttle and brake pedals, shown in Figure 2.9, were endowed with angular potentiometers (also visible in the picture), which measure the angle travelled by each pedal hinge. This measure is used as the reference signal for the pedals positions, which are among the inputs of the vehicle simulation model. The potentiometers are the SRS280 model from Penny and Giles, with an *electrical angle* of  $50^\circ$ . The working range was set from 0 V to 10 V using an external DC power generator (represented in Figure 2.10), which generates the reference DC signal of 10 V. However, the actual angular working range of the pedals is less than the nominal potentiometers angle of  $50^\circ$  and therefore just about 3 V are used.

These analogue signals of the potentiometers are acquired by the acquisition board which is connected to the Target PC, as already written in Section 2.1. Finally, inside the vehicle simulation model, the acquired signals in Volts are converted into signals in the range 0–1, as described



Figure 2.10: DC power generator.

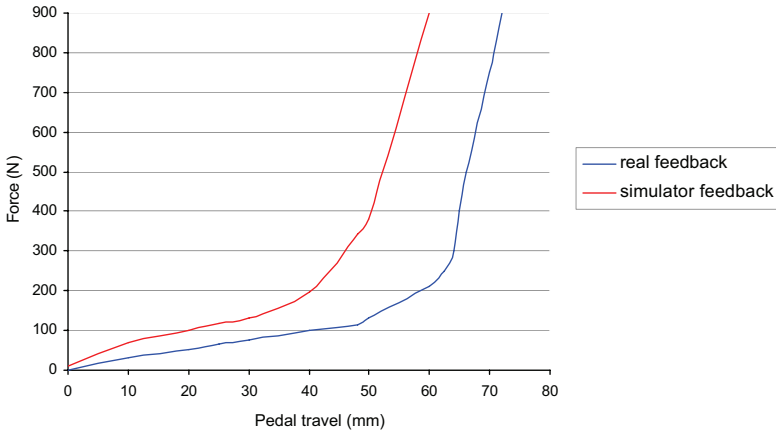


Figure 2.11: Passive feedback force on the brake pedal [43].

in Section 3.1.

In order to reproduce the behaviour of real pedals, both the driving simulator throttle and brake pedals have passive feedback systems. By means of them, the driver feels realistic reaction forces on the pedals during the simulated drive. The throttle pedal is endowed with its default return spring which is also on the original pedal. On the other side, for the brake pedal it has been necessary to emulate the reaction force due the pressure of the oil during braking. Starting from a real force – pedal travel curve, a cylinder with two springs has been designed to this aim [43]. The results of the simulator feedback force in comparison to the real one is represented in Figure 2.11. During the first part of the pedal



Figure 2.12: Steering system with electric motor for active torque feedback (on the right side of the picture).

travel, only the first steel spring works, whereas in the second part of the travel, a high stiffness rubber spring works in parallel to the previous one. This behaviour reproduces fairly good the real pedal characteristic, with a first part of low stiffness and a second part of very high stiffness due to the deformation of the braking system elements.

### 2.2.2 Steering system

The steering system of the driving simulator is shown in Figure 2.12. Starting from the left side of the picture, it is made of: the steering wheel, the steering wheel support with the electric power-assisted (currently disabled) steering unit (EPS), the steering column with the Hooke joints and the electric motor for the torque feedback. All components, except the electric motor, are of a Fiat Idea (supplied by TRW).

During this work period, in order to improve the system reproducing a realistic steering wheel torque, the active torque feedback with a brushless electric motor was implemented in the steering system. The electric motor is used also to acquire the steering wheel angle, which was previously measured by the EPS.

The active steering torque feedback chosen for the simulator is a

Table 2.2: Characteristics of the Control Technique Unimotor brushless electric motor.

Model name	115U2C30
Power supply voltage	3-phase, 380 V
Continuous stall torque	9.4 N m
Peak torque	28.2 N m
Maximum cogging	0.14 N m
Inertia	0.0009 kg m <sup>2</sup>
Weight	11.6 kg

brushless electric motor whose main characteristics are summarised in Table 2.2. This type of electric motor was considered the most suitable for this application, where running at very low speed giving high torques is required. A peak torque of 28.2 N m is sufficiently above the maximum steering torque applied by drivers of passenger vehicles.

The electric motor is driven by a converter which is shown in Figure 2.13 with its connection ports. The feedback torque control is carried out giving the signal of the torque reference as analogue input to the motor converter (using the input ports of the *Analog speed reference 2*), which interprets it as a current reference. This signal is computed by the vehicle simulation model as function of the actual driving conditions (see Section 3.7). It is then given to the converter, in the range 0 V–10 V from the National Instrument acquisition board connected to the Target PC. The default control parameters of the converter were kept, whereas some control of the feedback torque was implemented at the simulation model level.

As pointed out, the electric motor is used also to measure the steering wheel angle. This measure is performed by an internal encoder which gives the angular position of the motor with a resolution of  $2^{16}$  positions per round. This signal is an output of the converter (the output port *Speed* is used) in 0 V–10 V range and it is acquired by the National Instrument acquisition board. The conversion from Volts to the steering wheel angle is carried out in the input block of the vehicle simulation model (Section 3.1).

From the mechanical point of view, the electric motor is connected to the space frame of the driving platform by a sub-structure which was

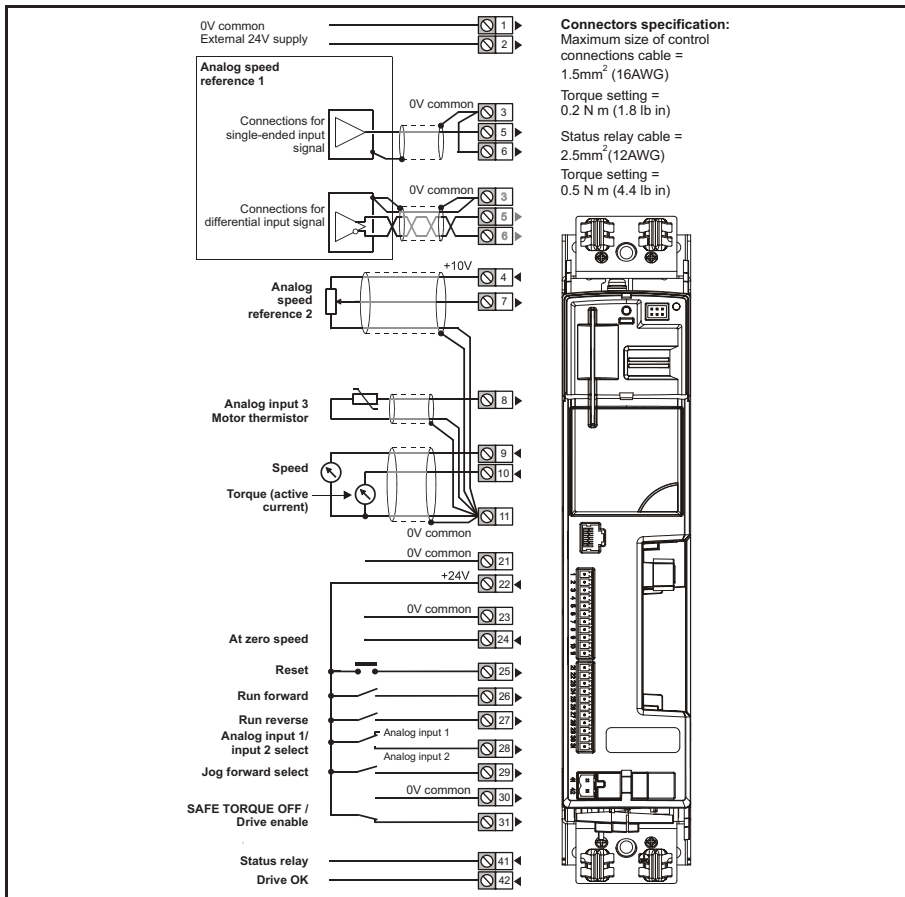


Figure 2.13: Digitax electric motor converter.

specifically designed and verified.

## 2.3 Control desk

Simulated drives are always followed by an operator who seats at the control desk. From this station, all fundamental elements of the driving simulator can be controlled using, as previously mentioned, the Host PC and the Instructor Station PC. In more detail, the functions of the control desk are:

- control the vehicle simulation model (Host PC);

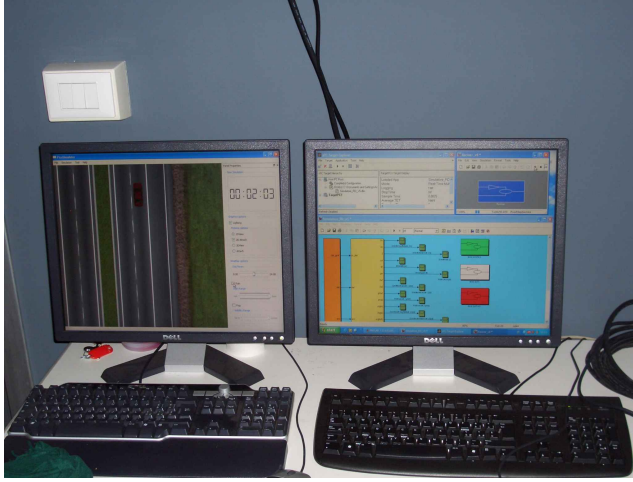


Figure 2.14: Driving simulator control desk with Host PC (at the right) and Instructor Station PC (at the left).

- data acquisition (Host PC);
- parameters change in the simulated drive (Host PC);
- graphical scenario monitoring (Instructor Station PC);
- parameters change in the graphical environment (Instructor Station PC).

The simulation model control has been already described in Section 2.1. The other functions related to the Host PC are topics of Section 4.2 and 4.3. At this point it is worth anticipating that, during the simulated drives it is theoretically possible to change every model parameter without stopping and restarting the simulation. Sudden events, such as a lateral skid or a change in a vehicle dimension, can be therefore commanded from the Host PC in the control desk.

In addition to controlling the vehicle simulation model, the operator at the control desk can monitor the vehicle behaviour in the graphical scenario with the Instructor Station PC, whose interface is shown in Figure 2.15. Moreover, it is possible to change some environmental parameters of the scenario. These currently include the rain, the fog and the daylight. An example of the fog in the scenario is shown in Figure 2.16. In the future developments, it will be possible to control



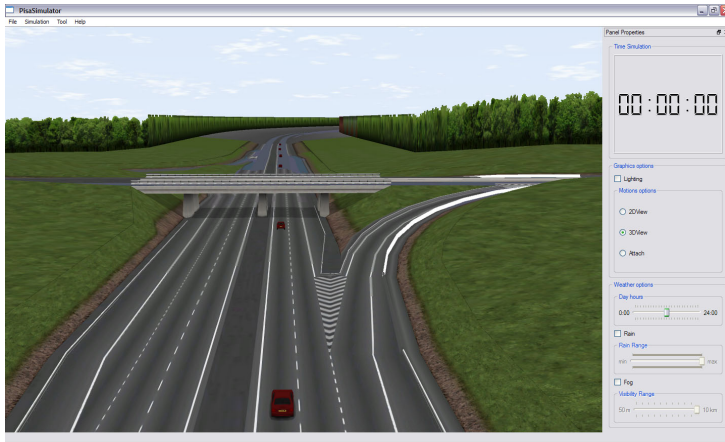


Figure 2.15: Instructor Station PC screen shot.

also the traffic intensity and to command sudden events in the graphical scenario, such as pedestrians crossing the road.

## 2.4 Visual system

The driving simulator visual system is made of a single front flat screen and an image projector, both shown in Figure 2.17. The image projected on the screen represents the driver's front view in the graphical scenario which is elaborated by the Traffic Generator PC. The NEC projector is therefore connected to this computer.

The visual system was calibrated to set the proper distance of the projector from the screen and of the screen from the driver's seat, so that the projected image has the right dimensions.

This visual system was suitable for the main aims of the driving simulator activities, i.e. for highway driving. As future development of the simulator, a three-screen visual system or single cylindrical screen system shall be installed to properly drive in the urban environment, having a wider visual field.

## 2.5 Graphical scenario

The graphical scenario is made of a highway environment connected to an urban area with two secondary roads. In the scenario, there other



Figure 2.16: Fog in the graphical scenario imposed from the Instructor Station PC.

autonomous vehicles, which are currently 300, with different target speeds and routes set-up at the beginning of the simulation. In the urban area there also pedestrians who cross the roads on zebra-crossings and parked vehicles.

The graphical scenario was developed by Anticyp Simulation and runs in Vega Prime, a dedicated commercial software application of Multigen–Paradigm. Vega Prime allows to create specifically designed three dimensional graphic environments for driving simulators with several features as: traffic management (number of vehicles, density, speed, etc.),

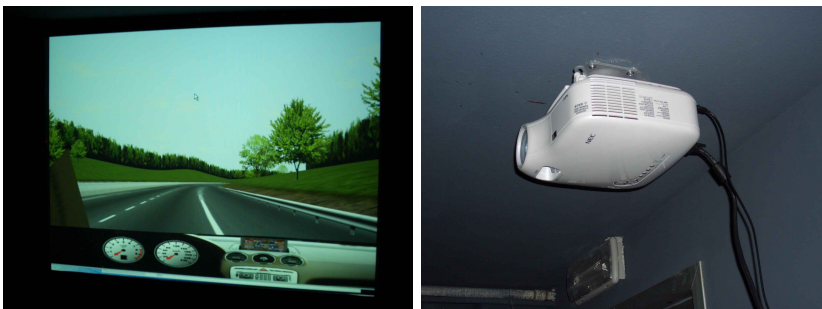


Figure 2.17: Driving simulator visual system: front screen (left) and image projector (right).

environment special effects (rain, fog, etc.) and sudden events in the scenario (such as pedestrians crossing the road). As written in Section 2.3, some of the control functions of the graphical environment can be carry out in real time during the simulated drive from the Instructor Station PC in the control desk. However, some others must be carry out in the Traffic Generator PC when the simulation is stopped. These include the set-up of the driver's front view (position and angles), the definition of the traffic parameters (number of vehicles, speed and route of each vehicle and pedestrians route and behaviour), and the definition of static objects in the scenario (such as parked vehicles, traffic signs and lights, etc.). With these functions, the environment can be completely customized for the needs of the specific tests which are carried out with the driving simulator.

During the simulated drive, the graphical scenario front view is continuously update with the signals computed by the vehicle simulation model and sent from the Target PC to the Traffic Generator and Instructor Station PCs. These signals, which mainly defined the position and orientation of the vehicle in the scenario, are the following:

- longitudinal coordinate of the vehicle centre of mass in a fixed reference ( $x$ );
- lateral coordinate of the vehicle centre of mass in a fixed reference ( $y$ );
- vehicle centre of mass height;
- longitudinal velocity of the vehicle centre of mass;
- lateral velocity of the vehicle centre of mass;
- yaw angle;
- pitch angle;
- roll angle;
- yaw velocity;
- pitch velocity;
- roll velocity;



Figure 2.18: Driver's front view in the highway environment.

- simulation real time;
- engine speed<sup>1</sup>.

Before sending the coordinates  $x$  and  $y$ , a translation and a rotation of  $90^\circ$  are performed in the model in order to align the fixed coordinate system of the model to that of the graphical scenario. An alignment of the time vectors must also be carried out to guarantee the real-time simulation; for this reason also the time signal is sent from the Target PC.

The driver front view (Figure 2.18) is completed by the virtual dashboard, which displays the vehicle and engine speeds and a virtual rear mirror. The position of these elements was set-up to correctly reproduce their actual position in the driver's view in real cars.

In Figure 2.18 and Figure 2.19 parts of the highway area are shown in the driver's front view and in a top view. The highway is a closed-loop about 20 km long with three radial parts and some junctions. The urban area, which was developed in a second phase of the project, is connected to the highway by secondary roads. This area was graphically built

<sup>1</sup>The engine speed signal is used to generate the engine noise.

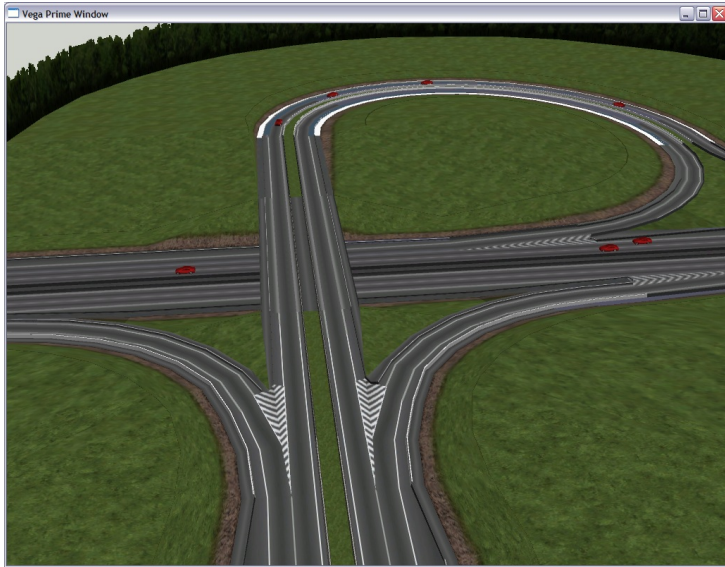


Figure 2.19: Top view of a highway junction.

starting from air photos of Rosignano (Livorno, Italy), reproducing some of its neighbourhoods. This part of the scenario, which is currently in development, will be completed with more traffic lights, traffic signs, parked vehicles and pedestrians. Example view of the current urban area are shown in Figure 2.20 and Figure 2.21.



Figure 2.20: Driver's front view in the urban environment.



Figure 2.21: Top view of the urban environment.

## Chapter 3

# Simulation model

The simulation model represents the core part of the driving simulator. The model receives the signals of the driver's inputs (throttle and brake pedal position and the steering wheel angle) and computes all output signals for the actual car position and orientation in the graphical scenario, for the active feedback on the steering wheel and for data acquisition. To these aims, the model simulates the complete vehicle dynamic behaviour and manages input and output signals as described in Section 2.1.

The model was developed in Matlab/Simulink environment and its main window, which shows its main structure, is represented in Figure 3.1. The model is made of four main parts:

- driver's inputs processing;
- vehicle model;
- output data sending (to Host PC for data acquisition, to Traffic Generator PC and Instructor Station PC for the signals needed by the graphical scenario);
- output scopes for off-line analyses.

The driver's input and the output parts are topic of Section 3.1, whereas the vehicle model is deeply described in the following sections focusing on its structure and on its subsystems.

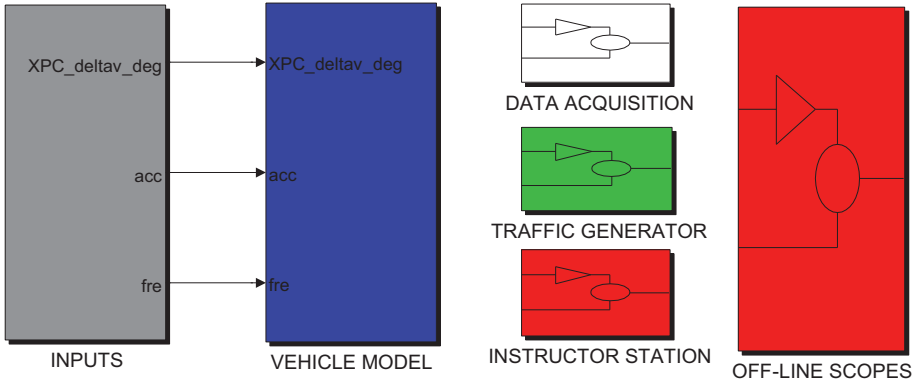


Figure 3.1: Simulink blocks in the main model window.

### 3.1 Input and output blocks

The content of the input block of Figure 3.1 is shown in Figure 3.2. The driver's input signals, acquired by the National Instrument acquisition board, are read by the model using the specific xPC Target block for the acquisition board, which was already described in Section 2.1. The signals of the throttle and brake pedal position and the steering wheel angle are available in the 0 V–10 V range. In this block, they are converted in model units, i.e. the pedal positions in signals from 0 (rest pedal position) to 1 (full pedal travel) and the steering signal in steering wheel angle in degrees. The  $a$  (throttle) and  $b$  (brake) signals are simply computed from the measured potentiometer signals  $V_a$  and  $V_b$  and their limit values, as follows:

$$a = \frac{V_a - V_{a,\min}}{V_{a,\max} - V_{a,\min}} \quad (3.1)$$

$$b = \frac{V_b - V_{b,\min}}{V_{b,\max} - V_{b,\min}}. \quad (3.2)$$

The steering wheel angle  $\delta_s$  is obtained from its corresponding voltage signal (which gives the angle in  $2^{16}$  units per round), with a specific function. A simple linear conversion, as that carried out for the pedal signals, can not be performed because the voltage signal is between 0 V and 10 V in a steering wheel round, but the model generally needs steering wheel angles bigger than  $360^\circ$  in both directions. Moreover, the angle at



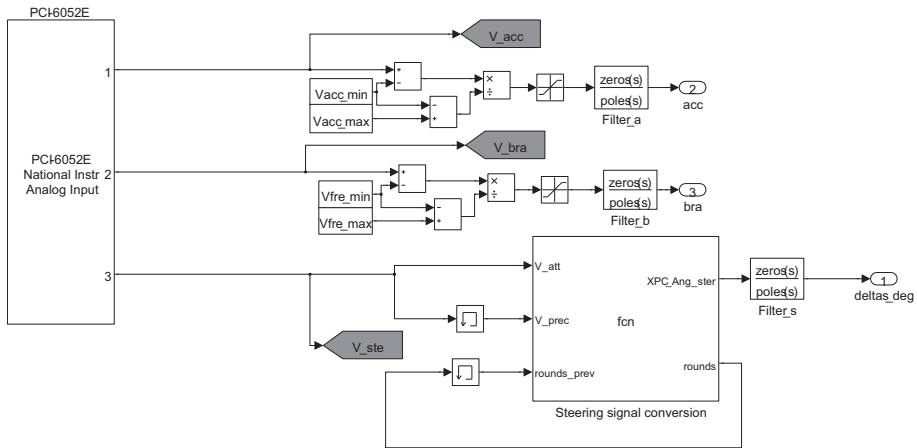


Figure 3.2: Driver's inputs block in the simulation model.

which the discontinuity in the voltage signal occurs can be theoretically everywhere between  $0^\circ$  and  $360^\circ$ , depending on the relative position of the motor encoder and the steering wheel. The function traces the steering wheel voltage signal counting the rounds and correctly computing the actual steering angle even if the signal jumps from 0 V to 10 V (or vice-versa). An offset value of the encoder position, which define the  $0^\circ$ , has to be set as parameter for the function.

In order to properly set the limits and the offset of the driver's input signals, a simple test model was made with a signal receiver. The former is made just of the input block of the simulation model and the sending block of the steering torque feedback and it is run in the Target PC. The latter is a simple signal receiver (Figure 3.3), running in the Host PC, which acquires the voltage signals of the driver's inputs together with the converted signals and allows the operator to choose a constant steering torque to be applied on the steering wheel.

In the simulation model, the converted values of the driver's input signals are filtered before being used for further computations in the vehicle model. Typical low-pass filters, with tunable cutting frequency and order, are used to eliminate high frequency measurement noise coming from the analogue sensors. The cutting frequencies, which were set in the filters, are very much above the maximum frequencies of the driver's input dynamics, so that the filter influence on the system dynamics is negligible.

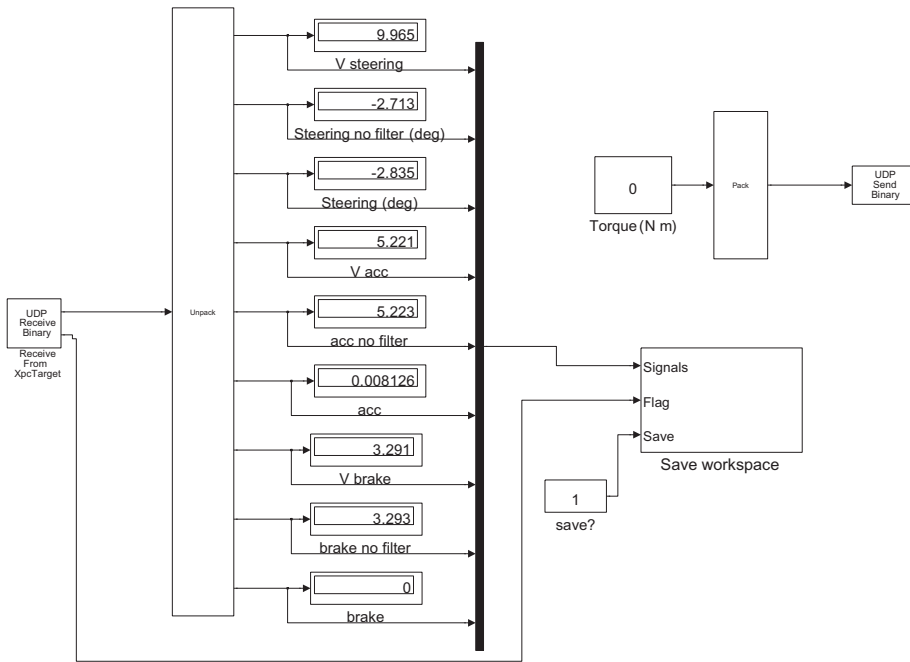


Figure 3.3: Test tool for driver's input signals and steering torque feedback.

All conversion and filter parameters can be easily set in the mask of the input block. Currently used parameters are shown in Figure 3.4.

For what concerns the output blocks, there are three blocks for the three computers to which output data are sent during the simulations. The structure of these blocks is the same, differences among them regard just a specific UDP send block, as described in Section 2.1. The signals sent to the computers dedicated to the graphical scenario have been already listed, whereas the signals acquired and stored by the Host PC are treated in Section 4.2.

When simulating the model outside the driving simulator (e.g. for development), the simulation is carried out directly in Simulink environment and the output signals can be observed with signal scopes collected in a specific block.

The steering torque feedback, which is also a model output, is treated in Section 3.7.

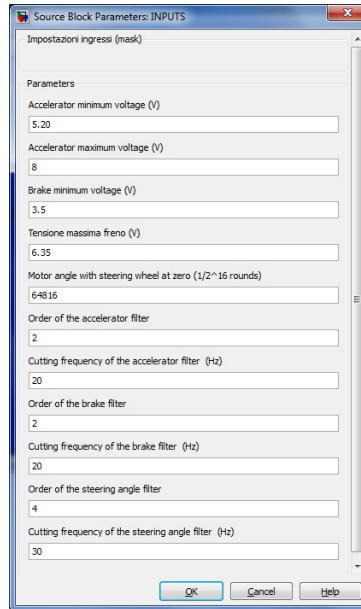


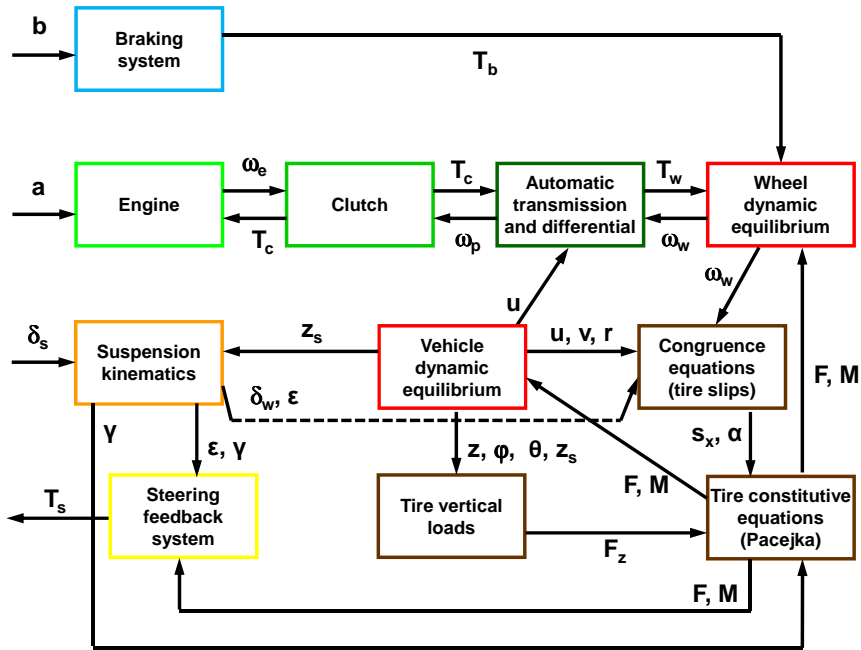
Figure 3.4: Mask parameters of the input block.

## 3.2 Structure of the vehicle model

The vehicle model reproduces the dynamic behaviour of a four wheel vehicle and its main subsystems. A functional scheme of the vehicle model is shown in Figure 3.5, where different colours are used to identify different subsystems. In this picture, just the main model functions and the main connections between them are shown, so that a clear overview of the model is provided. A list of symbols of the main quantities is also shown, whereas the other symbols needed will be introduced describing the single blocks with their equations.

The throttle pedal position is the input of the chain of powertrain blocks. The engine block uses this signal to compute the engine torque and solve the dynamic equilibrium of the engine. The engine speed is used by the clutch to obtain the transmitted torque, which is sent to the transmission with differential and, finally, to the wheels. As will be shown in the next section, the angular velocities are used as closed-loop feedback signals to solve the equations.

The drive torques, together with the braking torques computed by the braking system and the tire forces computed by the tire model, are



a: accelerator pedal position;  
 b: brake pedal position;  
 $\delta_s, \delta_w$ : steering angle (at the steering wheel and at the wheel);  
 $T_s$ : steering torque feedback;  
 u, v: longitudinal and lateral velocity;  
 r: yaw rate;  
 z,  $\varphi, \theta$ : vertical sprung mass displacement, roll and pitch;  
 F, M: tires forces and moments;  
 $T_b$ : braking torque;  
 $T_e, T_c, T_w$ : engine, clutch and wheel driving torque;  
 $\omega_e, \omega_p, \omega_w$ : engine, gearbox primary shaft and wheel angular velocity;  
 $s_x, \alpha$ : tire longitudinal slip and slip angle;  
 $z_s$ : suspension travel;  
 $\epsilon, \gamma$ : toe and camber angle of the wheel.

Figure 3.5: Block scheme of the vehicle model with the main subsystems and its main connections.

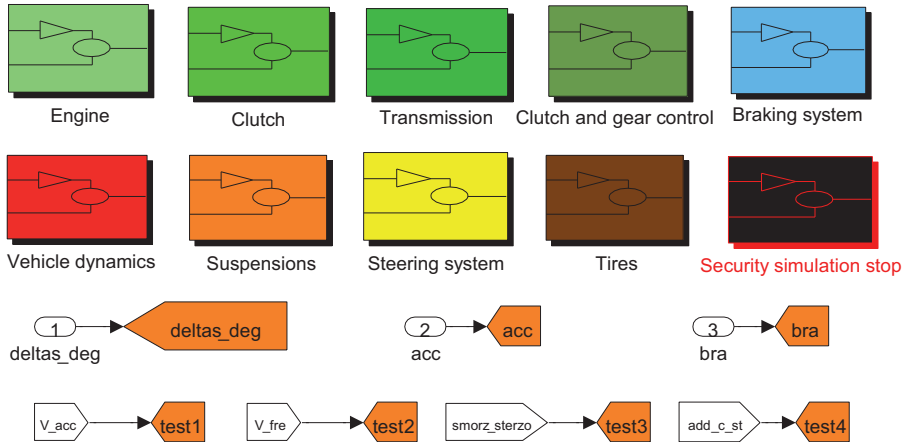


Figure 3.6: Simulink blocks in the vehicle model window. The same colours of Figure 3.5 are used.

the inputs of the wheel dynamic equilibrium, from which the angular velocity of the wheels is obtained. This result is used by the tire model to compute the longitudinal slip and the slip angle (congruence equations), using also the outputs of the vehicle dynamic equilibrium (vehicle linear and angular velocities) and the steering angle at the wheels. The tire model finally computes the tire forces and moments from the tire slips, the wheel camber angles and the vertical loads. These are computed by the tire model itself, from the sprung and unsprung masses kinetic quantities obtained from the vehicle dynamic equilibrium.

The part of the vehicle dynamic equilibrium solves the differential motion equations of the sprung mass and the four unsprung masses, having, as input, the tire forces and moments and, as output, the kinetic quantities describing the car body and the suspensions motion. A suspension kinematic model is also needed to compute the relative position and orientation of the wheels with respect to the car body as functions of the suspension travels and the driver steering angle.

Finally, the steering torque feedback is obtained from the tire loads and the position and orientation of the wheels and it is physically applied to the steering wheel.

The vehicle model was developed in Simulink following the described scheme. The function blocks of Figure 3.5 were organised as shown in

Figure 3.6, where the main window of the vehicle model is represented. Each block of the model represents a physical subsystem of the vehicle, except the vehicle dynamics block. In details, the vehicle model blocks are:

- engine;
- clutch;
- transmission (gearbox and differential);
- clutch and gear control (control logics for the automatic transmission);
- braking system;
- vehicle dynamics (equilibrium of sprung and unsprung masses and rotational equilibrium of the wheels);
- suspensions (kinematics, elastic and damping characteristics);
- steering system (steering torque feedback);
- tires (tire slips and tire loads);
- security simulation stop.

This model architecture allows to develop each vehicle subsystem independently and to have different levels of detail in each block, depending on the simulation aims. Moreover, other vehicle subsystems can be added if properly connected to the others, with no need to redevelop the current model. At the moment, the vehicle mechanics and the powertrain are reproduced with a sufficient detail for the driving simulator activities which were carried out. As future development, the model could be more detailed in some parts and other subsystems, such as the electrical system or the engine cooling system, could be added to deeply investigate some aspects of the vehicle behaviour.

In the following sections, all vehicle model blocks are described. At this point, it is worth briefly writing about the security stop block, which was added to the model for safety reasons. This block automatically stops the simulated drive if the yaw rate exceeds a threshold value, currently set to 5 rad/s, which represents abnormal driving conditions, such as

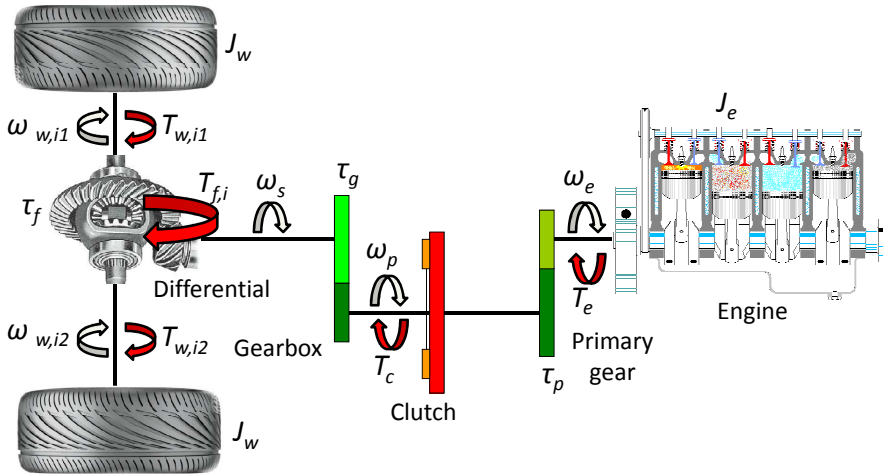


Figure 3.7: Powertrain of the vehicle simulation model. The configuration with two drive wheels is here represented (generic axle  $i$  with left (index 1) and right (index 2) wheels). The primary gear is optional.

numerical problems due to vehicle overturning or manoeuvres considered too extreme. Stopping the simulation, the steering torque feedback is switched off and there is therefore no risk of high and impulsive torques which can hurt the driver.

### 3.3 Powertrain and braking system blocks

The vehicle model powertrain is made of the blocks of: engine, clutch and transmission. A block for the clutch and gear control is also included, being the driving simulator with no direct driver control of the clutch and the gear shifting. As the powertrain, the braking system influences the longitudinal vehicle dynamics and its block is therefore described in this section.

The complete vehicle powertrain is represented in Figure 3.7 with the main symbols used in the following. The system is made of the following physical elements: the engine, an optional primary gear (with fixed gear ratio), the clutch, the gearbox (with variable gear ratio) and the differential. As already mentioned, the wheels are not considered part

of the powertrain and their dynamic equations are solved by the vehicle dynamics block. This block receives the final output of the powertrain chain, which are the driving torques at the drive wheels (and the braking torques) and gives back the wheel angular velocities.

The powertrain system is modelled with a single rotational inertia which represents the engine inertia and all other component inertias which are between the engine and the clutch disc. Other transmission inertias are neglected for simplicity, being their values much lower than the engine inertia. This means that there is just one differential motion equation in the engine block, whereas the other elements are all modelled with algebraic equations, which compute their output torque.

In Figure 3.7 two drive wheels are shown, without specifying to which axle they belong. Without modifying the model architecture it is, in fact, possible to have a front-wheel drive, a rear-wheel drive or a four-wheel drive with an open central differential. As it will be described, this can be done just modifying the car numerical parameters.

It is worth specifying at this point that all gear ratios are defined as the velocity of the driven gear divided by the velocity of the driver gear. Although in classic mechanics the opposite convention is more often used, in automotive field the ratios are computed in this way and it was therefore decided to follow this convention.

In the following, the equations and the Simulink models of the powertrain and braking system blocks are presented.

### 3.3.1 Engine

The engine block of the vehicle model, shown in Figure 3.8, solves the engine rotational dynamics, described by:

$$J_e \dot{\omega}_e = a T_e(\omega_e) l_e(\omega_e) - f(a) T_{r,e}(\omega_e) - \frac{T_c}{\tau_p}, \quad (3.3)$$

where  $J_e$  is the engine inertial term,  $\omega_e$  is the engine speed,  $T_e$  is the engine driving torque,  $T_{r,e}$  is the engine drag torque and  $T_c$  is the torque transmitted by the clutch, divided by the optional primary gear ratio  $\tau_p$ . The driving torque is function of the engine speed and it is employed in the model as a look-up table which represents the engine characteristic curve at full throttle. An example of the curve can be seen in Figure 3.8 in the engine torque block. The function is simply multiplied with the throttle pedal position signal  $a$  to compute the actual engine torque. It is also



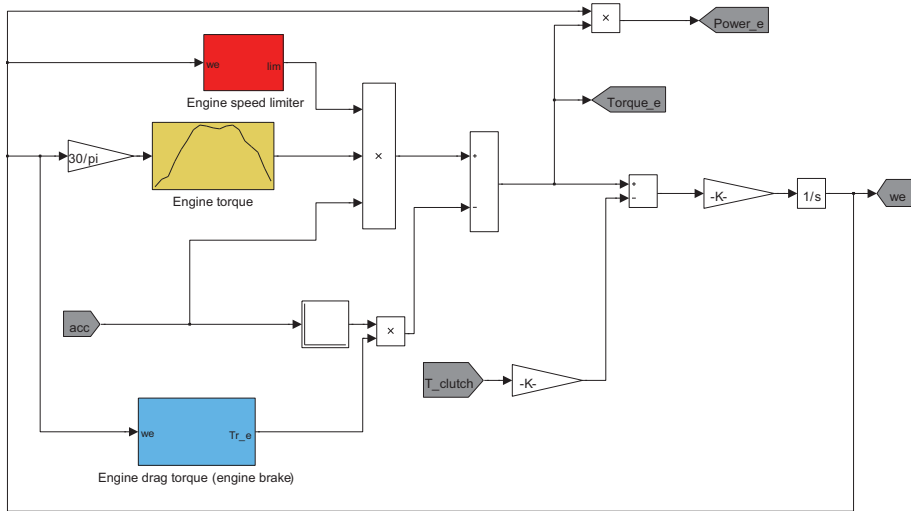


Figure 3.8: Engine block of the vehicle simulation model in Simulink.

multiplied with  $l_e$ , the output of an engine speed limiter function, which limits the driving torque to keep the engine speed below its maximum value.

When the engine is in coast (i.e.  $a$  almost 0),  $f(a)$  becomes 1 (otherwise it is null) and the engine drag torque  $T_{r,e}$  is transmitted. This torque is computed from the engine speed (expressed in rpm), using an empirical equation which takes into account the engine displacement ( $V_e$ , in  $\text{cm}^3$ ) together with some numerical coefficients [26]:

$$T_{r,e}(\omega_e) = 0.97 + \frac{0.15}{1000}\omega_e + \frac{0.05}{1000^2} \frac{9.81}{400\pi} V_e \omega_e^2. \quad (3.4)$$

It is worth noting that every type of driving motor can be employed in the model, if the torque–speed characteristic is available. Although up to now, just internal combustion engines have been simulated, there are no constraints to employ electric motors in the future.

### 3.3.2 Clutch

The clutch block (shown in Figure 3.9) computes the torque  $T_c$  which is transmitted to the gearbox, as function of the engine speed (reduced by the primary gear ratio, when present) and the primary shaft angular velocity  $\omega_p$ .

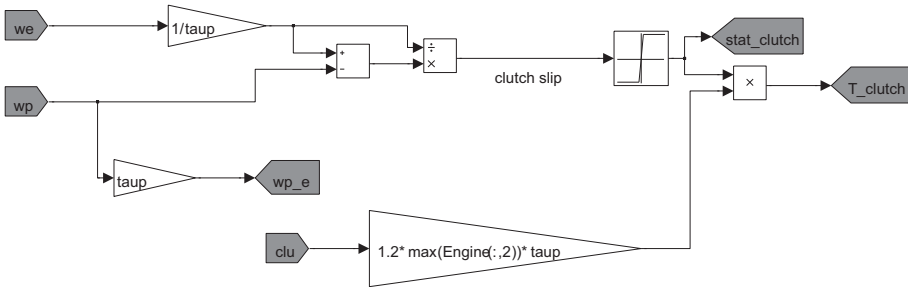


Figure 3.9: Clutch block of the vehicle simulation model in Simulink.

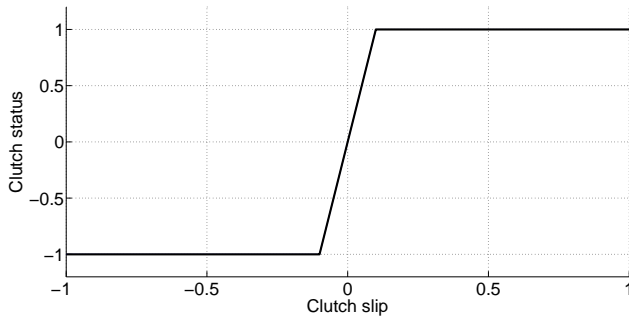


Figure 3.10: Clutch friction function.

In order to model the static and dynamic friction behaviour of the clutch with a single model architecture, a friction function was employed. This function depends on the clutch slip, defined as:

$$s_c = \frac{\omega_e/\tau_p - \omega_p}{\omega_e/\tau_p}. \quad (3.5)$$

The friction function  $f_f(s_c)$ , which is graphically represented in Figure 3.10, indicates the clutch status. When the clutch is slipping, the function absolute value is 1, whereas its value is between 0 and |1| when static friction occurs. In this condition, a small amount of slip is computed by the model (currently the slip threshold value between static and dynamic friction is set to 0.1 rad/s), so that the angular velocities of the input shaft ( $\omega_e/\tau_p$ ) and of the output shaft ( $\omega_p$ ) remain uncoupled degrees of freedoms. This allows to keep the same model architecture for both static and dynamic friction conditions, although a small (but acceptable) error is made in the former condition.

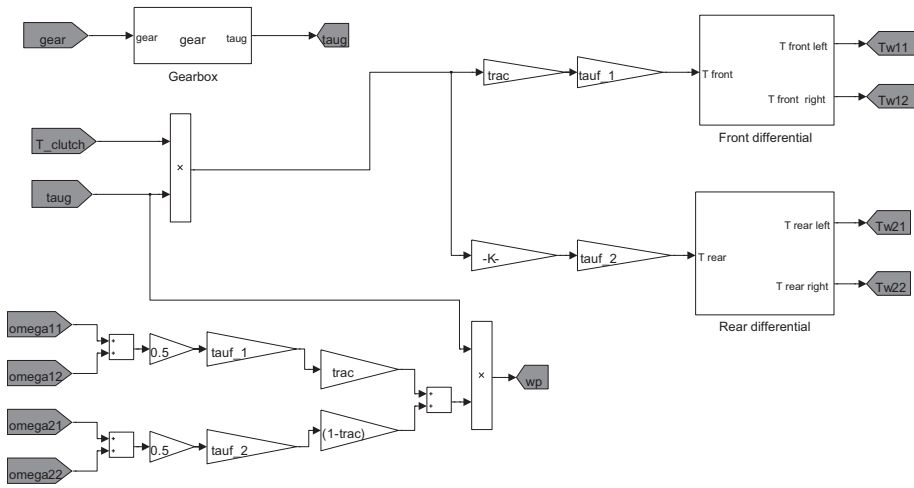


Figure 3.11: Transmission block of the vehicle simulation model in Simulink.

The friction function multiplies the current transmissible torque by the clutch, so that it is fully transmitted if dynamic friction conditions occur, whereas just an amount of it is actually transmitted in static friction conditions. This amount depends on the system equilibrium. The clutch torque is obtained as:

$$T_c = c \left( 1.2 T_{e,\max} \tau_p \right) f_f(s_c), \quad (3.6)$$

where  $T_{e,\max}$  is the maximum engine torque and  $c$  represents the clutch control signal (from 0 to 1). The clutch is made to transmit 1.2 times the maximum engine torque when engaged ( $c = 1$ ). During an engagement manoeuvre, the clutch torque that can be transmitted is modelled as a linear function of the clutch control signal.

### 3.3.3 Transmission

The transmission block contains the mathematical functions of the gears and the differential. It computes the driving torques on the drive wheels from the input torque given by the clutch block. Moreover, the angular velocity of the primary shaft is obtained as function of the velocities of the drive wheels (given by the vehicle dynamics block). As previously shown, this signal is needed by the clutch model to compute the transmitted torque.

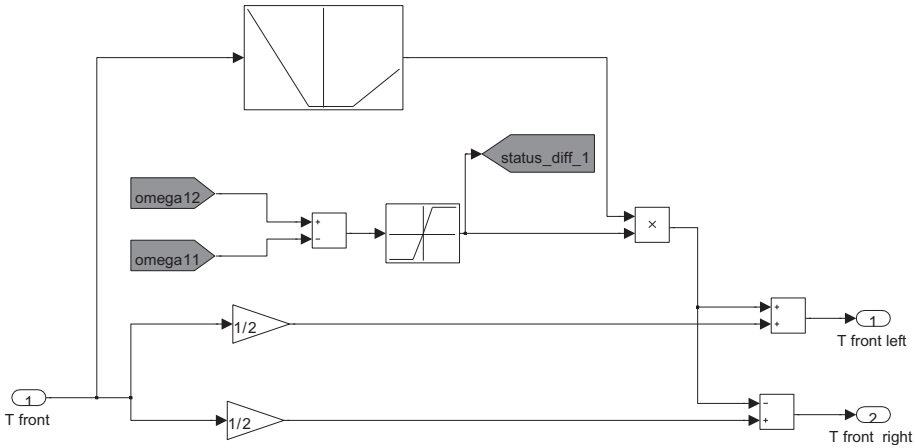


Figure 3.12: Differential block of the vehicle simulation model in Simulink.

The content of the transmission block is shown in Figure 3.11 where the functions introduced are clearly represented. The gear signal coming from the clutch and gear control block is used as index to select the actual gear ratio  $\tau_g$  from a vector. Currently there is not a dynamic model of the gear shifting, which occurs instantaneously when the gear control logic sends a new gear signal.

The driving torques for the front and the rear axles, which are  $T_{f,1}$  and  $T_{f,2}$  respectively, are obtained from the following equations:

$$T_{f,1} = T_c \tau_g t \tau_{f,1} \quad (3.7)$$

$$T_{f,2} = T_c \tau_g (1 - t) \tau_{f,2}, \quad (3.8)$$

where  $\tau_{f,1}$  and  $\tau_{f,2}$  are the front and rear final ratios on the differentials. The parameter  $t$  is used to select front-wheel ( $t = 1$ ) or rear-wheel ( $t = 0$ ) drive, keeping the same model block architecture. It is also possible to set  $t = 0.5$ , which represents the case of a four-wheel drive vehicle with an open central differential.

The final torques of the two axles are split between the two wheels with the differential functions. The (sub)block of the front differential is represented in Figure 3.12. The front and rear differentials are modelled in the same way; in the following equations the generic axle  $i$  is therefore taken into account.

The model reproduces the behaviour of a torque-sensitive limited-slip differential which can turn in a classic open differential, if its parameters

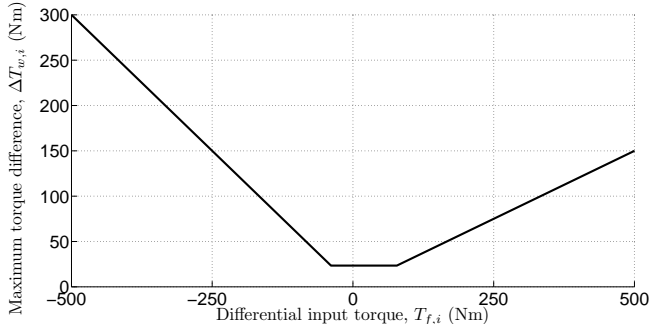


Figure 3.13: Differential maximum allowed torque difference between left and right wheels as function of the input torque. Example of the ET3 Formula SAE vehicle with 23.5 N m of preload, 0.3 blockage ratio in drive and 0.3 in coast mode.

are properly set. Without going into details of the mechanical behaviour of such differentials (see [18]), the maximum allowed torque difference  $\Delta T_{w,i,\max}$  between the two wheels is function of the input torque and depends on the preload and on the blockage ratio  $r_b$  of the differential. This ratio gives the maximum amount of torque difference with respect to the input torque, in drive and coast modes, as shown in Figure 3.13<sup>1</sup>.

The maximum allowed torque difference is actually transmitted when the differential is in slipping conditions, whereas just an amount of it is transmitted when the differential is locked. As for the clutch block, a friction function was employed to model these two conditions keeping a single model block architecture with no switches. The friction function  $f_f(\omega_{w,i2} - \omega_{w,i1})$  has the same shape of those shown in Figure 3.10, but depends on the difference of the angular velocities of the two wheels (of the generic axle  $i$ , with the second index  $j = 1$  for the left wheel and  $j = 2$  for the right wheel), which gives the amount of the differential slip.

The actual difference of the torque between the two wheels  $\Delta T_{w,i}$  can be written as:

$$\Delta T_{w,i} = \Delta T_{w,i,\max}(T_{f,i})f_f(\omega_{w,i2} - \omega_{w,i1}), \quad i = 1, 2. \quad (3.9)$$

<sup>1</sup>It is more common the use of the torque bias ratio (TBR), which indicates how much torque can be transmitted by the loaded wheel with respect to the unloaded one. The TBR is simply obtained as  $\frac{1+r_b}{1-r_b}$ , for both drive and coast modes.

The torques on the single wheels are then obtained as:

$$\begin{aligned} T_{w,i1} &= \frac{T_{f,i}}{2} + \Delta T_{w,i}, & i = 1, 2 \\ T_{w,i2} &= \frac{T_{f,i}}{2} - \Delta T_{w,i}, & i = 1, 2. \end{aligned} \quad (3.10)$$

It is worth noting that if the differential function  $\Delta T_{w,i,\max}(T_{f,i})$ , shown in Figure 3.13, is null (setting the preload and the blockage ratios to 0), the model reproduces the behaviour of a classic open differential, being the input torque equally split between the two wheels.

Finally, the transmission block computes the angular velocity  $\omega_p$  of the primary shaft as function of the wheel velocities, the final ratios, the current gear ratio and the parameter  $t$ .

$$\omega_p = \tau_g \left( \frac{\omega_{w,11} + \omega_{w,12}}{2} \tau_{f,1} t + \frac{\omega_{w,21} + \omega_{w,22}}{2} \tau_{f,2} (t - 1) \right). \quad (3.11)$$

### 3.3.4 Clutch and gear control

A clutch and gear control logic is needed, being the driving simulator with automatic transmission. To this aim, simple logic blocks were developed to carry out the basic functions of an automatic transmission. Although this part is very simple, it was considered sufficient for the current driving simulator aims. As other blocks, it can be easily developed implementing more complex functions.

The clutch logic controls the  $c$  signal of the clutch position as function of the engine speed. When  $\omega_e$  is below a threshold value, the clutch is disengaged ( $c = 0$ ). When the engine speed crosses this threshold,  $c$  is linearly incremented as function of  $\omega_e$  until the clutch is engaged ( $c = 1$ ). The engine speed at which the clutch begins to transmit torque and the slope of this linear function are set in the vehicle parameter.

The gear shift logic is a state logic which monitors the engine speed, the clutch position and the current gear. If the engine speed goes over a threshold value set for the up-shift, if the clutch is engaged and if a gear shifting has not been carried out in the last second, the gear output signal is set to the next gear (up-shift). On the other side, if the engine speed goes below the threshold down-shift value and the other conditions are verified, the gear output signal is set to previous gear (down-shift).

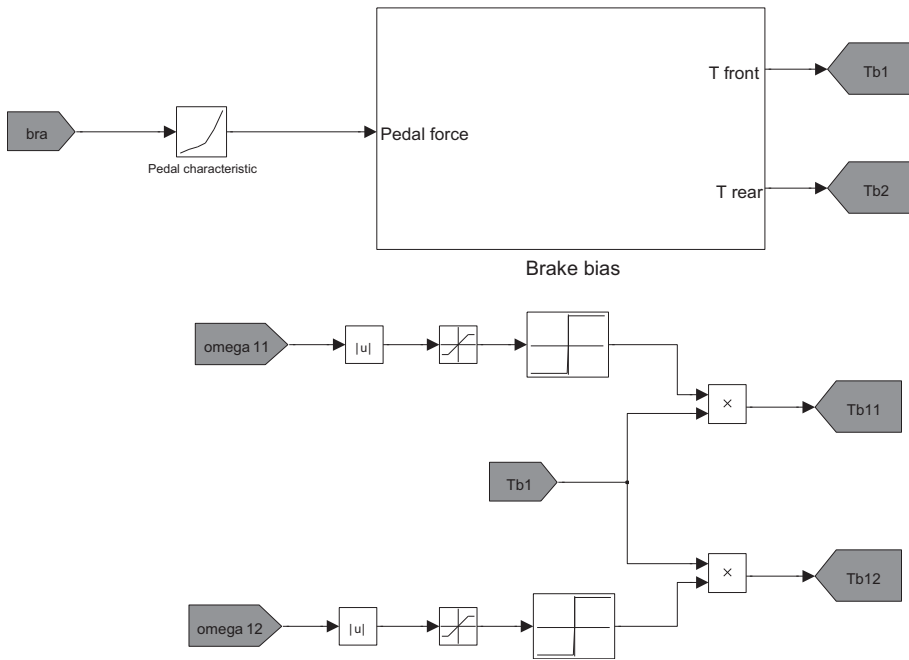


Figure 3.14: Braking system block of the vehicle simulation model in Simulink. The friction functions of just the front wheels is here represented (at the bottom).

### 3.3.5 Braking system

The braking system block, shown in Figure 3.14, computes the braking torques at the wheels (to be sent to the vehicle dynamics block for the wheels rotational equilibrium) from the driver's input of the brake pedal position  $b$ . This signal is firstly converted from a position to a force by implementing the pedal force–displacement characteristic in the model. This is made with a look-up table, visible in the block picture. The force value is normalized to 1.

The pedal force is transformed in braking wheel torque by two constants for the front and the rear brakes  $k_{b,1}$  and  $k_{b,2}$ . These constants take into account all main variables of the braking front and rear systems, i.e. the master cylinders diameter, the callipers cylinders number and diameter and the brake discs diameter. A brake bias parameter  $k_b$  can be additionally set to change the ratios between the front and rear braking torques if a tunable system is available in the modelled vehicle. The

braking torques for the front and the rear wheels are obtained as:

$$T_{b,1} = f_b(b)k_{b,1}k_b \quad (3.12)$$

$$T_{b,2} = f_b(b)k_{b,2}(1 - k_b). \quad (3.13)$$

In order to model also the condition of locked wheel, the previously obtained braking torques have to be multiplied by a friction function  $f_f$ , as already seen for the clutch and the differential. The braking torques at the four wheels can be then obtained with these equations:

$$T_{b,ij} = T_{b,i}f_f(\omega_{w,ij}) \quad i = 1, 2 \text{ and } j = 1, 2. \quad (3.14)$$

In this case, the argument of the function is the wheel angular velocity  $\omega_{w,ij}$ . The threshold value of the function, which defines the limits of the static and dynamic frictions is discussed in Section 3.6.5.

### 3.4 Vehicle dynamics

The vehicle dynamics block carries out the following tasks:

- dynamic equilibrium of the vehicle model bodies (car body and wheels);
- computation of aerodynamic forces and moments;
- computation of the steering torque;
- computation of auxiliary kinematic quantities from the model degrees of freedom.

The vehicle dynamics model is made of five rigid bodies with inertial properties: the car body (or sprung mass) and the four wheels (unsprung masses), which include rolling components (tire, rim, upright, brake disc, etc.) and no-rolling components (upright, brake calliper, etc.). The model solves the equilibrium equations of these bodies, receiving the external forces between tires and road from the tire model, the driving and braking torques from the powertrain and braking system blocks and the aerodynamic forces, which are currently computed inside the vehicle dynamics block. The equilibrium equations are integrated to obtain the state of the dynamic system, i.e. the degrees of freedom and their derivatives.



Independently from the suspension type, each wheel is constrained to the car body leaving just one relative degree of freedom or two degrees of freedom if the wheel can steer. However, the steering kinematics depends on the steering wheel angle (with algebraic relationships), which is, as already mentioned, an input of the driver. This second physical degree of freedom is therefore not considered an actual degree of freedom of the model. Thus, the motion of the wheels can be fully determined using a single variable for the relative suspension motion of each wheel, together with the wheel angular velocity. In synthesis, the model has 14 degrees of freedom, which are:

- 6 d.o.f. for the car body position and orientation in the global coordinate system;
- 4 d.o.f. for the relative positions of the wheels with respect of the car body (i.e. suspension travels);
- 4 d.o.f. for the rotational motion of the wheels.

More complex vehicle dynamics models are made of more bodies, such as the suspension control arms, thus having more degree of freedoms, and are of course more accurate in describing the vehicle dynamics. However, the required amount of modelling and computational effort is often too much if compared to the little increase in accuracy with respect to a 14 d.o.f vehicle model. For the aims of the driving simulator application, the introduced model was therefore considered suitable.

At the beginning, the vehicle dynamics model was taken from the literature [17] and, in a second phase, it was developed in a parallel work carried out in cooperation with the Formula SAE team of the University of Pisa [53]. Both models are made of 4 bodies and have the 14 degrees of freedom just described. The former have a fixed architecture with a specific suspension model which limits the possibilities of simulating different vehicles. On the other side, the internally-developed vehicle dynamics model was built without a specific suspension model, whose kinematic characteristics are given as look-up tables from the suspension block. This allows to simulate vehicles with different suspension architectures just changing the model parameters, as it is described in Section 3.5.

In the following, the vehicle dynamics model is just briefly described, being not directly developed in this work. For further details, the cited reference [53] should be considered.

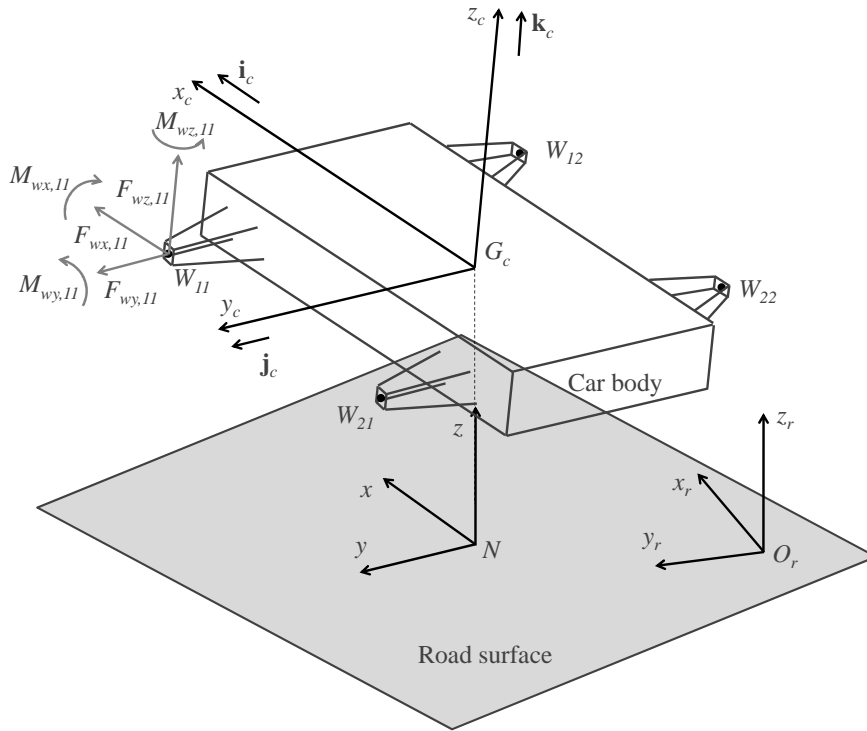


Figure 3.15: Car body model with forces and moments coming from a wheel.

In order to describe the car body motion, three coordinate system were used (see Figure 3.15): an absolute system fixed to the road with its  $z_r$  axis perpendicular to the road surface (supposed flat), a system fixed to the car body with its origin in the sprung mass centre of mass  $G_c$ , with the axes oriented as in the picture (typical conventions in vehicle dynamics) and an auxiliary system. This last coordinate system has its origin in the point  $N$ , the vertical projection of  $G_c$  on the road surface. Its axes are defined as the projection of the  $x_c$  and  $y_c$  axes on the road, being its  $z$  axis perpendicular to the road. This auxiliary system is rotated with respect to the absolute coordinate system of the yaw angle  $\psi$  (around  $z_r$ ).

The motion of the car body is determined using the longitudinal and lateral velocity ( $u$  and  $v$ ) of the point  $N$  (in the auxiliary coordinate

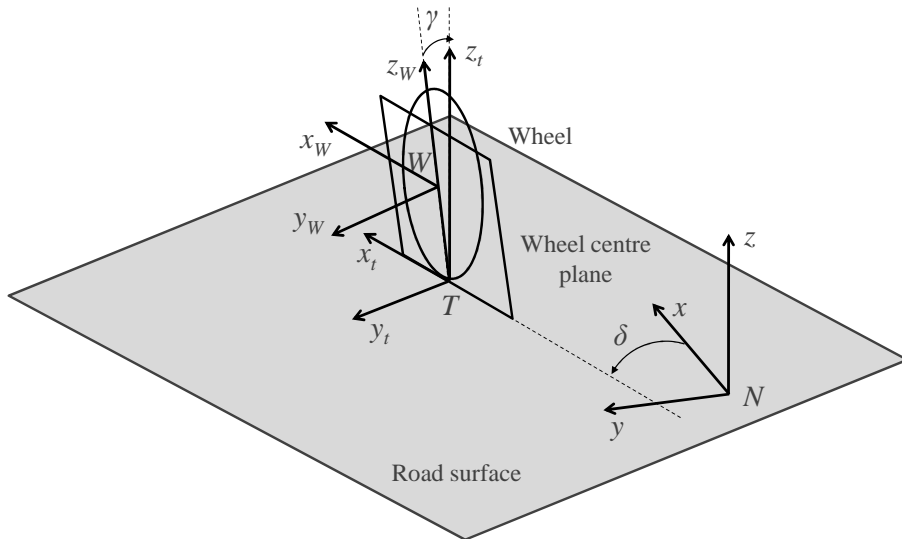


Figure 3.16: Wheel and tire local coordinate systems and wheel angles (indices  $i$  and  $j$  are suppressed for clarity).

system) and the vertical distance  $h$  of  $G_c$  from  $N$ . The orientation is defined, as usually in vehicle dynamics, with three consecutive planar rotations which transform the absolute coordinate system, aligning it with the car body coordinate system. The three rotations are made around current axes, defining (with this order of rotations): the yaw angle  $\psi$  (around  $z_r$ ), the roll angle  $\phi$  (around  $x$ ) and the pitch angle  $\theta$  (around  $y_c$ ). From the definition of these angles, the angular velocity vector of the car body can be easily obtained.

The forces and moments acting on the car body are given by the suspensions (control arms, springs and dampers), by the aerodynamic actions and the weight. The actions given by the suspensions are computed from the equilibrium of each unsprung mass, obtaining an equivalent force and a moment exchanged with the car body in the current wheel centre position.

In order to carry out the equilibrium of the wheels, the wheel kinematics has to be fully described. As previously pointed out, the total six degrees of freedom of each wheel can be reduced to just one degree of freedom by implementing the congruence relationships of the suspension (see Section 3.5). Being the relative motion of the wheel with respect to

the car body mainly vertical, the choice of the quantity describing this single degree of freedom was made on the vertical position  $z_{W,ij}$  of the wheel centre in the car body coordinate system. The difference of the current value of  $z_{W,ij}$  from the initial one represents the suspension travel measured at wheel centre. In addition to this degree of freedom, the wheel rotates around its axis, with its angular velocity  $\omega_{w,ij}$ . The motion of the front wheels due to steering is fully dependent on the input of the steering wheel angle and it is obtained by the congruence relationships of the suspensions.

The wheel has its inertial properties defined in its local coordinate system in the wheel centre  $W_{ij}$ , with axes  $x_{w,ij}$ ,  $y_{w,ij}$  and  $z_{w,ij}$ . The wheel axis is considered coincident with  $y_{w,ij}$ . The orientation of this local system also defines the wheel angles with respect to the car body, which are used to compute the components of the interaction forces and moments. The wheel local system (Figure 3.16) is once again defined with three planar rotations around current axes from the car body coordinate systems, which define: the wheel steering angle (or toe angle)  $\delta_{c,ij}$  (around  $z_c$ ), the camber angle  $\gamma_{c,ij}$  (around current  $x$ ) and the spin angle  $\chi_{c,ij}$  (around  $y_{w,ij}$ , without taking into account the wheel rotation). An auxiliary (tire) coordinate system on the tire–road contact point  $T_{ij}$  is used to obtain the tire forces, as conventionally done in vehicle dynamics [22]. This system has its  $z_{t,ij}$  axis perpendicular to the road surface and the  $x_{t,ij}$  axis on the intersection between the middle plane of the wheel with the road plane.

The tire forces are obtained from the tire model (Section 3.6) in this coordinate system and are used to compute the equilibrium of the wheel together with the suspension elastic and damping forces and the driving or braking torques, finally obtaining the actions on the car body.

The complete system of equations of the car body and wheels dynamics can then be written in the following form:

$$\mathbf{A}(\mathbf{x})\dot{\mathbf{x}} = \mathbf{b}(\mathbf{x}), \quad (3.15)$$

where the vector  $x$  of the unknowns is made of the velocities associated to the 14 degrees of freedom of the model:

$$\mathbf{x} = \left[ u \ v \ \dot{h} \ \dot{\psi} \ \dot{\phi} \ \dot{\theta} \ \omega_{w,11} \ \omega_{w,12} \ \omega_{w,21} \ \omega_{w,22} \ \dot{z}_{W,11} \ \dot{z}_{W,12} \ \dot{z}_{W,21} \ \dot{z}_{W,22} \right]^T. \quad (3.16)$$

The matrix  $\mathbf{A}(\mathbf{x})$  and the vector  $\mathbf{b}(\mathbf{x})$  are not constant and have to be computed at each step time of the solution, which is given by:

$$\mathbf{x} = \int \mathbf{A}^{-1}(\mathbf{x})\mathbf{b}(\mathbf{x})dt, \quad (3.17)$$

Positions and angles, such as the roll, pitch and yaw angles are obtained with a second step of integration.

The vehicle dynamics block computes also other quantities, such as the longitudinal and the lateral accelerations of the point  $N$  and the velocity of the global centre of mass, which are useful for analysing the vehicle behaviour.

The steering torque, whose signal is used as reference for the steering torque feedback, is also computed by this block. To this aim, the principle of virtual work is applied with the forces and moments between the front tires and the road and the torque on the steering wheel. In order to express the motion coordinates of the wheel in all directions as functions of the steering wheel angle, the kinematic suspension relationships (described in the next section) must be known.

Finally, as previously introduced, the vehicle dynamics block computes also the aerodynamic forces, which are, up to now, simply obtained with the classic quadratic equations from the vehicle speed and the drag and lift coefficients. As future development of the vehicle model, a specific aerodynamics block could be made with a more detailed aerodynamic model.

## 3.5 Suspensions

The vehicle suspensions are modelled with a specific block, in which the kinematic behaviour together with the elastic and the damping characteristics are reproduced. These three aspects are mathematically represented with algebraic functions, which are included in the vehicle simulation model as look-up tables. As already pointed out, this means that several types of suspension can be employed in the model without modifying its block architecture.

### 3.5.1 Suspensions kinematics

In this work, the suspension kinematics models of the double wishbone architecture and the MacPherson strut were developed. In both cases,

the objective of the suspension model is to obtain the relative position and orientation of the wheel with respect to the car body, varying the relative vertical position (unsprung mass degree of freedom) and the steering wheel angle  $\delta_s$  (just for the front wheels). The following algebraic functions have to be obtained:

$$\begin{aligned}
 x_W &= x_W(\Delta z_W, \delta_s) \\
 y_W &= y_W(\Delta z_W, \delta_s) \\
 \delta &= \delta(\Delta z_W, \delta_s) \\
 \gamma &= \gamma(\Delta z_W, \delta_s) \\
 \chi &= \chi(\Delta z_W, \delta_s),
 \end{aligned}
 \tag{3.18}$$

where the wheel indices  $i$  and  $j$  are suppressed for clarity as well as the index  $c$  for the angles, which are all relative to the car body. The function argument  $\Delta z_W$  is the suspension travel measured at wheel centre, i.e. the difference of the current  $z_W$  from the initial position at static load.

In order to solve the equilibrium equations, the vehicle dynamics block needs also the partial derivatives of the previous functions. In details, these are:

$$\frac{\partial x_W}{\partial z_W}, \frac{\partial x_W}{\partial \delta_s}, \frac{\partial y_W}{\partial z_W}, \frac{\partial y_W}{\partial \delta_s}, \frac{\partial \delta}{\partial z_W}, \frac{\partial \delta}{\partial \delta_s}, \frac{\partial \gamma}{\partial z_W}, \frac{\partial \gamma}{\partial \delta_s}, \frac{\partial \chi}{\partial z_W}, \frac{\partial \chi}{\partial \delta_s},$$

where, once again, the terms with  $\delta_s$  are not present for the rear wheels.

The functions in eq. (3.18) and 3.5.1 are computed by a Matlab script file, which runs in the initialization phase (see Section 3.8) and generates all the function look-up tables. This computation starts from the suspension mounting points, defined in the reference condition of static load. All suspension mounting points positions are taken from a point  $O$  on the car body, whose position is arbitrary, and are expressed in the car body coordinate system.

### Double wishbone

The model of the well known double wishbone suspension is shown in Figure 3.17. In order to analyse the suspension kinematic behaviour, the upper and lower A-arms were both considered as made of two links with coincident spherical joints on the wheel side (points  $C$  and  $F$ ). Thus, the double wishbone is treated as a particular case of a generic multi-link suspension with five links. The following congruence equations can

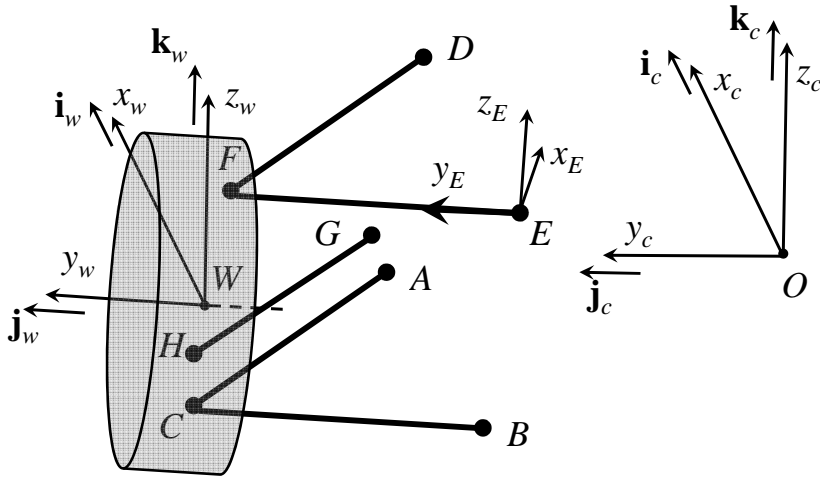


Figure 3.17: Double wishbone suspension model. The spherical joints are represented by big black points. The link local coordinate system is shown just for the link  $EF$ .

therefore be written (each equation is made of three scalar equations):

$$\begin{aligned}
 \mathbf{OA} + \mathbf{AC} &= \mathbf{OW} + \mathbf{WC} \\
 \mathbf{OB} + \mathbf{BC} &= \mathbf{OW} + \mathbf{WC} \\
 \mathbf{OD} + \mathbf{DF} &= \mathbf{OW} + \mathbf{WF} \\
 \mathbf{OE} + \mathbf{EF} &= \mathbf{OW} + \mathbf{WF} \\
 \mathbf{OG} + \mathbf{GH} &= \mathbf{OW} + \mathbf{WH}.
 \end{aligned} \tag{3.19}$$

It was chosen to write all vectors of these equations in the car body coordinate system, introducing rotational matrices for all other local coordinate systems needed. The vectors  $\mathbf{OA}$ ,  $\mathbf{OB}$ ,  $\mathbf{OD}$ ,  $\mathbf{OE}$  and  $\mathbf{OG}$  are fixed and already in the car body system.  $\mathbf{OW}$  is also in the same coordinate system and can be written as  $[x_W \ y_W \ z_W]^T$ , introducing the coordinates of the wheel center position. The vectors  $\mathbf{WC}$ ,  $\mathbf{WF}$  and  $\mathbf{WH}$  have fixed components in the wheel coordinate system, which, as already written in the previous section, has the origin in  $W$  and unit vectors  $\mathbf{i}_W$ ,  $\mathbf{j}_W$  and  $\mathbf{k}_W$  along its axes (see picture). This system is defined from the car body system with the three planar rotations (sequence 312),

which define the wheel angles (see Section 3.4)  $\delta$ ,  $\gamma$  and  $\chi$ . The rotational matrix, which transforms the components in the wheel coordinate systems in components in the car body system, is:

$$\mathbf{R}_w(\delta, \gamma, \chi) = \begin{bmatrix} c\chi c\delta - s\chi s\gamma s\delta & -c\gamma s\delta & c\delta s\chi + c\chi s\gamma s\delta \\ c\delta s\chi s\gamma + c\chi s\delta & c\gamma c\delta & -c\chi c\delta s\gamma + s\chi s\delta \\ -c\gamma s\chi & s\gamma & c\chi c\gamma \end{bmatrix}, \quad (3.20)$$

where the sin and cos functions are shortened in  $s$  and  $c$ .

In order to write **AC**, **BC**, **DF**, **EF** and **GH**, local coordinate systems for each link are considered, as shown in the picture just for the link  $EF$ . The origin of these systems is on the points on the car body side. The orientation of them are defined, as the wheel coordinate system, from the car body system with the same 312 order of rotations so that the local  $y$  axis (e.g.  $y_E$  in the picture) corresponds to the link axis. The last rotation around this axis is actually not required because it does not affect the position of the points, which are, of course, lying on the link axis. Considering as example the link  $EF$ , the rotation matrix is therefore the following:

$$\mathbf{R}_E(\delta_E, \gamma_E) = \begin{bmatrix} c\delta_E & -c\gamma_E s\delta_E & s\gamma_E s\delta_E \\ s\delta_E & c\gamma_E c\delta_E & -c\delta_E s\gamma_E \\ 0 & s\gamma_E & c\gamma_E \end{bmatrix}. \quad (3.21)$$

Equations 3.19 can now be written as:

$$\begin{aligned} \mathbf{OA} + \mathbf{R}_A(\delta_A, \gamma_A) [0 \ l_{AC} \ 0]^T &= [x_W \ y_W \ z_W]^T + \mathbf{R}_w(\delta, \gamma, \chi) \mathbf{WC}^w \\ \mathbf{OB} + \mathbf{R}_B(\delta_B, \gamma_B) [0 \ l_{BC} \ 0]^T &= [x_W \ y_W \ z_W]^T + \mathbf{R}_w(\delta, \gamma, \chi) \mathbf{WC}^w \\ \mathbf{OD} + \mathbf{R}_D(\delta_D, \gamma_D) [0 \ l_{DF} \ 0]^T &= [x_W \ y_W \ z_W]^T + \mathbf{R}_w(\delta, \gamma, \chi) \mathbf{WF}^w \\ \mathbf{OE} + \mathbf{R}_E(\delta_E, \gamma_E) [0 \ l_{EF} \ 0]^T &= [x_W \ y_W \ z_W]^T + \mathbf{R}_w(\delta, \gamma, \chi) \mathbf{WF}^w \\ \mathbf{OG} + \mathbf{R}_G(\delta_G, \gamma_G) [0 \ l_{GH} \ 0]^T &= [x_W \ y_W \ z_W]^T + \mathbf{R}_w(\delta, \gamma, \chi) \mathbf{WH}^w, \end{aligned} \quad (3.22)$$

where  $l$  are the lengths of the links and  $\mathbf{WC}^w$ ,  $\mathbf{WF}^w$  and  $\mathbf{WH}^w$  are expressed in the wheel local coordinate system. These vectors are constant and computed from the point coordinates in the initial static condition (index 0):

$$\begin{aligned} \mathbf{WC}^w &= \mathbf{R}_w^T(\delta_0, \gamma_0, \chi_0) \mathbf{WC}_0 \\ \mathbf{WF}^w &= \mathbf{R}_w^T(\delta_0, \gamma_0, \chi_0) \mathbf{WF}_0 \\ \mathbf{WH}^w &= \mathbf{R}_w^T(\delta_0, \gamma_0, \chi_0) \mathbf{WH}_0. \end{aligned} \quad (3.23)$$



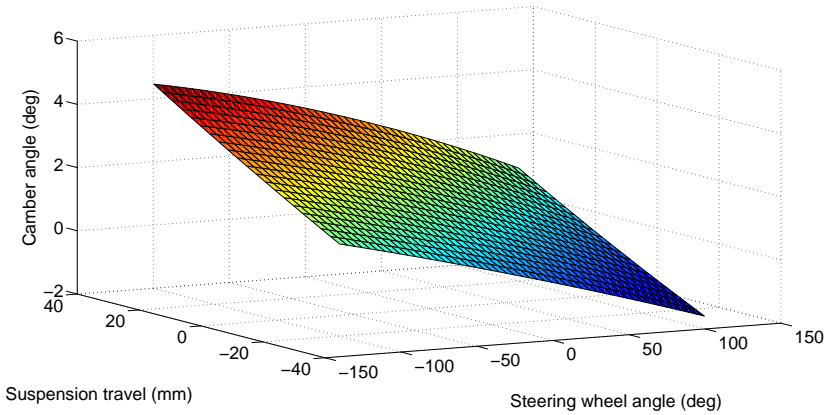


Figure 3.18: Graphical representation of the camber angle look-up table of the ET3 Formula SAE car front suspension.

Equations 3.22 are 15 algebraic non-linear scalar equations, with the following unknowns:

$$z_W, y_W, \delta, \gamma, \chi, \delta_A, \gamma_A, \delta_B, \gamma_B, \delta_D, \gamma_D, \delta_E, \gamma_E, \delta_G, \gamma_G.$$

Their solution represents the functions in eq. (3.18), considering:

$$\begin{aligned} z_W &= z_{W,0} + \Delta z_W \\ OG_y &= OG_{y,0} + \tau_s \delta_s, \end{aligned} \quad (3.24)$$

where  $\tau_s$  is the steering ratio expressed as the amount of lateral (along  $y_c$ ) travel of the steering rack (point  $G$ ) with respect to the steering wheel angle  $\delta_s$  (for the front wheels).

The suspension equations are solved in the initialization phase, before the simulation begins, varying the inputs  $\Delta z_W$  and  $\delta_s$  in a specific range with discrete values. The solutions are imported in the vehicle simulation model (in the suspension block) as look-up tables. An example is shown in Figure 3.18.

### MacPherson

The implementation of the MacPherson suspension follows most of what already described for the double wishbone. The architecture of the suspension is shown in Figure 3.19. The congruence equations for the

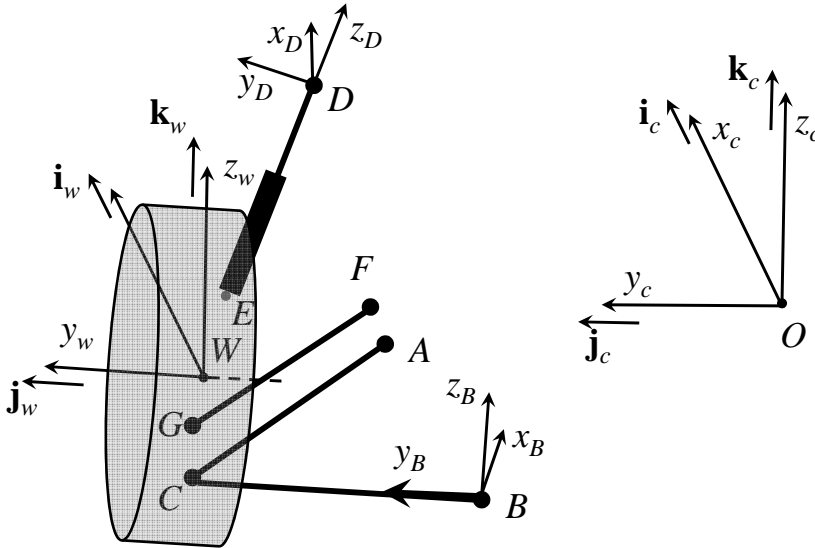


Figure 3.19: MacPherson suspension model. The spherical joints are represented by big black points; the translational joint is also clearly represented. The link local coordinate system is shown just for the link  $BC$ . The local coordinate system of the damper is also represented (which is defined in  $D$ ).

lower arm and the steering rod are the same of the double wishbone. The damper, which in MacPherson suspension is part of the mechanism, represents a translational joint between the wheel and the damper rod, which is connected to the car body with a spherical joint.

In order to write the congruence equations of the translational joint, a local coordinate system in  $D$  was introduced (see picture), which has its  $z_D$  axis along  $\mathbf{ED}$  and the other axes arbitrarily defined in the initial static condition. The orientation of the system is defined as the wheel coordinate system, using the index  $D$  for its angles.

The congruence equations of the translational joint can now be written, in scalar components, as two equations for the in-line primitive joint, i.e.  $\mathbf{ED}$  must be along  $z_D$ , and three equations for the constant relative orientation of the wheel and the damper rod. The complete system of

the suspension equations is:

$$\begin{aligned}
\mathbf{OA} + \mathbf{AC} &= \mathbf{OW} + \mathbf{WC} \\
\mathbf{OB} + \mathbf{BC} &= \mathbf{OW} + \mathbf{WC} \\
\mathbf{i}_D \cdot (\mathbf{OW} + \mathbf{WE} - \mathbf{OD}) &= 0 \\
\mathbf{j}_D \cdot (\mathbf{OW} + \mathbf{WE} - \mathbf{OD}) &= 0 \\
\mathbf{i}_w \cdot \mathbf{i}_D &= c_x \\
\mathbf{j}_w \cdot \mathbf{j}_D &= c_y \\
\mathbf{k}_w \cdot \mathbf{k}_D &= c_z \\
\mathbf{OF} + \mathbf{FG} &= \mathbf{OW} + \mathbf{WG},
\end{aligned} \tag{3.25}$$

where  $c_x$ ,  $c_y$  and  $c_z$  are obtained from the initial static condition as:

$$\begin{aligned}
c_x &= \mathbf{R}_w(\delta_0, \gamma_0, \chi_0) [1 \ 0 \ 0]^T \cdot \mathbf{R}_D(\delta_{D,0}, \gamma_{D,0}, \chi_{D,0}) [1 \ 0 \ 0]^T \\
c_x &= \mathbf{R}_w(\delta_0, \gamma_0, \chi_0) [0 \ 1 \ 0]^T \cdot \mathbf{R}_D(\delta_{D,0}, \gamma_{D,0}, \chi_{D,0}) [0 \ 1 \ 0]^T \\
c_x &= \mathbf{R}_w(\delta_0, \gamma_0, \chi_0) [0 \ 0 \ 1]^T \cdot \mathbf{R}_D(\delta_{D,0}, \gamma_{D,0}, \chi_{D,0}) [0 \ 0 \ 1]^T.
\end{aligned} \tag{3.26}$$

As for the double wishbone case, equations 3.25 can be written introducing the rotational matrices and the vectors of the wheel and link points expressed in local coordinate systems, so that they remain constant. The equations are:

$$\begin{aligned}
\mathbf{OA} + \mathbf{R}_A(\delta_A, \gamma_A) [0 \ l_{AC} \ 0]^T &= [x_W \ y_W \ z_W]^T + \mathbf{R}_w(\delta, \gamma, \chi) \mathbf{WC}^w \\
\mathbf{OB} + \mathbf{R}_B(\delta_B, \gamma_B) [0 \ l_{BC} \ 0]^T &= [x_W \ y_W \ z_W]^T + \mathbf{R}_w(\delta, \gamma, \chi) \mathbf{WC}^w \\
\mathbf{R}_D(\delta_D, \gamma_D, \chi_D) [1 \ 0 \ 0]^T \cdot (\mathbf{OW} + \mathbf{R}_w(\delta, \gamma, \chi) \mathbf{WE}^w - \mathbf{OD}) &= 0 \\
\mathbf{R}_D(\delta_D, \gamma_D, \chi_D) [0 \ 1 \ 0]^T \cdot (\mathbf{OW} + \mathbf{R}_w(\delta, \gamma, \chi) \mathbf{WE}^w - \mathbf{OD}) &= 0 \\
\mathbf{R}_w(\delta, \gamma, \chi) [1 \ 0 \ 0]^T \cdot \mathbf{R}_D(\delta_D, \gamma_D, \chi_D) [1 \ 0 \ 0]^T &= c_x \\
\mathbf{R}_w(\delta, \gamma, \chi) [0 \ 1 \ 0]^T \cdot \mathbf{R}_D(\delta_D, \gamma_D, \chi_D) [0 \ 1 \ 0]^T &= c_y \\
\mathbf{R}_w(\delta, \gamma, \chi) [0 \ 0 \ 1]^T \cdot \mathbf{R}_D(\delta_D, \gamma_D, \chi_D) [0 \ 0 \ 1]^T &= c_z \\
\mathbf{OF} + \mathbf{R}_F(\delta_F, \gamma_F) [0 \ l_{FG} \ 0]^T &= [x_W \ y_W \ z_W]^T + \mathbf{R}_w(\delta, \gamma, \chi) \mathbf{WG}^w.
\end{aligned} \tag{3.27}$$

where  $l$  are the lengths of the links and  $\mathbf{WC}^w$ ,  $\mathbf{WE}^w$  and  $\mathbf{WG}^w$  are computed from the point coordinates in the initial static condition as follows:

$$\begin{aligned}
\mathbf{WC}^w &= \mathbf{R}_w^T(\delta_0, \gamma_0, \chi_0) \mathbf{WC}_0 \\
\mathbf{WE}^w &= \mathbf{R}_w^T(\delta_0, \gamma_0, \chi_0) \mathbf{WE}_0 \\
\mathbf{WG}^w &= \mathbf{R}_w^T(\delta_0, \gamma_0, \chi_0) \mathbf{WG}_0.
\end{aligned} \tag{3.28}$$

In this case, equations 3.27 are 14 scalar equations, with the following 14 unknowns:

$$x_W, y_W, \delta, \gamma, \chi, \delta_A, \gamma_A, \delta_B, \gamma_B, \delta_D, \gamma_D, \chi_D, \delta_F, \gamma_F.$$

As in the previous case, the solution of the congruence equations gives the functions in eq. (3.18), considering the inputs  $\Delta z_W$  and  $\delta_s$  as in eq. (3.24), substituting the point  $G$  with the actual steering rack end in the MacPherson suspension (point  $F$ ).

### 3.5.2 Suspensions stiffness and damping

In order to solve the wheel equilibrium, the vehicle dynamics block needs the elastic and damping forces of the suspensions. These are simply obtained as functions of the suspension travel and its derivative. These functions are once again implemented in the vehicle model with look-up tables.

The elastic force due to the suspension spring is defined as follows:

$$F_{e,ij} = F_{e,i}(\Delta z_{w,ij}). \quad (3.29)$$

This function, which represents the elastic characteristic measured at the wheel centre, must be supplied in the vehicle parameters file.

The vehicle could be endowed with anti-roll bars, which represent an additional stiffness force  $F_{a,i}$  depending on the suspension travels of both wheels on a single axle. The following equation is used to model the anti-roll bars, with a constant stiffness  $k_{a,i}$ :

$$F_{a,i} = k_{a,i}(z_{w,i1} - z_{w,i2}). \quad (3.30)$$

Finally, the suspension interacts with the car body also by a damper. The damping force  $F_{d,ij}$  of each wheel is written as a function of the suspension travel velocity, once again considering all quantities at the wheel centre:

$$F_{d,ij} = F_{d,i}(\dot{z}_{w,ij}). \quad (3.31)$$

## 3.6 Tire model

The tire model is shown in Figure 3.20, where the coordinate systems of the wheel and of the tire (on the road contact point) are represented.

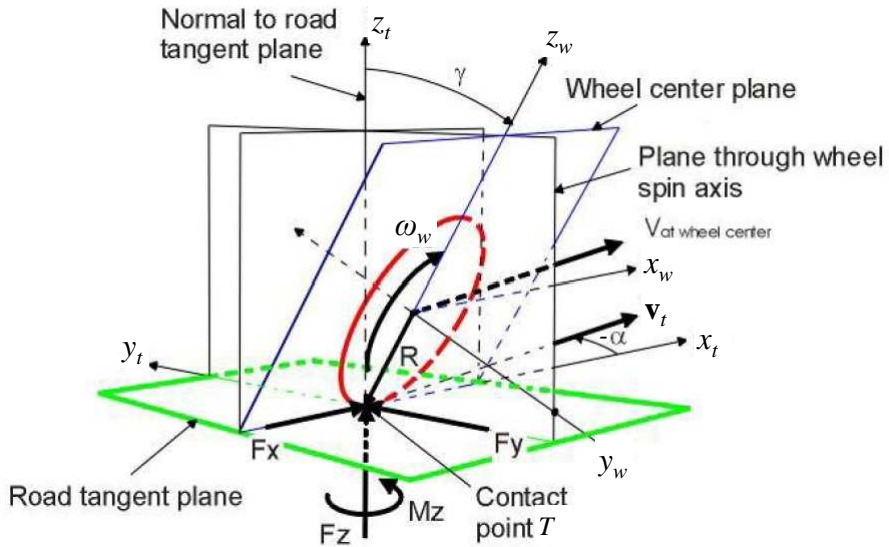


Figure 3.20: Tire model with coordinate systems and basic quantities.

The tire is considered a body with no mass (which is included in the wheel mass), with a radial spring-damper. The velocity of contact point is also represented, which is given by the vehicle dynamics block from the wheel and the car body equilibrium. The longitudinal and lateral components in the tire coordinate systems will be further called  $u_t$  and  $v_t$ . The tire kinematic conditions are fully determined knowing also the camber angle  $\gamma$  (with respect to the road, as in the picture), the wheel angular velocity  $\omega_w$  and the variation of the wheel centre height from the road surface <sup>2</sup>  $h_t$ . The indices  $i$  and  $j$  are once again suppressed for clarity. All these quantities are given by the vehicle dynamics block.

The objective of the tire model is to compute the forces and moments received from the road, which depend on its kinematic conditions, as it is described in the following sections.

<sup>2</sup>This is supposed vertical with respect to the road surface because the camber angle has a small value, so that  $\cos \gamma \simeq 1$ .

### 3.6.1 Vertical load

The tire vertical load is obtained from the vertical equilibrium, as function of the tire deflection ( $-h_t$ ) and its velocity:

$$F_z = -k_t h_t - c_t \dot{h}_t. \quad (3.32)$$

A constant tire radial stiffness  $k_t$  and a constant radial damping  $c_t$  are employed; their values are determined in the tire parameters file.

The vertical load represents an input for the computation of the other forces and components, as shown in Section 3.6.4.

### 3.6.2 Rolling radius and deformed radius

The tire rolling radius  $R_r$  is used to compute the longitudinal rolling velocity  $\omega_w R_r$ . Its value is very close to the unloaded tire radius  $R_0$ , and it is obtained following this empirical relationship [47]:

$$R_0 - \frac{F_{z,0}}{k_t} \left( D_r \arctan\left(-B_r \frac{h_t}{F_{z,0} k_t}\right) - F_r \frac{h_t}{F_{z,0} k_t} \right), \quad (3.33)$$

where  $B_r$ ,  $D_r$  and  $F_r$  are tire coefficients and  $F_{z,0}$  is the reference tire vertical load at which the coefficients are evaluated (with an experimental test).

The tire deformed radius  $R$ , i.e. the distance of the wheel centre from the road surface, is simply obtained as:

$$R = R_0 + h_t. \quad (3.34)$$

### 3.6.3 Tire slips

In order to generate forces from the interaction with the road, the tire must be subjected to slips in longitudinal and lateral directions. The classic relationships of the so called tire practical slips are [22, 51]:

$$\begin{aligned} s_x &= \frac{\omega_w R_r - u_t}{u_t} \\ s_y &= -\frac{v_t}{u_t}, \end{aligned} \quad (3.35)$$

where  $s_x$  is the longitudinal slip and  $s_y$  is the lateral slip. It is also common the use of the tire slip angle (instead of the lateral slip), which is defined as:

$$\alpha = \tan s_y = \tan -\frac{v_t}{u_t}. \quad (3.36)$$

These relationships are widely used for vehicle dynamics simulations but are not suitable for driving simulator applications because of two main limits. One problem is that, in such applications, the vehicle should be able to stop and start again. This is not possible using eq. (3.35), where the longitudinal speed  $u_t$  at the denominator would lead to infinite slips and hence numerical problems. The second issue regards reverse drive. Even if it is not simulated in the driving simulator of this work, the relationships of the slips should consider also this case because a negative longitudinal speed could exist for numerical reasons (when the vehicle is stopped) or in extreme manoeuvres (e.g. when the vehicle slips round). With eq. (3.35) the slips are not correctly computed if  $u_t < 0$ .

In [6], these problems are overcome implementing the tire relaxation lengths  $l_{r,x}$  and  $l_{r,y}$  in the slip equations (and not in the force equations as usually done in vehicle dynamics) and using appropriate absolute values and sign functions:

$$\begin{aligned} \frac{l_{r,x}}{|u_t|} \dot{s}_x + s_x &= \frac{\omega_w R_r \text{sign}(u_t) - |u_t|}{|u_t|} \\ \frac{l_{r,y}}{|u_t|} \dot{s}_y + s_y &= -\frac{v_t}{|u_t|}. \end{aligned} \quad (3.37)$$

In simulations,  $\dot{s}_x$  and  $\dot{s}_y$  should be obtained (and then integrated), thus eliminating  $u_t$  from the denominators of the fractions:

$$\begin{aligned} \dot{s}_x &= -\frac{|u_t|}{l_{r,x}} s_x + \frac{\omega_w R_r \text{sign}(u_t) - |u_t|}{l_{r,x}} \\ \dot{s}_y &= -\frac{|u_t|}{l_{r,y}} s_y - \frac{v_t}{l_{r,y}}. \end{aligned} \quad (3.38)$$

As shown in [6], the sign function and the absolute value in the nominator of the steady-state longitudinal slip (second term at the right side of the equation) allow to correctly compute the slip in forward and reverse drive. Then, in order to have the correct signs of the forces, the tire longitudinal force  $F_x$  must be multiplied by the sign function of  $u_t$ .

The first term at the right side of both equations 3.38 represents the speed of the exponential law (which tends to the steady-state term, when  $\dot{s} = 0$ ) and hence a sort of damping. This depends on  $u_t$ , being quite zero at very low speed. For this reason, in [6] an additional damping term is added when the vehicle speed is close to zero to avoid system low damping.

However, as shown in [6], with this slip formulation, the convergence to the zero solution when the vehicle stops is not guaranteed. In general, slips, and hence forces, other than zero can remain even if the vehicle is in equilibrium at zero speed. This occurs because, when the vehicle is stopped, the exponential speed of the slip equations becomes zero and then, being the steady-state slip also zero, equations 3.38 lead to  $\dot{s} = 0$ .

In this work, this issue was solved starting from the result in [6]. At the same time, as eq. (3.38), the modifications introduced in the slip equations allow to solve also the initial problems of zero speed and reverse drive.

In order to avoid zero slips and forces when the vehicle is stopped, the longitudinal speed terms  $u_t$  in the denominators of eq. (3.37) were limited to a minimum value, with generally two different thresholds (marked by different accents) for the steady-state term (right side of the equations) and the exponential speed term (left side). In general, these two values can also be different between the longitudinal and lateral slip equations, even if they are further marked with the same accent for clarity. The slip equations, with the lateral one written using the slip angle, become:

$$\begin{aligned} \frac{l_{r,x}}{|\hat{u}_t|} \dot{s}_x + s_x &= \frac{\omega_w R_r - u_t}{|\bar{u}_t|} \\ \frac{l_{r,y}}{|\hat{u}_t|} \dot{\alpha} + \alpha &= -\tan \frac{v_t}{|\bar{u}_t|}. \end{aligned} \quad (3.39)$$

In the simulation model, as already written for eq. (3.37),  $\dot{s}_x$  and  $\dot{\alpha}$  should be obtained to be integrated, thus implementing the slip equations as:

$$\begin{aligned} \dot{s}_x &= -\frac{|\hat{u}_t|}{l_{r,x}} s_x + \frac{\omega_w R_r - u_t}{|\bar{u}_t|} \frac{|\hat{u}_t|}{l_{r,x}} \\ \dot{\alpha} &= -\frac{|\hat{u}_t|}{l_{r,y}} \alpha - \frac{v_t}{|\bar{u}_t|} \frac{|\hat{u}_t|}{l_{r,y}}. \end{aligned} \quad (3.40)$$

If the limits of  $|\bar{u}_t|$  and  $|\hat{u}_t|$  are the same, these terms can be simplified in the last part of both equations 3.40. In this case the steady-state terms of the equations become very similar to those of eq. (3.38) (other differences related to the sign function are discussed in the following). However, the exponential coefficient (coefficient of  $s$  in the first term) is now limited to a minimum because of the absolute value, avoiding solutions, and then equilibriums, with  $s \neq 0$  when the vehicle is stopped (i.e. when angular and linear velocities are both null).



The limit of  $|\bar{u}_t|$  is set to avoid the denominator from being zero at zero speed. In order to correctly compute the slips, this value has to be close to zero and was set to 0.1 m/s. The limit of  $|\hat{u}_t|$  for the longitudinal and lateral equations can be set to have an acceptable damping of the system at very low speeds. As it is shown in the following, the damping due to the thresholds on  $|\hat{u}_t|$  can not avoid vibrations on the tire slip and forces at low speeds. An additional damping term (as that in [6]) was not implemented in the present work for simplicity and because such vibrations occur just at very low speed, without influencing the car body dynamics and thus the driver's feelings.

The problem of the vehicle behaviour at speed close to zero was investigated in more detail and it is presented in Section 3.6.5, describing also how the threshold value of  $|\hat{u}_t|$  was set.

It should be noted that the aim of these modifications of the classic slip equations is not to reproduce the actual behaviour of the tire at very low speed. This could be done only implementing tire models with real inertial, radial stiffness and damping properties, which require higher computing efforts but do not change significantly the behaviour at speeds other than very low. For the aims of the driving simulator application, it is important just to have a realistic behaviour of the complete vehicle at low speed (with realistic forces), allowing to stop it and start it again. Simulated drives are then carried out mostly at speeds higher than the limits of these approximations, computing the right slip values.

It is also worth noting that, in order to avoid numerical problems related to the sign function (which is in eq. (3.37)), slip equations 3.39 are written with a different numerator of the longitudinal slip. This leads to a little error in the slip computation in reverse drive, if the longitudinal force-slip characteristic is not symmetric. However, this was not considered a problem, being the error not big and having reverse drive conditions just when the car slips round or as numerical errors when the car is stopped.

### 3.6.4 Tire forces and moments

Once obtained the longitudinal and lateral slips (or slip angle), the tire model computes the forces and moments coming from the interaction with the road. In general, being the vertical load already obtained as described in Section 3.6.1, the following functions (tire constitutive relationships)

must be evaluated:

$$\begin{aligned}
 F_x &= F_x(F_z, \alpha, \gamma, s_x) \\
 F_y &= F_y(F_z, \alpha, \gamma, s_x) \\
 M_x &= M_x(F_z, \alpha, \gamma, s_x) \\
 M_y &= M_y(F_z, \alpha, \gamma, s_x) \\
 M_z &= M_z(F_z, \alpha, \gamma, s_x).
 \end{aligned} \tag{3.41}$$

Depending on the detail of the tire model employed, some of these functions can be not represented and their expressions can be more or less complex. However, even a basic tire model must compute at least the lateral and longitudinal forces, which are both modelled with the well known *Magic Formula* by Pacejka [51, 22]:

$$F = D \sin \left( C \arctan \left( B \bar{s} - E \left( B \bar{s} - \arctan(B \bar{s}) \right) \right) \right) + O_v, \tag{3.42}$$

where  $F$  is the generic force component,  $\bar{s}$  the corresponding corrected slip (or slip angle), given by  $s + O_h$  and  $B$ ,  $C$ ,  $D$ ,  $E$ ,  $O_v$  and  $O_h$  are coefficients specific for each tire. The slope of this curve  $F(s)$  in the origin is known as slip stiffness (longitudinal or lateral) and is:

$$K = BCD. \tag{3.43}$$

In a basic tire model, the coefficients of the *Magic Formula* can be constant (except  $D$  which depends on the vertical load), whereas they depend on the other tire variables (i.e. the function arguments of eq. (3.41)) in more complex models. In this latter case, several other tire coefficients, which are experimentally evaluated, are introduced for these relationships.

In the present work, the Pacejka 2002 tire model (PAC2002) is employed [47, 51]. This gives the functions of eq. (3.41) using several tire coefficients, which are supplied to the vehicle model with a tire property file. The complete equations of this tire model are presented in the appendix A. They are included in the vehicle simulation model in Simulink in specific Embedded Matlab blocks. As example, in Figure 3.21 the lateral force versus the slip angle of an Avon tire for Formula SAE is shown.

The model is suitable also for combined longitudinal and lateral forces when specific tire coefficients for combined equations are supplied. However, in many cases these coefficients are not available because the specific tests were not carried out. For these cases, the combined behaviour

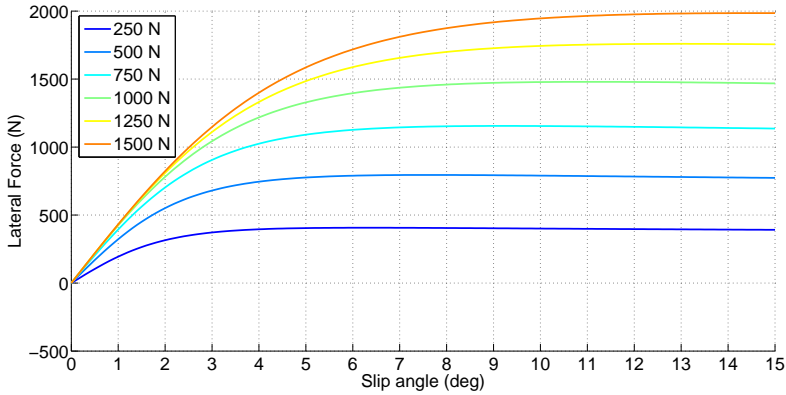


Figure 3.21: Lateral force characteristic with different vertical loads ( $\gamma = 0$  and  $s_x = 0$ ). The tire is an Avon racing tire for Formula SAE.

of the tire was simply modelled considering the maximum grip ellipse, with limits  $D_x$  and  $D_y$  on the two axis. These represent the maximum of the longitudinal and lateral *Magic Formula*, neglecting possible vertical offsets  $O_{v,x}$  and  $O_{v,y}$ . If  $\left(\frac{F_{x,0}}{D_x}\right)^2 + \left(\frac{F_{y,0}}{D_y}\right)^2 > 1$ , where  $F_{x,0}$  and  $F_{y,0}$  are the independently computed forces, the actual longitudinal and lateral forces are obtained as:

$$F_x = \frac{\text{sign}(F_{x,0})}{\sqrt{\left(\frac{1}{D_x}\right)^2 + \left(\frac{F_{y,0}}{F_{x,0}D_y}\right)^2}} \quad (3.44)$$

$$F_y = F_x \frac{F_{y,0}}{F_{x,0}}.$$

An other modification on the original Pacejka tire model regards the rolling resistance moment  $M_y$ . If the specific experimentally obtained coefficients are not available, a rolling resistance must however be computed for a realistic behaviour of the driving simulator. In this case, this is obtained following this equation:

$$M_y = -f_f(\omega_w)F_zR\left(f_r + k_r(R_r\omega_w)^2\right), \quad (3.45)$$

where  $f_r$  is the rolling friction coefficient and  $k_r$  an other tire coefficient. These coefficients can be easily determined using values from the literature.

It is worth noting that a friction function  $f_f(\omega_w)$ , with the same shape of that shown in Figure 3.10 at page 62, was employed. This is necessary to avoid a non-zero moment when the tire is not rolling. The effect of this friction function on the dynamics at very low speed is discussed in the next section.

Friction functions are employed also for the other tire force and moment components if they are not zero when the tire angular and linear velocities are null.

### 3.6.5 Tire model corrections for simulation at very low speed

One of the main problem of vehicle dynamics simulation in driving simulator applications is the vehicle behaviour (and especially the tire behaviour) at very low speed. As already described in Section 3.6.3, the classic tire slips equations are not suitable for these applications and alternative equations were proposed.

It should once more noted that the modifications, which were introduced, and the analyses which follow, were not intended to properly model the tire and the vehicle behaviour at very low speed. The main aim is, in fact, to reproduce acceptable tire and vehicle dynamics which allows to stop and start again the vehicle, giving a realistic (even if not properly correct) model behaviour.

The analyses which follow are focused on the dynamics at very low speed, especially on the model damping. The influence on it of the threshold value on  $\hat{u}_t$  (introduced in Section 3.6.3) and of the friction functions of the rolling resistance and the braking torque were investigated.

In the following, the vehicle behaviour at very low speed is analysed using a linearised simplified model for the longitudinal and lateral dynamics. A single wheel with tire is considered, with the mass of a quarter of the car and the actual inertia of the wheel of the complete model.

#### Longitudinal dynamics

The equations of the simplified model for the longitudinal dynamics analysis take into account the longitudinal tire force, the rolling resistance moment, the braking torque and the drive torque. The equations represent the linear (along  $x$ ) dynamics, the wheel rotational dynamics and the

tire slip dynamics, as follow:

$$\begin{aligned}
 m\dot{u}_t &= F_x \\
 \dot{s}_x &= -\frac{|\hat{u}_t|}{l_{r,x}}s_x + \frac{\omega_w R_r - u_t}{|\bar{u}_t|} \frac{|\hat{u}_t|}{l_{r,x}} \\
 J_w \dot{\omega}_w &= -F_x R + M_y - T_{b,w} + T_w,
 \end{aligned} \tag{3.46}$$

where  $m$  is the mass (a quarter of the car),  $J_w$  is the inertia of the wheel,  $T_{b,w}$  and  $T_w$  are the braking torque and the drive torque at the wheel.

The state of the system is given by  $[\omega_w \ s_x \ u_t]^T$ ; the drive torque represents the input of the system. The equations are then linearised around the zero state, using the following relationships:

$$\begin{aligned}
 F_x &= K_x s_x \\
 M_y &= -f_r m g R p \omega_w \\
 T_{b,w} &= T_b q \omega_w,
 \end{aligned} \tag{3.47}$$

where  $p$  and  $q$  are the slopes of the friction functions (which represent the reciprocal of the limit between static and dynamic friction) and  $T_b$  is the maximum available braking torque (with dynamic friction), called  $T_{b,i}$  in eq. (3.14). The rolling resistance equation is obtained linearising eq. (3.45) with  $\omega_w$  around zero. The equations of the system become:

$$\begin{aligned}
 \dot{u}_t &= \frac{K_x}{m} s_x \\
 \dot{s}_x &= \frac{R_r c_{\hat{u}_t}}{l_{r,x} c_{\bar{u}_t}} \omega_w - \frac{c_{\hat{u}_t}}{l_{r,x}} s_x - \frac{c_{\hat{u}_t}}{l_{r,x} c_{\bar{u}_t}} u_t \\
 \dot{\omega}_w &= -\left( \frac{f_r m g R p}{J_w} + \frac{T_b q}{J_w} \right) \omega_w - \frac{K_x R}{J_w} s_x + T_w,
 \end{aligned} \tag{3.48}$$

where the constants  $c$  represent the different threshold values.

The limit  $c_{\hat{u}_t}$  and the slope  $p$  of the rolling resistance friction function were investigated and set considering the free response of the system with no braking torque, whereas the influence of the slope of the braking torque friction function was analysed considering the free response of the system loaded with the maximum braking torque. The influence of the threshold parameters on the eigenvalues of the system is shown in Figure 3.22 and Figure 3.23, considering a numerical example of a C-segment car. The threshold values were set considering the following objectives:

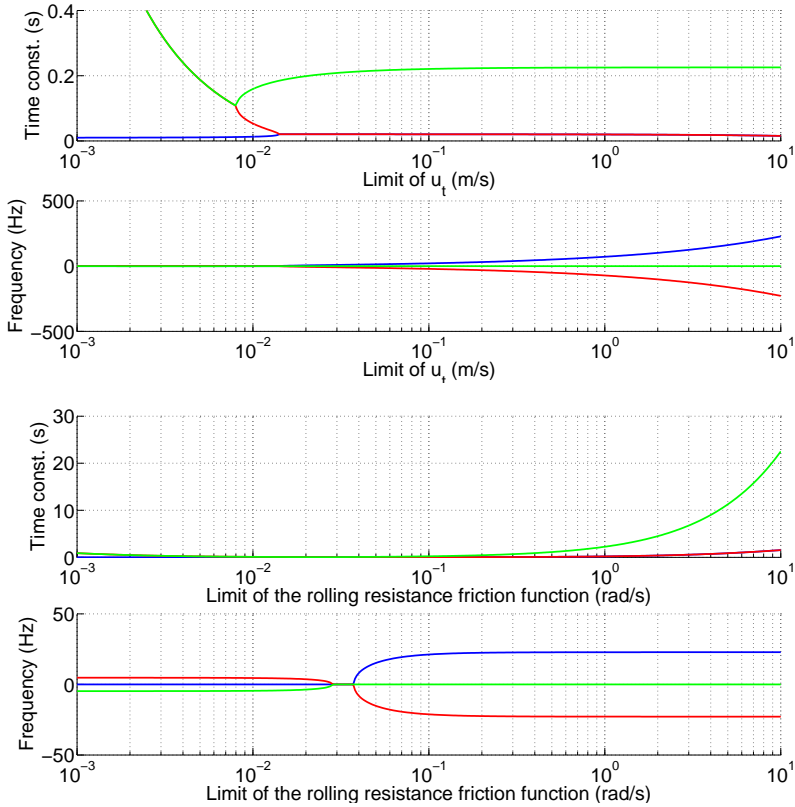


Figure 3.22: Real and imaginary parts of the eigenvalues of the longitudinal dynamics model with no braking, as function of  $c_{\hat{u}_t}$  (first two graphs, with  $\frac{1}{p}=0.1$  rad/s) and  $\frac{1}{p}$  (last two graphs, with  $c_{\hat{u}_t}=0.1$  m/s). The (negative) real part is expressed with the reciprocal (i.e. the time constant of the eigenmode); the imaginary part is expressed in terms of frequency.

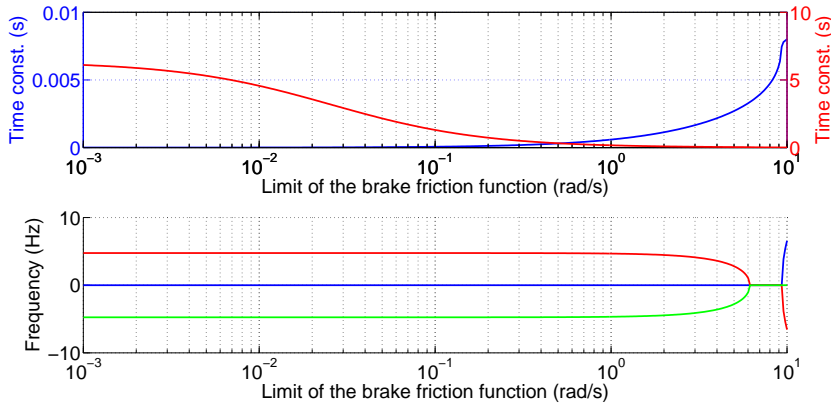


Figure 3.23: Real and imaginary parts of the eigenvalues of the longitudinal dynamics model with braking as function of  $\frac{1}{q}$  (i.e. the limit of static-dynamic in the friction function of the braking torque). The (negative) real part is expressed with the reciprocal (i.e. the time constant of the eigenmode); the imaginary part is expressed in terms of frequency.)

- lower the time constant of the eigenmodes in order to have acceptable values of damping (i.e. time constants of about 0.2 s – 0.5 s);
- avoid time constant of the eigenmodes lower than 1 ms, otherwise the model solver, which has a time step of 2.5 ms, is not able to solve the equations;
- avoid too high threshold values of  $c_{\hat{u}_t}$ ,  $\frac{1}{p}$  and  $\frac{1}{q}$ , which will extend the field where the model is not correct from the physical point of view.

Comparing the results of different vehicles with different parameters, the threshold values were manually set to fixed values. An automatic procedure based on the presented criteria, which sets the thresholds depending on the specific vehicle parameters could be developed in the future.

From the graphs presented, it could be noted how, when no braking torque is applied, the vehicle longitudinal damping is mainly due to the rolling resistance moment and the influence of  $c_{\hat{u}_t}$  is quite negligible. For this reason,  $c_{\hat{u}_t}$  was set to 0.1 s, the same value of  $c_{\hat{u}_t}$  (Section 3.6.3). The

static-dynamic friction limit of the rolling resistance moment was set to 0.1 rad/s ( $p = 10$ ) and that of the braking torque to 2 rad/s ( $q = 0.5$ ).

### Lateral dynamics

A similar procedure of that for the longitudinal dynamics was carried out for the lateral dynamics around zero speed. In this case, the equations of the simplified single-wheel model are the lateral linear dynamics and the tire slip dynamics:

$$\begin{aligned} m\dot{v}_t &= F_y \\ \dot{\alpha} &= -\frac{|\hat{u}_t|}{l_{r,y}}\alpha - \frac{v_t}{|\bar{u}_t|} \frac{|\hat{u}_t|}{l_{r,y}}. \end{aligned} \quad (3.49)$$

The model is linearised around  $u_t = 0$ , implementing the linearization of the tire lateral constitutive equation:

$$F_y = K_y\alpha, \quad (3.50)$$

thus having:

$$\begin{aligned} \dot{v}_t &= \frac{K_y}{m}\alpha \\ \dot{\alpha} &= -\frac{c_{\hat{u}_t}}{c_{\bar{u}_t}l_{r,y}}v_t - \frac{c_{\hat{u}_t}}{l_{r,y}}\alpha, \end{aligned} \quad (3.51)$$

where the state of the system is  $[\alpha \ v_t]^T$ .

In this case, the only constant to be determined is  $c_{\hat{u}_t}$  which, as already written, can be different from that of the longitudinal slip equation. The criteria used to determine it are the same described for the longitudinal dynamics.

Having just a two-dimensional model, the eigenvalues can be easily obtained, however, they are here just graphically presented (in Figure 3.24). Having no other damping term than that depending on  $c_{\hat{u}_t}$ , the system is much more less damped than in the longitudinal direction. Although the damping coefficient is still very low, the threshold was set to 2 m/s in order to avoid an incorrect tire slip dynamics at higher speeds.

The effects of these modifications of the tire model are also pointed out in the results of the simulations with the complete vehicle model, shown in Section 4.4.



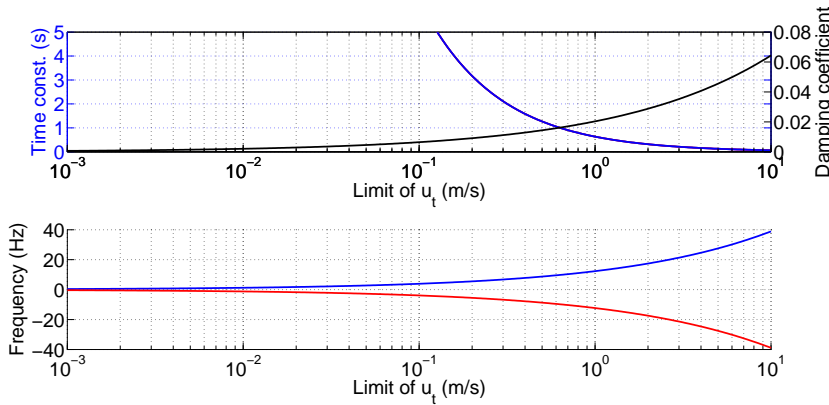


Figure 3.24: Real and imaginary parts of the eigenvalues of the simplified model for the lateral dynamics as function of  $c_{\hat{u}_t}$ . The (negative) real part is expressed with the reciprocal (i.e. the time constant of the eigenmode); the imaginary part is expressed in terms of frequency.). The damping coefficient is also showed.

### 3.7 Steering system

The steering system block of the vehicle simulation model is shown in Figure 3.25. The steering kinematics is treated in the suspension block, as it is described in Section 3.5.1. In the steering system block, the following two main functions are carried out:

- computing the final steering torque and sending it to the feedback electric motor (via the National Instrument PCI board);
- computing the final steering angle.

The steering torque  $T_s$ , which is computed by the vehicle dynamics block, can be corrected by an additional damping term, simply obtained as  $c_s \dot{\delta}_s$ . This term is required in some cases because of few damping in the driving simulator steering system. The physical system is not complete and it has therefore different inertial and friction properties which can lead, in some cases depending on the vehicle parameters, to a low-damped system. At high speeds, instability can also occur. To avoid this, the damping coefficient  $c_s$  can be set to a proper value which damps the system without too much drag torque when steering very quickly. An estimation of the damping coefficient required was carried out using

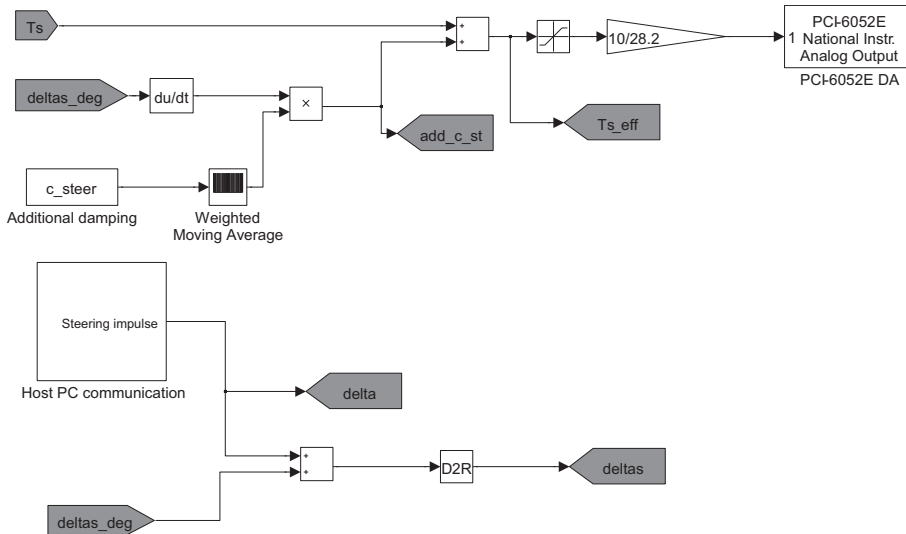


Figure 3.25: Steering system block of the vehicle simulation model in Simulink.

a simple single-track vehicle model with linear tires. Its eigenvalues were analysed at different speeds, finding the proper damping coefficient depending on the vehicle model parameters.

The final value of the steering torque is then converted in Volts<sup>3</sup> and sent as reference to the feedback electric motor, using the already described specific block of the National Instrument board.

As future development of the model, a power-assisted steering model could be implemented. Currently, the maximum torque is limited with a saturation block to 10 N m to avoid excessive driver's effort.

The second function of the steering system block is the possibility of adding an impulse to the steering angle to simulate a lateral sudden skid. To do so, an additional steering angle with a square function is added (just in the simulation environment) to the current steering angle imposed by the driver for a specified time. As already anticipated, this is done by the operator, which follows the simulation at the control desk, sending the amplitude and the duration time from the Host PC via the LAN. The specifically developed block, called *Host PC communication* in Figure 3.25, has a UDP receiver block and a function which generates

<sup>3</sup>10 V correspond to 28.2 N m, which is the peak torque of the motor.

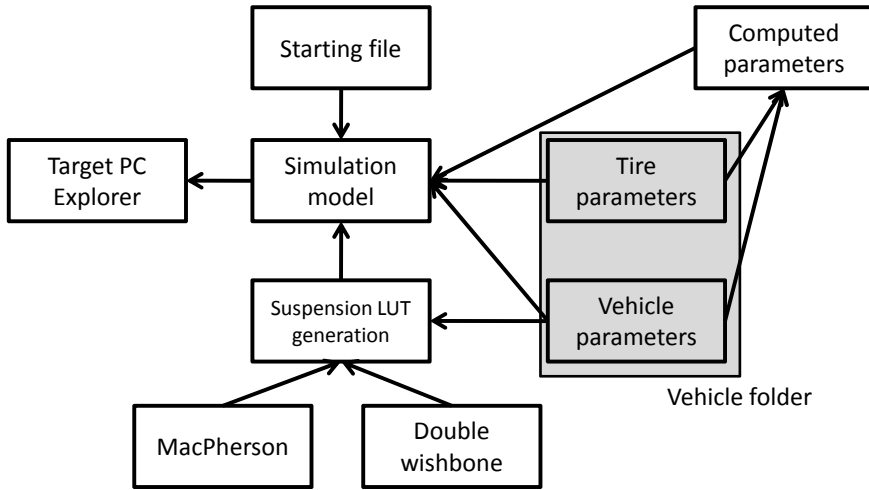


Figure 3.26: Block scheme of the data flow between the files involved in the initialization phase of the simulation.

the square signal. The software running in the Host PC, which is used to send this impulse, is described in Section 4.3.

### 3.8 Parameters and file organization

The developed vehicle simulation model is completely parametric. Every vehicle parameter, the suspension type and the tire properties can be changed without modifying the model block architecture. A specific folder is dedicated to each vehicle, where its parameter files are stored and can be modified. Up to now, two different vehicles are available for simulated drives: a small family car (belonging to the so called C-segment) and the Formula SAE race car of the Università di Pisa. The former has a 1600 cm<sup>3</sup> gasoline engine, front double wishbone suspensions and rear MacPherson struts. Most parameters, such as the suspension mounting points and the tire model coefficients, were available, whereas other were estimated. The Formula SAE car is a single-seat 550 cm<sup>3</sup> race car with front and rear double wishbone suspensions; its tire parameters were available from the Formula SAE Tire Testing Consortium, whereas all vehicle parameters were known, being the car completely internally designed.

The vehicle parameters include: dimensions and inertial properties of the sprung and the unsprung masses, suspension type and mounting points, suspension stiffness and damping, tire type and coefficients, engine characteristic, transmission parameters, braking system parameters, aerodynamic coefficients and simulation initial conditions.

Before starting the simulated drive, an initialization phase must be carried out in the Host PC, loading all basic vehicle parameters and computing some other derived parameters. The data flow and the files involved in this phase are shown in Figure 3.26. A starting Matlab m-file (script file) performs all initialization operations calling back and executing the other files. Moreover, the simulation and the data sending frequencies are also set in this file.

Running the starting file, the operator is asked to choose the vehicle type. By doing this, the parameter m-file of the selected vehicle is called back and run; the vehicle parameters are stored in the Matlab workspace, so that the simulation model can read them. Then, an m-file, which computes the derived parameters, is run. This automatically load the tire coefficients of the selected vehicle and save the derived parameters to the workspace.

The last set of parameters to be loaded regards the suspensions. The suspension look-up table generation m-file is called back and executed. This reads the vehicle parameters (suspension type, coordinate of the mounting points, etc.) and, calling back the specific Matlab functions for the suspension types, solve the suspension congruence equations 3.22 and 3.27. The look-up tables generated are saved in the workspace, ready to be imported by the simulation model. Finally, the starting file opens the Target PC Explorer (shown in Figure 2.3 in Section 2.1), compiles the model in C-code and transfers the execution model file in the Target PC, ready for the simulation. At this point, the operator at the control desk interacts with the Target PC Explorer interface, starting and stopping the simulated drive. The driving simulator functions available during the drives are topic of the next chapter.

## Chapter 4

# Real-time driving simulation

### 4.1 Simulation model performances

During the simulated drives, the Target PC must be able to acquire the driver's input signals, to solve the simulation model equations and to send the output data to other computers through the LAN. All these operations have to be completed in each step of the simulation within the step time. If the time required is longer than the step time chosen, the real-time simulation is no more guaranteed and the driving simulator does not work properly.

The time required for all the Target PC operations is called, in the xPC Target Toolbox, *Task Execution Time* (TET). This time is not constant during the simulation, depending on the difficulties of the solver in integrating the model equations. In order to guarantee the real-time simulation, the mean TET should not be longer than 80% of the simulation fixed step time.

Both the TET and the step time have constraints on their values depending on the application. The step time is usually chosen to correctly integrate the differential equations of the vehicle simulation model. Typical values in vehicle simulations are between 1 ms and 10 ms, i.e. frequencies between 100 Hz and 1000 Hz. Shorter step times, if not needed, would require shorter TET and must be therefore avoided. On the other side, if the TET can not be shortened, the step time can be increased just if the dynamics of the model can be followed without the risk of numerical problems.

The TET depends on the Target PC computing performance and on

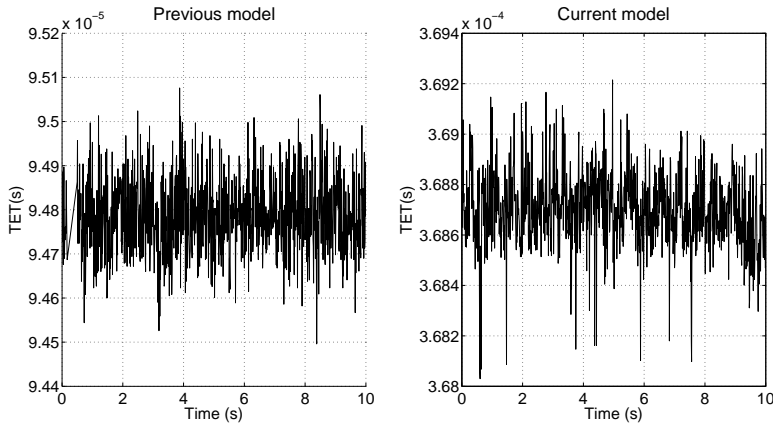


Figure 4.1: Task Execution Time (TET) of the previous version of the model (left) and the current one (right).

the simulation model complexity. Complex functions and communications with I/O interfaces (such as the National Instrument board) increase the TET.

In the present application, as already written in Section 2.1, the Runge-Kutta solver was chosen (ode4) with a fixed step time of 2.5 ms (solver frequency: 400 Hz). The TET during a generic manoeuvre is shown in Figure 4.1 for the older and the current version of the vehicle simulation model. As shown in the graphs, the mean TET of the old version is about 0.09 ms, whereas the current model has a mean TET of about 0.37 ms. This results is about four times the TET of the previous version due to the increased detail, and hence complexity, of the current model. However, the real-time simulation is still guaranteed with a big margin, being the mean TET shorter than 80% of the simulation fixed step time (2 ms).

## 4.2 Data acquisition

During the simulated drives, the Target PC sends several model output signals to the Host PC. These signals are acquired, monitored in real time and stored by the operator at the control desk, using a specific data acquisition software running in the Host PC. This is a home-developed Simulink model, whose front interface, during a simulated drive, is shown

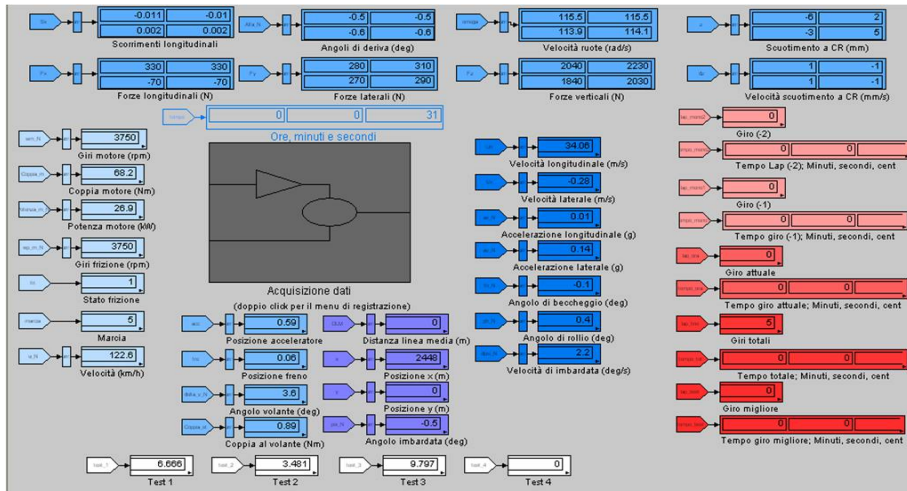


Figure 4.2: Data acquisition screen shot during a simulated drive.

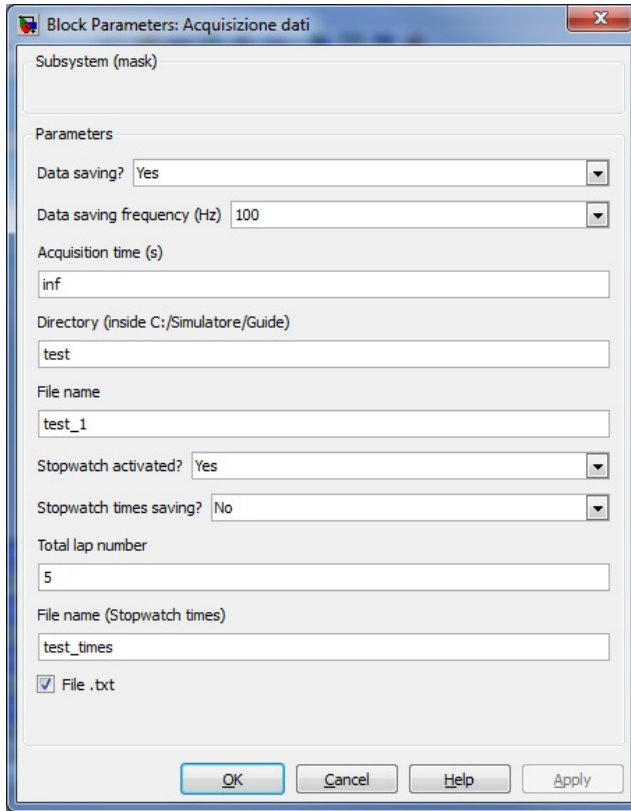
in Figure 4.2.

The acquired signals are currently 60 and are listed in Table 4.1. There are signals about the tire kinematic conditions (angular speed and slips), the tire forces, the driver's interfaces, the powertrain, the vehicle dynamics and the suspension travels. Moreover, four additional test channels are provided to send other signals from the model to the data acquisition software. The content of these channels has to be set in the simulation model before compiling it.

The data acquisition software receives the signals from the Target PC at a frequency of 100 Hz. These can be stored at the same frequency, keeping every data, or capturing one data element every two (the frequency is then 50 Hz), every three (33 Hz), or every four (25 Hz). All signals are then packed into a single matrix, which is saved as mat-file and/or txt-file for further data analyses.

During the acquisition in the simulated drives, the acquired signals are elaborated, to change some units into more practical ones, and then displayed in real time in the main window of the software (Figure 4.2).

Before the acquisition begins, the operator can set some options with a user-friendly mask (shown in Figure 4.3). The frequency of the data saving, the acquisition time, the directory and the file names and the txt-file output option can be edited. In addition to these, some options about the stop watch function are available, such as the number of laps



Block Parameters: Acquisizione dati

Subsystem (mask)

Parameters

Data saving? Yes

Data saving frequency (Hz) 100

Acquisition time (s)

inf

Directory (inside C:/Simulatore/Guide)

test

File name

test\_1

Stopwatch activated? Yes

Stopwatch times saving? No

Total lap number

5

File name (Stopwatch times)

test\_times

File .txt

OK Cancel Help Apply

Figure 4.3: Input mask for the parameters of the data acquisition software.

and the output file name for the lap times.

The stop watch function was added to the data acquisition software to accurately measure the driving times in a loop path. The lap times are computed considering a starting/finishing line, whose coordinates of the extreme points must be provided. In the graphical interface of the software, the last three laps are displayed together with the total time and the best lap time.



Table 4.1: Data acquired and stored during simulated drives. In the table: FL: front-left, FR: front-right, RL: rear-left, RR: rear-right.

#	Symbol	Unit	Quantity
1	$t$	s	Real time
2	$\omega_{w,11}$	rad/s	Wheel angular velocity FL
3	$\omega_{w,12}$	rad/s	Wheel angular velocity FR
4	$\omega_{w,21}$	rad/s	Wheel angular velocity RL
5	$\omega_{w,22}$	rad/s	Wheel angular velocity RR
6	$s_{x,11}$	-	Longitudinal tire slip FL
7	$s_{x,12}$	-	Longitudinal tire slip FR
8	$s_{x,21}$	-	Longitudinal tire slip RL
9	$s_{x,22}$	-	Longitudinal tire slip RR
10	$\alpha_{11}$	-	Tire slip angle FL
11	$\alpha_{12}$	-	Tire slip angle FR
12	$\alpha_{21}$	-	Tire slip angle RL
13	$\alpha_{22}$	-	Tire slip angle RR
14	$F_{x,11}$	N	Longitudinal tire force FL
15	$F_{x,12}$	N	Longitudinal tire force FR
16	$F_{x,21}$	N	Longitudinal tire force RL
17	$F_{x,22}$	N	Longitudinal tire force RR
18	$F_{y,11}$	N	Lateral tire force FL
19	$F_{y,12}$	N	Lateral tire force FR
20	$F_{y,21}$	N	Lateral tire force RL

Continued on next page

Table 4.1 – continued from previous page

#	Symbol	Unit	Quantity
21	$F_{y,22}$	N	Lateral tire force RR
22	$F_{z,11}$	N	Vertical tire force FL
23	$F_{z,12}$	N	Vertical tire force FR
24	$F_{z,21}$	N	Vertical tire force RL
25	$F_{z,22}$	N	Vertical tire force RR
26	$a$	-	Throttle pedal position
27	$b$	-	Brake pedal position
28	$\delta_s$	deg	Steering wheel angle
29	$T_s$	Nm	Steering wheel torque
30	$\omega_e$	rad/s	Engine speed
31	$T_e$	Nm	Engine torque
32	$P_e$	W	Engine power
33	$f$	-	Clutch position
34	$\omega_p$	rad/s	Primary shaft angular speed
35	gear	-	Gear
36	-	-	Clutch friction function value
37	-	-	Differential friction function value
38	DLM	m	Distance from lane centreline
39	$u$	m/s	Longitudinal velocity (point $N$ )
40	$v$	m/s	Lateral velocity (point $N$ )
41	$a_x$	m/s <sup>2</sup>	Longitudinal acceleration (point $N$ )
42	$a_y$	m/s <sup>2</sup>	Lateral acceleration (point $N$ )
43	$\phi$	rad	Roll angle
44	$\theta$	rad	Pitch angle
45	$\dot{\psi}$	rad/s	Yaw rate
46	$\psi$	rad	Yaw angle
47	$x$	m	Absolute coordinate x (point $N$ )

Continued on next page

Table 4.1 – continued from previous page

#	Symbol	Unit	Quantity
48	$y$	m	Absolute coordinate $y$ (point $N$ )
49	$\Delta z_{W,11}$	m	suspension travel FL
50	$\Delta z_{W,12}$	m	suspension travel FR
51	$\Delta z_{W,21}$	m	suspension travel RL
52	$\Delta z_{W,22}$	m	suspension travel RR
53	$\dot{z}_{W,11}$	m/s	suspension travel velocity FL
54	$\dot{z}_{W,12}$	m/s	suspension travel velocity FR
55	$\dot{z}_{W,21}$	m/s	suspension travel velocity RL
56	$\dot{z}_{W,22}$	m/s	suspension travel velocity RR
57	test1	?	Test variable 1
58	test2	?	Test variable 2
59	test3	?	Test variable 3
60	test4	?	Test variable 4

### 4.3 Real-time parameter changing

The vehicle parameters are generally loaded at the beginning of the simulation. If they are modified, the model should be recompiled and the simulation must be restarted. However, it is possible to change parameters in real-time during the simulation. As already anticipated in Section 2.1, the UDP Simulink blocks are used to send the new value of the parameter from the Host PC and to receive it in the simulation model. To this aim, before compiling the model, one or more UDB receive blocks with the same communication properties of the corresponding UDP send block must be implemented. From the Host PC, the parameters can be changed just running a basic Simulink model with a constant block connected to the UDP send block.

This method can be used to changed every parameter of the vehicle model, such as the engine power, the friction coefficient between tire and road or the anti-roll bar stiffness. This allows to study the driver's reactions to sudden changes in vehicle conditions.

In the present work, as already written in Section 3.7, this method was used to simulate a sudden lateral vehicle skid (which could be due to a sudden wind blow). This is done adding to the simulation steering wheel angle, a square function with a given amplitude and duration time. From

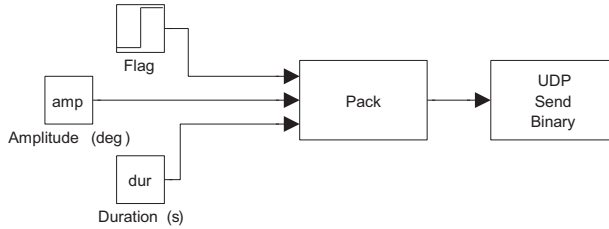


Figure 4.4: Block scheme of the model for sending the steering impulse.

the Host PC, using the simple Simulink model represented in Figure 4.4, the operator can send the amplitude, the duration time and a flag signal, when this model is run. The square function is built from these values with a specific function inside the steering system block of the vehicle model.

The amplitude of the signal was set to different values (between  $10^\circ$  and  $25^\circ$ ) depending on the vehicle speed. The duration time was typically set around 0.5 s.

## 4.4 Example of simulated manoeuvres

Before describing, in the next chapter, the experimental campaigns carried out with the driving simulator, the results of some typical manoeuvres are presented in this section. These are carried out in the driving simulator with a human driver and represent a sort of test for the driving simulator itself, and especially for the vehicle simulation model, in different driving conditions. These manoeuvres are:

- acceleration and braking manoeuvre;
- lane change manoeuvre;
- step steer manoeuvre;
- acceleration and braking manoeuvre with loss of grip;
- step steer manoeuvre with loss of grip.

The first three are performed with the C-segment vehicle, whereas the manoeuvres with the loss of grip are performed with the Formula SAE

vehicle. In these two last manoeuvre it is demonstrated that the vehicle simulation model allows the loss of grip continuing computing the solution. The driver can then keep once more the control of the vehicle and continue the simulated drive.

#### 4.4.1 Acceleration and braking manoeuvre

In this manoeuvre, which results are shown in Figure 4.5, the vehicle starts with zero speed. As it can be seen in the graphs, the driver firstly acts on the braking pedal, then the vehicle is smoothly accelerated and finally braked reaching zero speed. As it is clear from the signals, the vehicle model has no problem in computing the static condition (i.e. all signals are zero even if little numerical errors occurs) also when the brake signal is 1. At zero speed the system is well damped, as it can be observed in the final part of the manoeuvre, when the braking is completed. Longitudinal forces, wheel speeds and tire slips go to zero without vibrations.

At low speed, when drive torque is applied, there are some little vibrations in the rear slip and longitudinal force signals (rear drive vehicle). This occurs because of the lack of additional damping, as anticipated in Section 3.6.3. However, as pointed out, this has no influence on the vehicle speed and hence in the driver's feelings.

In the graphs it is also shown how the powertain behaves, especially the engine and the clutch. After an initial slipping phase, the clutch is engaged and the primary shaft velocity curve follows the engine speed curve. The more the engine torque, the more the curves are spaced out because of the clutch friction function (based on the clutch slip).

The gear shifts, which are easily identifiable by the engine speed variation, gives peaks in the longitudinal forces of the drive wheels, and hence in the tire slips, in the acceleration and in the pitch angle signals. These are due to the instantaneous change of the gear ratio and thus of the inertial properties of the powertrain. In signals integrated from the previous (such as the velocities) these peaks are filtered and are therefore not felt by the driver.

#### 4.4.2 Lane change manoeuvre

The results of a lane change manoeuvre performed at 80 km/h in the highway are shown in Figure 4.6. From the driver's input signal of the steering wheel angle it can be seen how the vehicle is firstly steered on

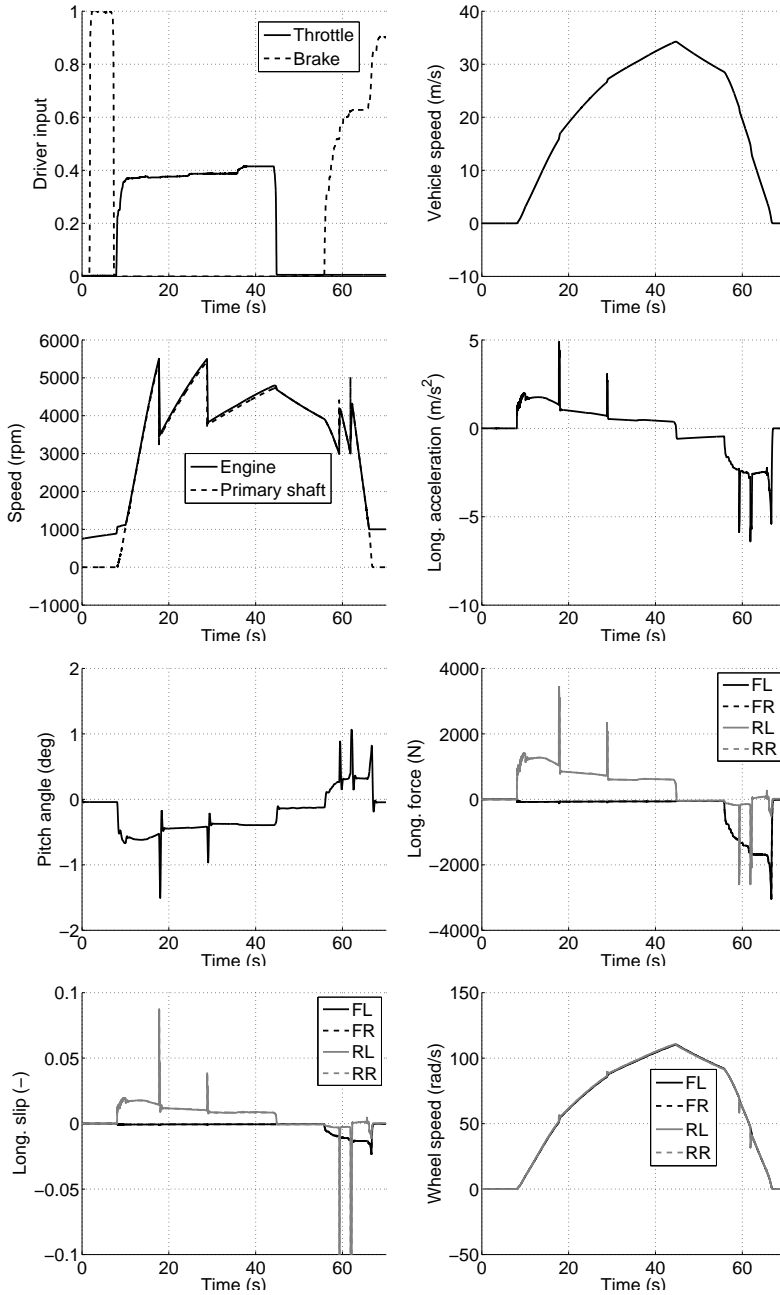


Figure 4.5: Results of an acceleration and braking manoeuvre with the C-segment car.

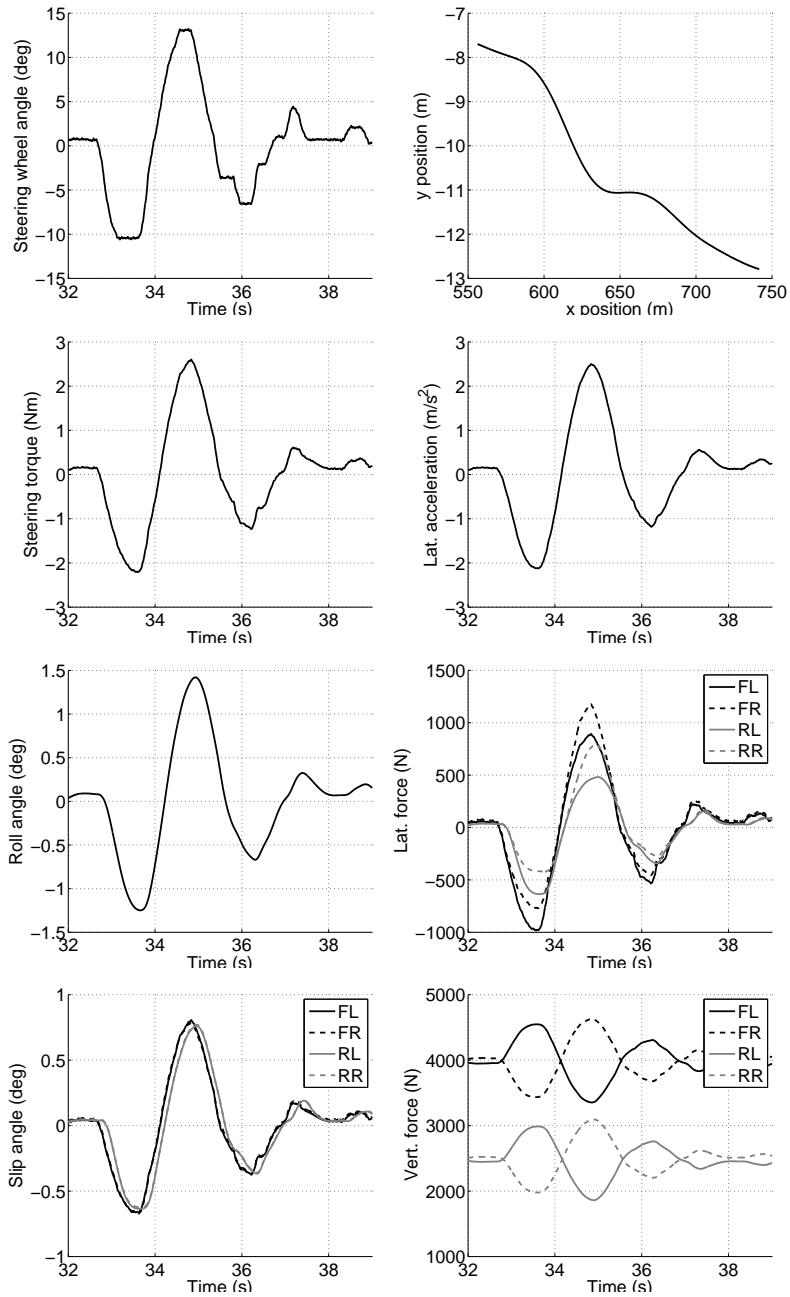


Figure 4.6: Results of a lane change manoeuvre at 80 km/h with the C-segment car.

the right to change lane and then on the left to align its trajectory with the road. The manoeuvre is carry out quickly, the driver needs to do, in fact, two more corrections on the steering wheel to keep the vehicle on the lane. This can be easily seen also in the trajectory graph.

Even if carried out quickly, the manoeuvre is not extreme, having a peak of the lateral acceleration of just  $3 \text{ m/s}^2$  and slip angles below  $1^\circ$ .

#### 4.4.3 Step steer manoeuvre

In Figure 4.7 the same signals, just seen for the lane change, are shown in a step steer manoeuvre performed at  $80 \text{ km/h}$ . In this manoeuvre the driver suddenly increases the steering wheel angle from almost zero (straight driving) to  $90^\circ$ . After a fast transient (which dynamics depends on the vehicle and tire properties, such as the tire relaxation lengths), the vehicle turns round in steady state conditions (as it can be seen in the trajectory graph). The effect of the tire relaxation lengths can be easily observed in the slip angle signals. Although the front tires are almost instantaneously steered, the front slips appear with a delay and grow smoothly because of the exponential law of the tire slips.

With respect to the previous one, this manoeuvre is much more near the grip limit. The lateral acceleration is, in fact, more than  $1 g$ , the roll angle reaches  $6^\circ$  and the steering torque, felt as feedback by the driver, is about  $10 \text{ Nm}$ .

Focusing on the vertical loads, it can be seen that the rear inner wheel (i.e. the left wheel) is lifted, being the corresponding  $F_z = 0$  (and hence  $F_y = 0$ ). The car does not turned over, having load on the front left wheel, and the solution is still computed without any problem by the simulation model.

#### 4.4.4 Acceleration and braking manoeuvre with loss of grip

This manoeuvre is similar to the first one described. In this case the driver gives full throttle with the Formula SAE vehicle, making the rear wheel slipping. As it can be seen in Figure 4.8, the rear wheel speed increases very quickly, whereas the front wheel speed is increasing with a slower rate, indicating that there is an excessive drive torque making the (rear) drive wheel slipping. The rear tire longitudinal slip reaches almost 2 and remain in the slipping range until the the vehicle velocity



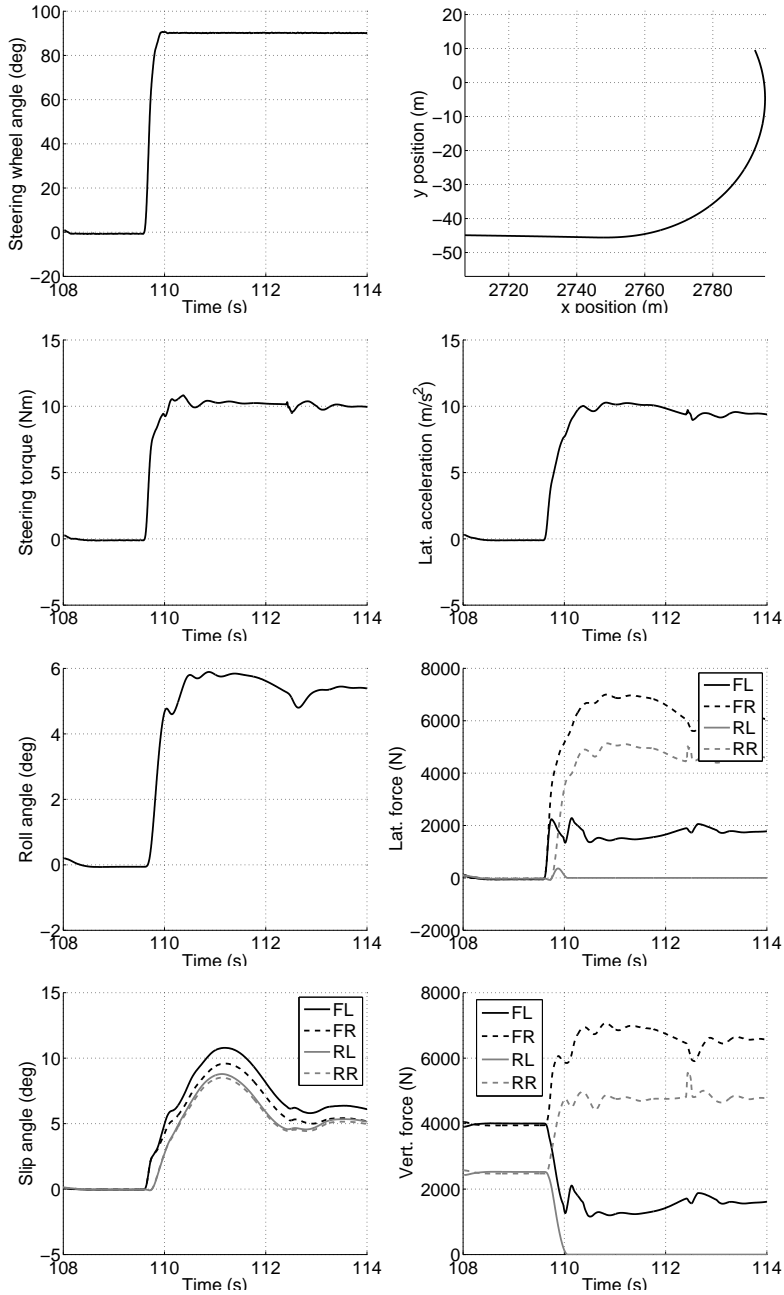


Figure 4.7: Results of a 90° step steer manoeuvre at 80 km/h with the C-segment car.



Figure 4.8: Results of an acceleration and braking manoeuvre with full throttle with the Formula SAE car.

has reached a value enough to stop the wheel slipping. The longitudinal force is then increased and the rear wheel speed, as well as the powertrain speeds, decreases. During the quick increase of all the powertrain speeds (and therefore also the engine speed), all gear shifting occurs, going the engine speed above the range for upshift.

After the vehicle has reached its maximum speed, the driver suddenly brakes at the maximum allowable braking force (the brake signal goes to 1). With the current brake bias, the rear wheels are normally braked, whereas the front wheels are locked (wheel speed goes very quickly to zero and the tire slip to  $-1$ ). When the vehicle is stopped all signals go to zero, except the engine speed which goes to the idle speed. Then, the vehicle starts again with full throttle.

With this manoeuvre, it was shown how the vehicle model can handle with no problem tire slipping in both acceleration and braking. Moreover, even if an extreme braking with tire slipping is carried out, the vehicle is stopped with all signals reaching zero and it is able to start again.

#### 4.4.5 Step steer manoeuvre with loss of grip

The last manoeuvre shown is a step steer of  $90^\circ$  performed at 100 km/h with the Formula SAE car. Having this car a little steering ratio, the steering angle at the wheels results very high (about  $16^\circ$ ).

Looking at the tire slip angles, it can be observed how the front tires lose grip, reaching slip angles of more than  $20^\circ$ , whereas the rear tires still have slip angles within the grip limit. Also in this case, the model can handle these extreme conditions computing correctly all the variables and without instability. Then, when the steering wheel is brought to the straight position, the car can move in the longitudinal direction and all lateral dynamics quantities have correctly gone to zero.

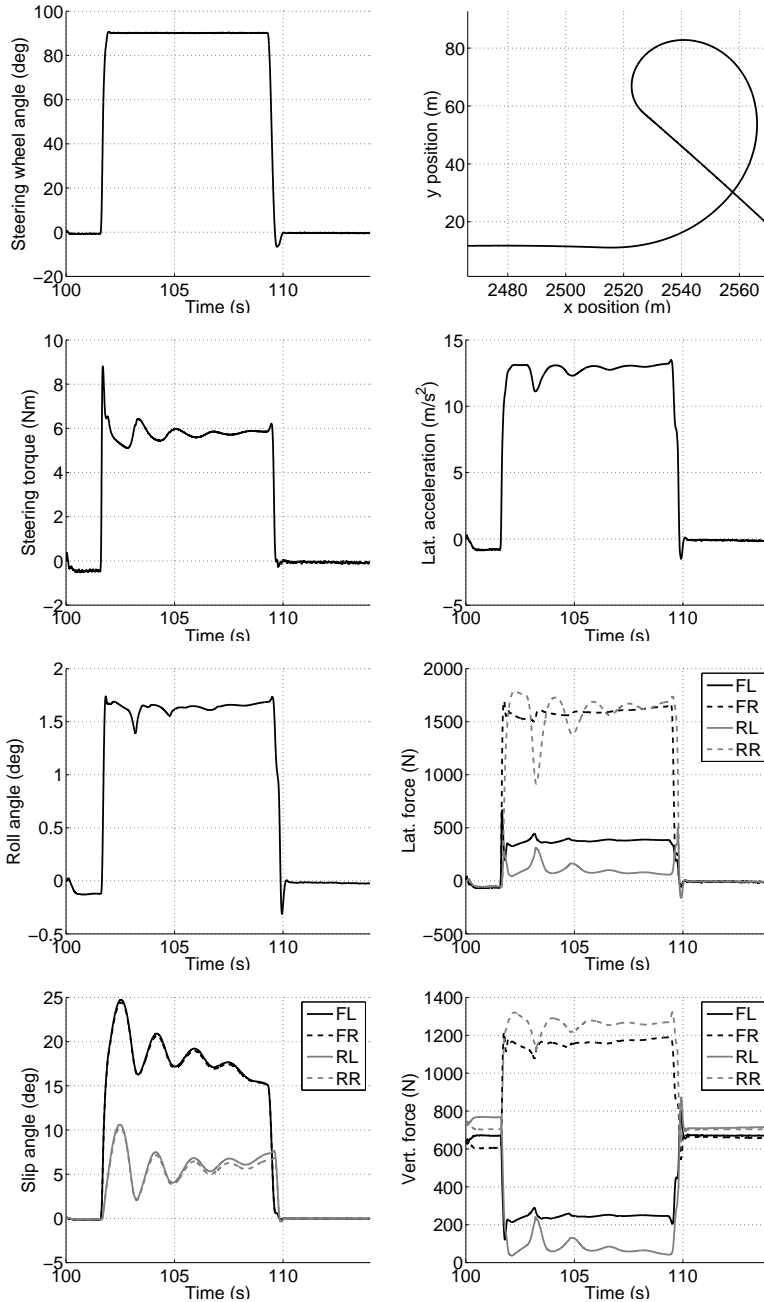


Figure 4.9: Results of a step steer manoeuvre at 100 km/h with the Formula SAE car.

# Chapter 5

## Experimental tests and campaigns

### 5.1 Introduction

After a first test phase, the driving simulator developed and built in the DIMNP was used, and it is currently still in use, for experimental campaigns mainly focused on road safety. The system was able to complete several hours of simulation without encountering any problem, allowing to collect an important amount of data about simulated drives.

The experimental campaigns carried out in the period of this work involved other university partners and are summarized in the following list:

- driving simulator calibration (with *Dipartimento di Ingegneria Civile-Vie e Trasporti, Università di Pisa*), see Section 5.2;
- development of diagnostic systems for the driver's attention level (with *Dipartimento di Ingegneria dell'Informazione, Università di Pisa* and *Dipartimento di Meccanica e Tecnologie Industriali, Università degli Studi di Firenze*), see Section 5.3;
- alcohol effects on driving style, especially on reaction times (with *Dipartimento di Biologia* and *Dipartimento di Ingegneria Civile-Vie e Trasporti, Università di Pisa*)

Before the experimental campaigns were carried out, a test session with 10 persons was planned in order to test the driving simulator for a



Figure 5.1: Simulated drive during an experimental campaign.

longer time than single drives and to collect a first set of data. This was used to analyse to potentiality of the system and for the development of data analyses techniques by the project partners before the experimental tests took place. The driver's were asked to drive at different speeds on the highway scenario and to carry out some typical manoeuvres such as acceleration, braking, lane change and combination of them. An example of the results of a manoeuvre is shown in Figure 5.2. This consists in in reaching the speed of 40 km/h, changing the lane and then braking until the vehicle is stopped. Signals of two different drivers are shown together to qualitatively highlight the differences in the driving style between them. Even if they were asked to perform the same manoeuvre, looking at the graphs, it is possible to detect clear differences between the signals of two drivers.

## 5.2 Driving simulator calibration

As already written at the beginning of this thesis, a driving simulator is a virtual reality tool which aims at reproducing a real human-machine-interaction. The more the machine, the environment and their interaction with the driver are similar to the reality, the more the driver would feel

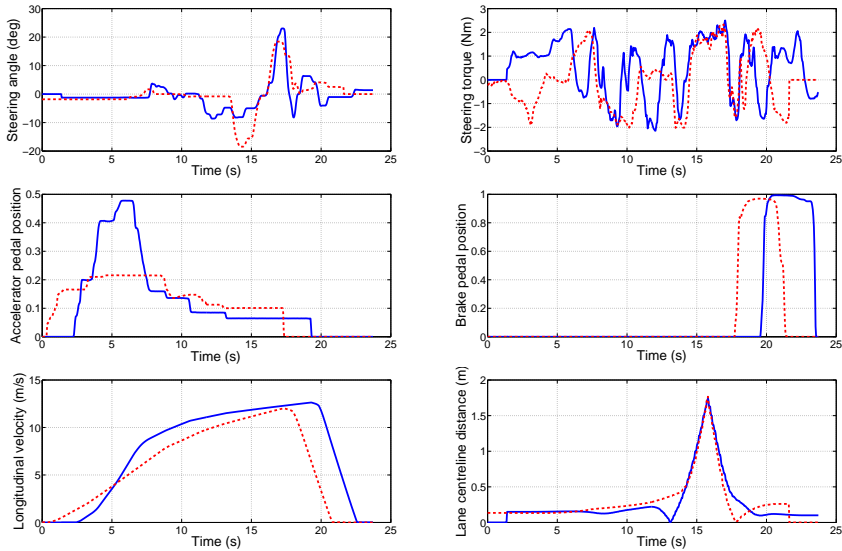


Figure 5.2: Lane change and braking manoeuvre performed by two different drivers (solid and dashed lines). The time vectors of the two data sets are aligned when the car crosses the line between the lanes (maximum distance from lane centreline).

himself as in the real world and would behave naturally. The reproducing of the real feelings on the driver and the correspondence of the driver's actions to the reality are therefore the main challenges of the driving simulator as a virtual reality tool. This means, not only to recreate the physical car environment and the road environment in the graphical scenario, but mainly to have consistent reactions of the system to the driver's inputs, to have realistic force feedbacks on the driver's commands and, when a moving platform is available, to reproduce the inertial effects on the driver's body.

For the driving simulator of this work, in order to verify the capabilities of reproducing real driving conditions, it was decided to carry out a correlation between simulated and real drives. The simulated drives were performed in the urban scenario of the driving simulator (Section 2.5), so that the real drives could be carried out in the correspondent roads of Rosignano (Livorno). The calibration was based on the signals of the vehicle speed and the steering wheel angle which, as found in literature, represent more than others the driver's behaviour. By comparing these

signals between the real and the simulated drives, it was possible to evaluate the driving simulator capability of reproducing real drives.

These calibration tests and the results analysis were carried out by the project partner and are therefore just briefly summarized.

### 5.2.1 Test protocol

For this experimental campaign 94 people were selected, aged between 18 and 35 years, with statistically variable sex, origin and other parameters.

They were firstly asked to drive on open roads (with low traffic intensity) of Rosignano following the predefined path for the test. This was about 3.2 km long and was divided in 8 sections by points of braking, such as traffic lights, pedestrian crossings, roundabouts, etc.. During the drives, the steering wheel angle the car speed signals, together with other vehicle signals, were acquired from the vehicle CAN and stored for further analyses. A vehicle with constructive parameters very close to those of the driving simulator was employed.

The simulated drives were carried out in the same roads in the urban scenario. In order to reproduce the real environment, traffic lights, pedestrian crossings and roundabouts were graphically reproduced in the scenario. In addition to this, similar traffic conditions (with randomly driven autonomous vehicles) to those in the real drives were set in the driving simulator; pedestrians with predefined walking paths were also included. Other vehicles and pedestrians were necessary to reproduce also traffic-related causes of braking.

### 5.2.2 Results and discussion

In Figure 5.3 the comparison between the results of a real and a simulated drive performed by the same driver is shown. Both the vehicle speed and the steering wheel angle signals visually show a good agreement between the two drives. This seems to indicate that the driver, when in the driving simulator, follows almost the same trajectory of the drive with the real car (steering wheel angle correlation) and acts similarly on the brake and accelerator pedals (speed correlation).

A statistical analysis was carried out on the 94 samples, using, for the speed quantity, the positive peak in each section. This was considered more significant than the mean speed (which was also evaluated) because of the lower influence on it of traffic and environment related speed



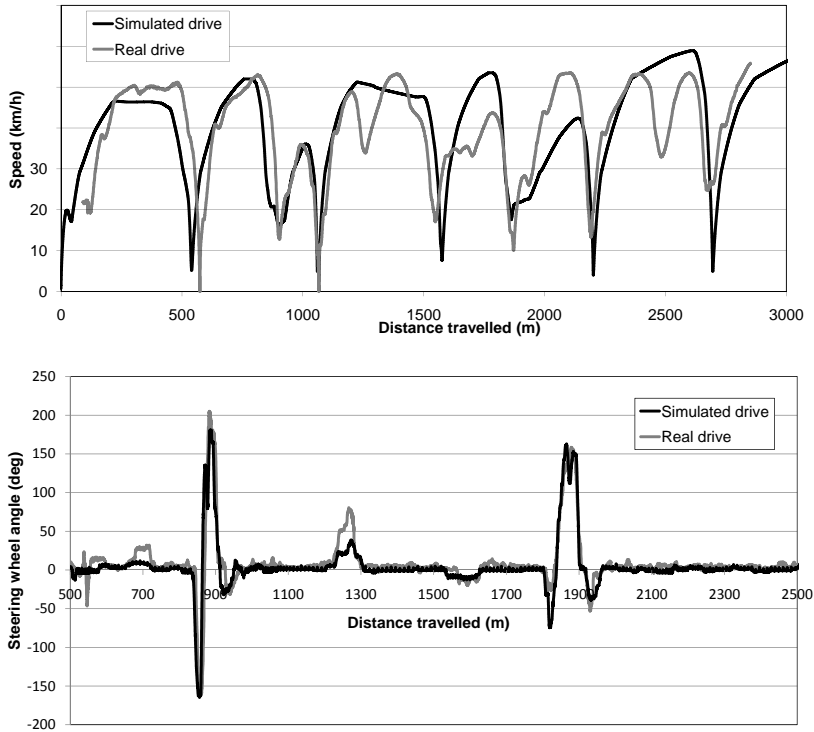


Figure 5.3: Comparison, based on the vehicle speed, of a real and a simulated drive of the same driver (top); comparison based on the steering wheel angle (bottom).

reducing.

With reference to the first section of the drives, the difference of the speed peak value between the real and the simulated drives for all the drivers is shown in Figure 5.4. The values of the speed difference are almost normally distributed with a mean of  $-2.22$  km/h and a standard deviation of 8.40 km/h.

A test  $t$  for paired samples was applied, finding that this little difference of the mean values is however significant, having a very large sample group. Similar results were found out in the other sections of the drives. In fact, in 6 sections out of 8, the null hypotheses, of having the same mean value of speed between real and simulated drives, was rejected with an error probability of just 1%. In the other sections the probability was

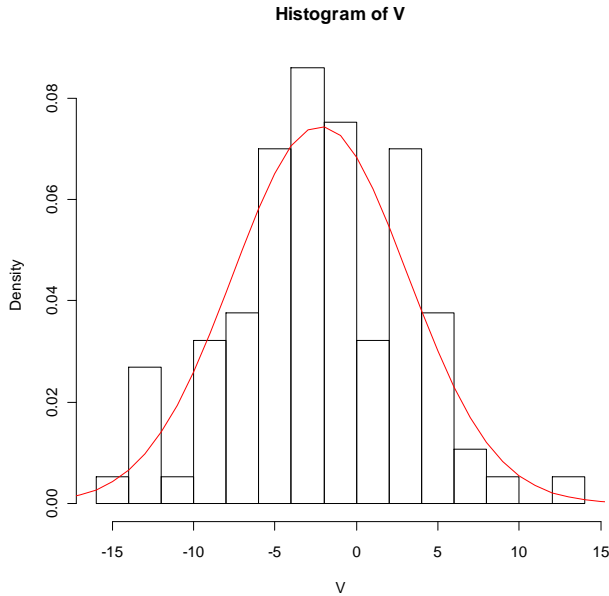


Figure 5.4: Distribution of the difference of the first section speed peak between real and simulated drives.

between 5% and 10%.

Having this little but significant difference on the speed values, a further step was taken, carrying out a linear regression analysis. The results of this analysis, in terms of the regression parameter  $R$ , were between 0.65 and 0.8 for the various drive sections.

The steering wheel angle was analysed just by mean of the regression, considering the peak values in specific points of the path. This signal showed a very good correlation, having  $R > 0.8$  in many sections. This means that in the simulator the drivers chose almost the same trajectory with respect to the real drives.

From the analyses on the speed signal, it can be concluded that there is a little difference between the real and the simulated driving conditions, measuring a higher speed in the drives at the driving simulator. This was mainly attributed to:

- the absence of side view in the visual system (which is made of a single frontal channel). The sensation of speed depends a lot on the movement of the objects near the driver's point of view;

- the absence of inertial and vibrational effects on the driver.

However, being this value below a threshold of 5 km/h, it can be concluded that this difference is negligible for the driving simulator aims. In addition, even if the test  $t$  was highly significant, cross-check tests on many drivers showed similar differences between two real drives of the same person with analogue traffic conditions. Then, considering also the good correlation of the steering wheel angle signal, and hence of the trajectory, the developed driving simulator is able to partially reproduce actual driving conditions. This means that the following experimental campaigns based on the analyses of the driving style could be carried out considering their results representative for real driving conditions.

### 5.3 PRIN experimental campaign

The main experimental campaign during the period of this work was carried out in the framework of the PRIN project in cooperation with the other project partners. The main objectives of the study, which have been already presented in Chapter 1, were the development of diagnosis systems for detecting the drivers' attention level. In specific, the activities were focused on the driver's drowsiness and on its influence on the driving style. People were asked to drive in the highway scenario in normal rested conditions and in tired conditions (after sleep deprivation of some hours), following the test protocol described in Section 5.3.1.

As anticipated in Section 1.2, the analyses were based on driver's input signals and on vehicle dynamics signals, avoiding direct measures of physiological or behavioural human variables, which can be felt as intrusive by many people. Among all signals available from the driving simulator acquisition, the steering wheel angle signal was found being the most representative of the driving style. This is, in fact, confirmed by the literature, as written in Section 1.2. This signal can be related to driver's attention level noting that the micro-corrections made by the driver (i.e. little amplitude and slow frequency motions) tend to decrease when the drowsiness level increases. However, the steering angle signal has also the information about the path followed by the vehicle. In specific, the signal can be considered as made of two contributions:

- a slow frequency part which depends on path followed by the vehicle;

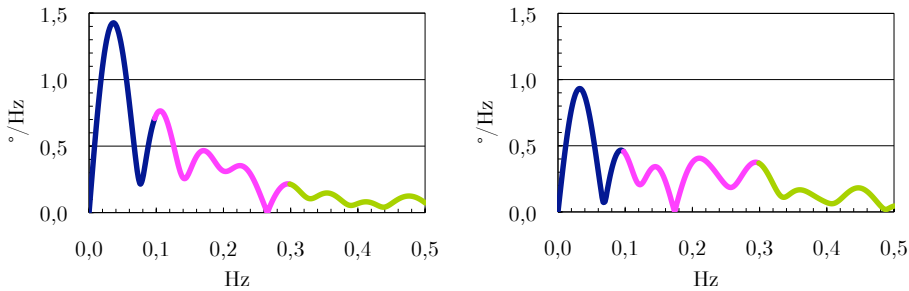


Figure 5.5: Spectrum of the steering wheel angle signal, represented with 3 ranges, for a single driver in rested condition (left) and tired condition (right).

- higher frequencies parts which depend on the driver's micro-corrections and are typical of each person and condition (i.e. rested, tired, ecc.), indicating the driving style.

An example of the frequency spectrum of the steering wheel angle signal is shown in Section 5.5, for both rested and tired test conditions of a single driver. The graph is divided in 3 frequency ranges to highlight the spectrum part related to the path and those related to the driver's correction. These ranges were analysed in terms of mean amplitude, centroid position and maximum amplitude for each driver, finding that the frequency limits should be adjusted for each driver, thus having a big number of parameters to analyse. For this reason, in order to have a reasonable number of parameters to work with, the analysis was focused on the first time derivative of the steering wheel angle signal.

This signal, which has a zero mean value in a simulated drive, has oscillations with frequency and amplitude depending, as the steering wheel angle signal, on the followed path and on the driving style. In addition, these parameters depend on the specific path and on the vehicle mean speed. For the following analyses, which results are briefly shown in Figure 5.3.2, it was then developed a fuzzy logic which is based on the following parameters, evaluated in a short driving time (20 s):

- vehicle speed;
- mean steering wheel angle value;
- peaks frequency of the derivative of the steering wheel angle;

- mean peaks amplitude of the derivative of the steering wheel angle.

These represent the input of the fuzzy logic, whereas the output is a parameter indicating the driving style, set as indicated in the next section. A fuzzy logic was considered the most suitable mathematical tool, being the function between the inputs and output unknown. The so called membership functions of the parameters and the fuzzy logic rules were set automatically using genetic algorithms, carrying out the algorithm learning with a first set of test data. For details on these aspects, which were carried out by the project partners, see [5].

### 5.3.1 Test protocol

For the experimental campaign, 12 people were selected among different age groups and were asked to drive in the driving simulator following a specific test protocol. They all performed the drives in rested and tired conditions in two different days. It was therefore possible to acquire an amount of data for the development and the test of the fuzzy logics aimed at detecting driver's drowsiness.

The test protocol was based on the following variables:

- **Driver's conditions (test conditions):**
  - rested (normal condition);
  - tired (sleep deprivation of some hours).
- **Simulated drive type:**
  - normal highway driving for 5 min;
  - highway driving using the mobile phone for 2 min;
  - highway driving of about 1 min with 2–3 sudden simulated lateral vehicle skids (as described in Section 4.3) carried out to measure the driver's response. These tests were performed just at 70 km/h and 130 km/h.
- **Vehicle speed:**
  - 70 km/h;
  - 90 km/h;
  - 110 km/h;

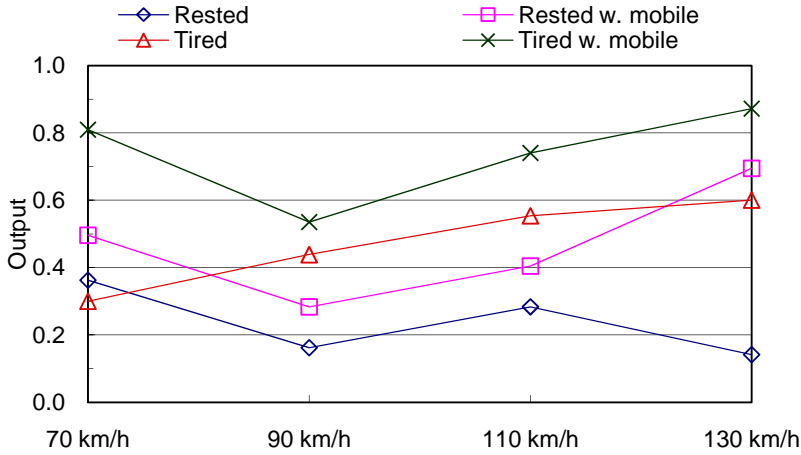


Figure 5.6: Comparison of the algorithm mean output value of driver A in the different test conditions.

– 130 km/h.

All drivers, before starting the test drives of the experiment, performed a 5 min drive to become confident with the driving simulator behaviour. This time was found being sufficient, having a good level of virtual reality reproduction of the system.

Employing the described test protocol, each driver drove for about 45 min for both the drives in rested and in tired conditions.

From the fuzzy logic point of view, four test conditions were reproduced, in which it is expected to have different driving styles. These conditions, with the correspondent value set for the output parameter of the fuzzy logic are: rested (0), rested with mobile phone (0.33), tired (0.66) and tired with mobile phone (1).

### 5.3.2 Results and discussion

The developed and tested algorithm based on fuzzy logic was applied to the acquired data of the experimental campaign. The analyses were carried out by *Dipartimento di Meccanica e Tecnologie Industriali* of the *Univeristà degli Studi di Firenze* and their results are in the following briefly described.

Table 5.1: Algorithm output value of driver A in all test conditions and speeds. The mean value for each test condition is also shown together with the difference (percentage) with respect to the normal rested conditions.

Condition	Speed (km/h)				Mean	Diff. (%)
	70	90	110	130		
Rested	0.363	0.162	0.284	0.141	0.237	0.0
Rested w. mobile	0.496	0.284	0.405	0.695	0.470	97.9
Tired	0.300	0.439	0.554	0.601	0.473	99.5
Tired w. mobile	0.809	0.535	0.740	0.872	0.739	211.4

In Figure 5.6 the results of the output of the fuzzy logic algorithm are shown for a driver (driver A) in the four different test conditions. The same results are summarized also in Table 5.1. It is shown how the output parameter, when the system parameters and rules are set on other data of the same driver, is able to detect the different driving conditions with clear differences in the output parameter. However, for this driver, the rested condition with mobile phone scores a similar output of the tired condition. The importance of the influence of the vehicle speed is also shown, highlighting how this is not easy to be predicted.

In Figure 5.7 the relative score with respect to the normal rested condition is shown for four different drivers. The output parameter shows once more a good correlation with the driver's attention level. However, there are important differences in the driving style, and thus in the output of the algorithm, among the different drivers. As driver A, also driver B scores a very similar output in the rested condition with mobile phone and in the tired condition; in this case the output in the tired condition is even lower. In addition to this, it was seen that the output of the algorithm can change a lot if the learning phase of the fuzzy logic is carried out on data from an other driver [5].

From the results shown, it can be concluded that the output index of the developed algorithm demonstrated a high correlation with the driver's attention level, indicating the possibility of development of a diagnosis tool based on this concept. However, as expected, the fuzzy logic must be set for each driver, performing a learning phase before the system is able to work properly and hence recognize the driving style.

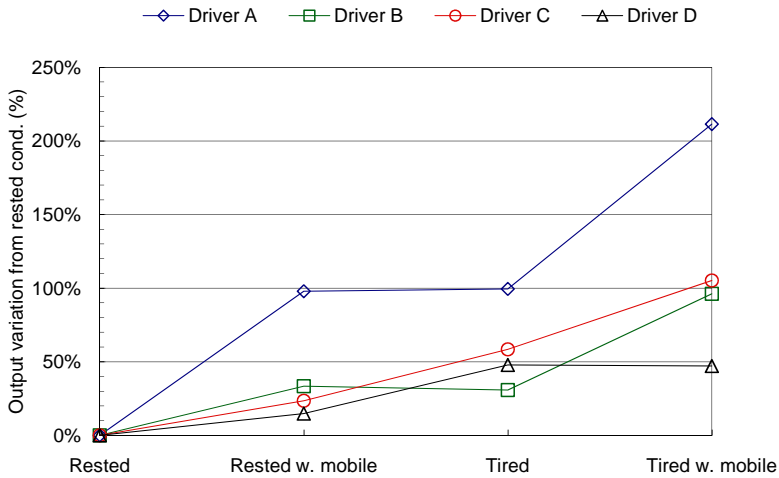


Figure 5.7: Comparison of the algorithm mean output value of different drivers.

Thus, in perspective of a possible industrial application of such a tool, the system should learn the basic driving style of each driver identifying periods in which the vehicle is driven at almost constant speed and store the information for each driver.

### 5.3.3 Reactions to sudden vehicle lateral skid

As shown in Section 5.3.1, in the test protocol of the experimental campaign some tests with the vehicle lateral skid were also included. These were carried out to test the real-time parameter changing feature described in Section 4.3 and to analyse the drivers' response to such a disturb.

Acquired data were analysed in the time domain computing the reaction times and the drivers ability times. The reaction time was considered as the time between the impulse on the steering angle, given by the operator from the control desk, and the reaction of the driver on the steering wheel. The ability time was considered the time the driver needs, after the reaction, to complete the manoeuvre and bring back the vehicle to the straight direction.



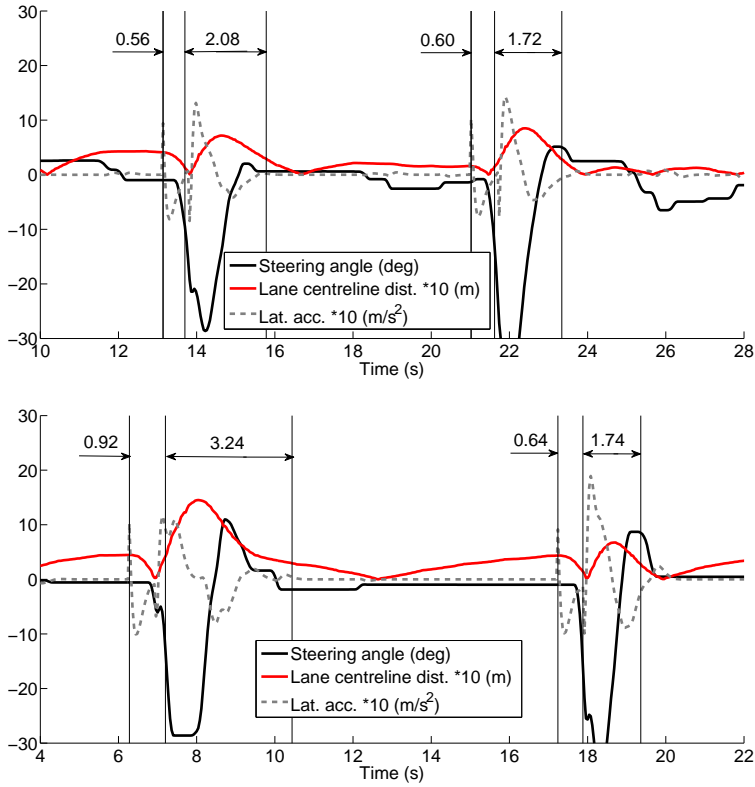


Figure 5.8: Acquired signals during two vehicle lateral skids at 70 km/h with a driver in rested condition (top) and in tired condition (bottom). Reaction times and driver's ability times are also shown.

Figure 5.8 shows, as example, the signals of two lateral skids at 70 km/h with a driver in both rested and tired conditions. After the time instant of the lateral skid (first vertical line), the derivative of the distance from the lane centreline changes, becoming much higher than before. The vehicle crosses the lane centreline (the signal is always positive, but this can be detected with a cusp at zero) and the driver, after a reaction time, reacts on the steering wheel to avoid the vehicle from excessive lateral skidding. The reaction time was evaluated considering a percentage of the first peak of the steering wheel angle (currently set to 30%). From this time instant, the driver is concentrated on the manoeuvre and tries to bring back the vehicle on its original path. To do this, he often needs

to make more corrections on the steering wheel (as in the example in the picture for the tired condition). The manoeuvre is then considered completed when the distance from the lane centreline goes and remains below a threshold value (currently set to 0.3 m). Similarly, the lateral acceleration signal can be used with an opportunely set threshold. The ability time is computed as the time from the finish of the reaction phase to the end of the manoeuvre.

The application of this analysis to all drivers of the experimental campaign gave the following results. Analogue reaction times were found between rested ( $0.65 \pm 0.08$  s) and tired conditions ( $0.64 \pm 0.07$  s). On the other side, tired drivers were found having longer ability times, with a mean difference of about 0.1 s ( $2.95 \pm 1.12$  s for rested drivers and  $3.09 \pm 1.97$  s for tired drivers). However, these data appear to be very much scattered and, being the sample of just 12 people, no significant conclusion can be made.

The test demonstrated however the potentialities of the real-time interaction with the simulated drives and further developments will be carried out for the next experimental campaigns, such as considering disturbs which should lead the drivers to act also on the brake pedal to better highlight their reactions.

## Part II

# Analysis and design of an automatic transmission for motor-scooters



## Chapter 6

# Background of the research and studied transmission

### 6.1 Energy efficiency problems of motor-scooter transmissions

In last years, environment protection has become one of the main issues for the automotive industry. At the beginning, the research efforts were focused on the engines and especially on their pollution emissions, such as HC, NO<sub>x</sub> and CO. More recently, an increasing attention has been devoted also to the overall efficiency of the vehicle, in order to find out all possible ways for reducing the fuel consumption and hence the carbon dioxide emissions (main responsible for the greenhouse effect).

For this reason, the research field has extended from the engine to all the powertrain, to reduce its energy loss. In addition to this, researches are more generally focused on all the vehicle subsystems, with the aim of increasing their efficiency and to reduce all the inertias.

Considering the two-wheelers class, and in specific motor-scooters (Figure 6.1), the mechanical continuously variable transmission (CVT) represents the main source of energy dissipation of the powertrain. This transmission, shows in details in Figure 6.2, is widely (almost always) employed in motor-scooters, being a simple automatic transmission with low manufacturing cost and high comfort performance due to the infinite transmission ratios. The classic CVT is made of two conic pulleys, which both have a fixed flange and a movable flange, and a rubber V-belt. The control of the transmission ratio is completely mechanical, carried out



Figure 6.1: Vespa Motor-scooter (left) and CVT assembly (right).

by a centrifugal variator (with rollers) on the drive pulley and a reaction spring on the driven pulley.

The energy losses on the CVT are due to the rubber V-belt, which is employed in motor-scooter applications. The hysteresis of the rubber, which is highly deformed when the belt is running on low radii of the pulleys, is one source of energy loss. The other one is the slip between the belt and the pulley contact surfaces, which leads to inefficiency the more the contact surface is wide in radial direction. The maximum overall efficiency can be typically of the order of 80%, but it is generally very much lower outside the ideal operating conditions [20, 19, 10], as shown in 6.3.

Metallic or hybrid belts, developed for the automotive industry to transmit more torque with respect to the rubber belt, have slightly increased the mechanical CVT efficiency, mainly reducing the hysteresis phenomenon. More recently, specific chains for CVT have been developed and launched in the market (such as in the Audi Multitronic [1]). In addition to the maximum transmissible torque, they have increased the mechanical CVT efficiency, reducing very much the radial dimension of the contact area between chain and pulley (which then gives less slip). This, in turns, requires high pressure to transmit the driving torque and therefore high cost for the materials employed. In these solutions, both with metallic belt and chain, a controlled active system is generally employed to control the pressure of the belt – pulley interface to the minimum required for the torque transmission, avoiding extra pressure,

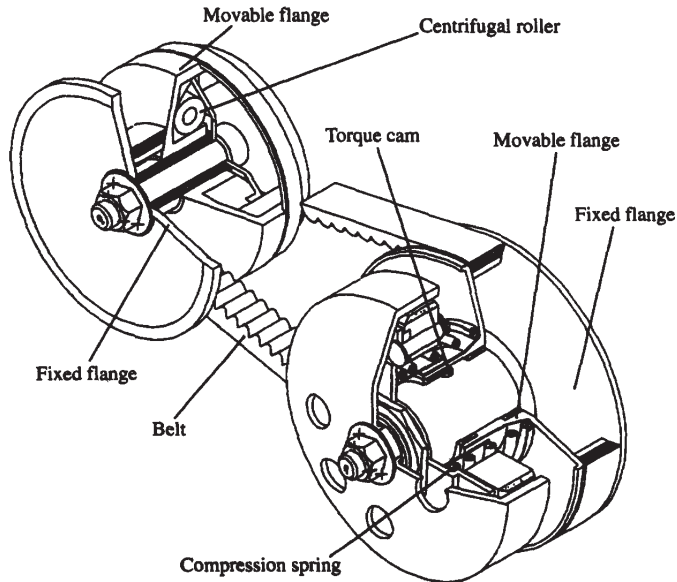


Figure 6.2: Scheme of a classic Continuously Variable Transmission (CVT) with V-belt. [10].

which is responsible for higher friction forces and slip losses. This system, which is typically hydraulic is associated with higher cost, higher weight and layout issues for all the components.

Because of the limits of the CVT, in motor-scooters (and in general in small power vehicles), where an automatic transmission is required for driver's comfort, there is the need of looking for low-cost automatic transmissions with high efficiency. In the next section the state of the art of automatic transmissions is briefly treated, focusing on innovative solutions suitable for the present application.

A high efficiency automatic transmission, specifically designed for small to medium displacement two-wheelers, becomes of particular interest also for applications with electric motors in both pure electric and hybrid vehicles. Indeed, even if electrical motors have a nominal characteristics (at constant power), which is well suited for a direct connection to the driving wheels, the maximum torque limit and the required maximum velocity may suggest a powertrain with the possibility of changing gear ratio. This can increase the maximum road slope that the vehicle can ascend and, at the same time, let the vehicle reach a reasonable top speed.

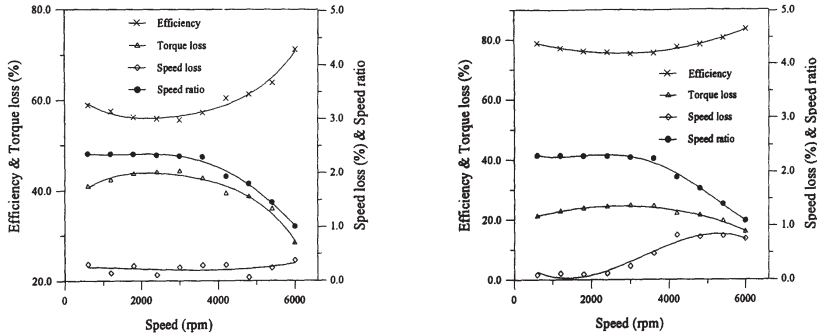


Figure 6.3: CVT efficiency at two different input torque values [10].

By this way, the electrical motor may become downsized (i.e. designed for a lower torque), with sensible advantages in terms of dimensions and costs also related to the batteries.

In addition to this, even if a variable ratio transmission has lower efficiency than a direct single speed transmission, the use of more transmission ratios can let the electric motor work nearer to the ideal speed and torque ranges, where its efficiency is maximum.

## 6.2 Alternative automatic transmissions

Several types of automatic transmission have been developed and are currently employed in the market for different vehicle applications, from small mopeds to big trucks. In general, a comparison between different solutions can be made focusing on these aspects:

- transmission energy efficiency;
- comfort;
- performance (e.g. gear shifting time);
- manufacturing cost.

From the comfort point of view, it is worth noting that a fundamental characteristic of some automatic transmissions, is the so called power-shift. This means that the changing of the gear ratio is carried out without interruption of the torque flow from the engine to the wheels,



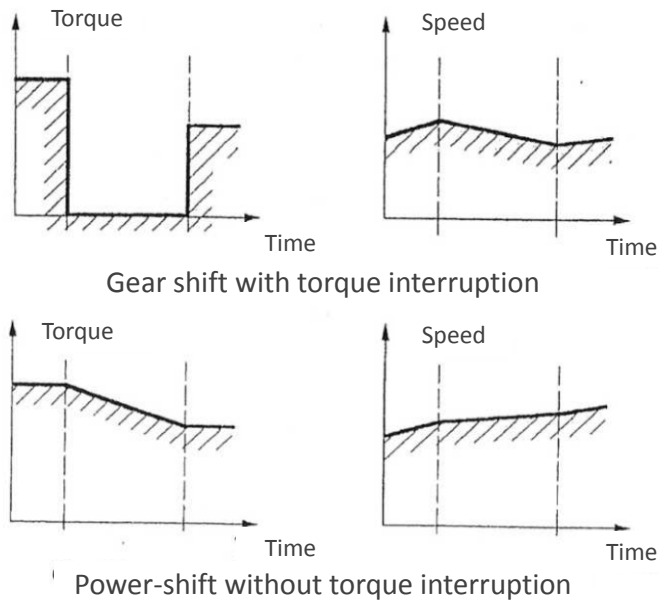


Figure 6.4: Torque and speed in a traditional gear shift and in a power-shift.

as shown in Figure 6.4. If the torque is interrupted (e.g. during the synchronization in a manual transmission) the acceleration of the vehicle sinks to negative values (the speed decreases) and then, when the new gear is engaged, becomes once more positive. This leads to high jerks, which are demonstrated to be associated with low comfort. On the contrary, in a power-shift the vehicle acceleration is always positive thus having a good comfort for the driver and the passengers.

Depending on the application, the transmission objective previously listed can have different priority. For motor-scooters, low manufacturing costs and comfort have always been important features of the powertrain. As pointed out, energy efficiency has recently become an other important objective. Performance is not as important as the other features, being motor-scooters less sport-oriented than motorbikes.

An innovative transmission for motor-scooters should then be competitive with the classic CVT from these point of views. Increasing the energy efficiency is the main objective but, at the same time, in order to be competitive, low manufacturing costs and high comfort typical of

CVT should be kept or just slightly worsen.

Among the theoretically possible transmissions for two-wheelers applications, there are several systems, which will be briefly described in the following sections. It is worth noting that two typical automotive solutions were not taken into account: the automated manual transmission (AMT) and the classic automatic transmission with torque converter and epicyclic gearings. The former, even if it has the very high mechanical efficiency typical of transmissions based on gears, does not carry out the power-shift and has therefore low comfort. The latter has dimensions and costs which are not suitable for the present application, even if the comfort can be very high.

### **6.2.1 Electronic controlled continuously variable transmission (ECVT)**

This automatic transmission can be simply derived from the conventional mechanically controlled CVT by implementing an active control on at least one pulley. The active system can be electrical or hydraulic: the former characterized by less cost and less axial forces on the pulley, whereas the latter has higher cost due to the hydraulic components but can reach higher axial forces, thus transmitting higher driving torques.

In two-wheeler applications, compact dimensions and low manufacturing cost are fundamental. For these reasons, the solution of a controlled CVT with an electric motor replacing the centrifugal variator appears to be the most suitable. An industrial solution based on this concept has been already introduced in the market by Piaggio Aprilia. In this solution, the control logic can follow different automatic settings (for low fuel consumption or maximum performance) or force the system to work on discrete transmission ratios, implementing a pseudo-sequential seven speed manual.

By implementing control logics which let the engine work around the best operating conditions from the efficiency point of view, the global energy efficiency of the powertrain can be increased with respect to a mechanically controlled CVT. However, without controlling the pressure on both the pulleys and using a rubber belt for low manufacturing cost, the energy efficiency of the mechanical system does not change with respect to the conventional CVT.

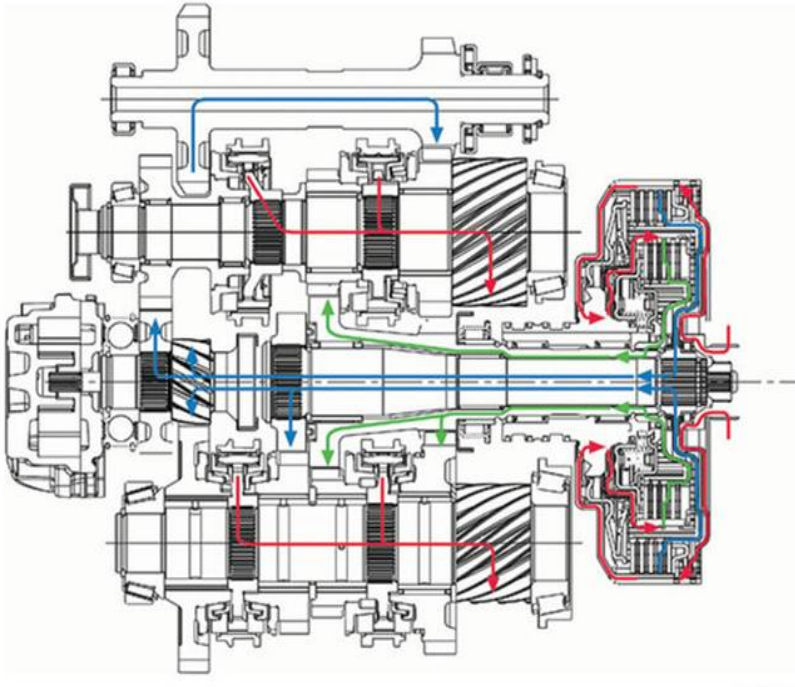


Figure 6.5: Dual clutch transmission with torque flows. Input and output torque: red; odd speeds: blue; even speeds: green.

### 6.2.2 Dual clutch transmission (DCT)

Dual clutch transmissions (DCT) represent an evolution of automated manual transmissions (AMT). The main innovation of DCT is the power-shift, which is performed thanks to the use of the two clutches [21, 36].

The system, which is shown in Figure 6.5, is basically a multi-speed automated manual transmission with two primary shafts, which are connected to the engine by two different multi-disc clutches. The first clutch engages the primary shaft of the odd speeds (and the reverse speed in cars), whereas the second clutch engages the primary shaft of the even speeds. The clutches are usually concentric, as well as the primary shafts, which are assembled one inside the other. Depending on the specific system, it can be a single secondary shaft for all the speeds or two different shafts for the odd and the even speeds (as that in the picture).

During a gear shift, the clutch of the gear to be engaged begins to

transmit torque, while the clutch of the current speed begins to open. During a synchronization phase, the torque is transmitted by both clutches (flows blue and green in the picture), thus carrying out the power-shift.

The transmission elements are actuated by a hydraulic system controlled by a specific electronic unit.

The main advantages of DCT are the high efficiency typical of mechanical transmissions based on gears and the power-shift. With the developing of complex logics, this system has reached a very high level of comfort and performance at the same time. It is worth noting that during the gear shift, avoiding the engine from falling to low speeds and then accelerating, the DCT generally leads to higher energy efficiency than a manual transmission.

On the other side, the DCT has high costs due to the hydraulic and the control systems. These systems leads also to more complex mechanical assemblies and layouts than a corresponding manual transmission, increasing also the global weight. Finally, the control logics, which are needed to reach high comfort and performance, are complex and need a fine tuning (high cost and developing times).

Thanks to its many advantages, the DCT has gained interest in the automotive industry in last years. Current solutions are the DSG from Volkswagen and the DCT from Renault. More recently, the Honda Dual Clutch system has been developed, representing the first application on two-wheelers [27].

### 6.2.3 Zeroshift

The Zeroshift transmission is an innovative solution based on classic manual transmissions, where the synchronizers are replaced by specific designed rings. These rings are automatically actuated by a controlled active electric, pneumatic or hydraulic system, which allows quick power-shifts [25].

The Zeroshift rings, shown in Figure 6.6 for a gear pair, work together and represent a dog engagement between the central hub (fixed to the output shaft) and the frontal dogs on the gears. The dog is split in two rings, in order to eliminate the backlash typical of dog engagement transmissions. The first ring is engaged to take up the drive torque coming from the gear, whereas the second is brought in afterwards to take up the backlash. Each ring has two different faces on each side. One is used to transmit torque, the other is a ramp for disengagement. Each ring



Figure 6.6: Zeroshift transmission elements for a gear pair [25]. The rings are in red and blue.

can transmit torque just in one direction, i.e. coupled with one of the two gears, whereas in the other is employed as backlash limiter. When the first gear is engaged, the ring which is not transmitting torque can be axially moved towards the other gears engaging it instantaneously. The previous gear is disengaged, thanks to the ramp profile, by the overrunning of the ring with respect to the gear dogs.

This system is still prototypical and, up to now, no industrial applications in commercial vehicles have been presented. The main advantages are similar to those of the DCT, even if a less comfortable power-shift is expected. On the other side, being the axial force for the ring movements very low, the size and the complexity of the controlled active system is expected to be lower. Also from the mechanical point of view, the system is simple having modified few components from the manual transmission. Finally, there is a few know-how, being this system innovative.

#### 6.2.4 Automated manual transmissions with centrifugal clutches

Other systems, derived from the classic manual transmission, make use of centrifugal clutches to connect the gears to the primary or secondary shaft of the gearbox. The centrifugal clutches, whose engagement is related to the vehicle speed, replace the synchronizers of manual transmissions,

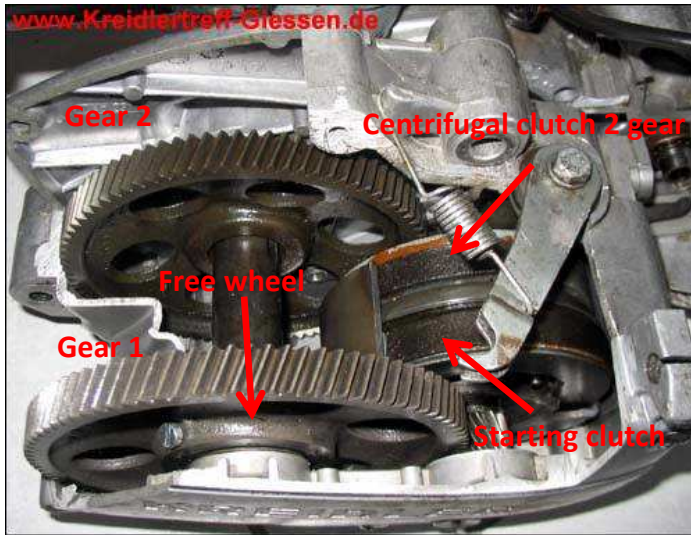


Figure 6.7: Kreidler Flory gearbox [35].

carrying out the same functions automatically at fixed vehicle speeds. The free wheels are needed to disconnect the non working gears from the shafts when a new gear is engaged<sup>1</sup>.

This system represents a mechanically controlled automatic transmission, which performs also the power-shift. In fact, during the synchronization phase, the centrifugal clutch transmits drive torque to the the wheels [35].

Transmissions based on this principle were employed in the seventies in small displacement mopeds in the German and Austrian industry. Examples of this application are represented by: the Puch Maxi, the Kreidler Flory, which is shown in Figure 6.7, and the Sax Saxonette. In these cases, the automatic transmissions was offered as alternative to the stock manual transmission.

These systems, which have only two speeds, did not found wide applications due to their limits in terms of comfort and performances, compared to the low cost CVT belt transmission, which becomes widely employed in the eighties.

However, being the transmission based on gears, they generally have higher energy efficiency than the CVT and therefore have nowadays

<sup>1</sup>The principle of this kind of transmission is described in detail in Section 6.3.

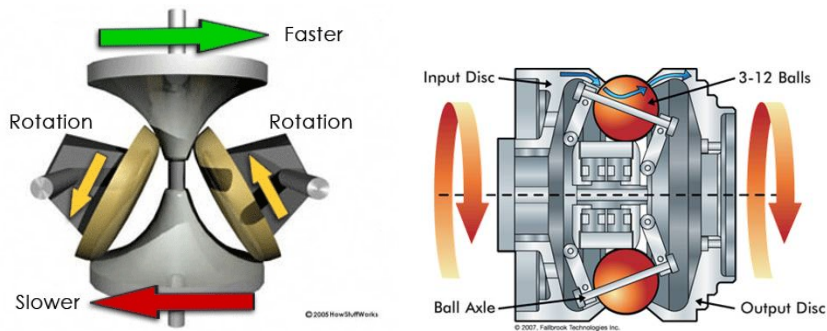


Figure 6.8: Half-toroidal CVT (left, displayed vertical) and NuVinci transmission (right, displayed horizontal).

gained new interest. It is also worth noting that, from the mechanical point of view, the system is quite simple, thus having low manufacturing cost, few layout problems and low weight. On the other side, if pure mechanical control of the gear shift is kept for low cost, the comfort of the transmission is lower than a classic CVT because of the feeling of the gear shift when the free wheel is disengaged.

Other possible powertrain solutions based on similar concepts can be found in the technical literature, as those presented in [7, 24]. Those systems, mainly due to their complexity, have not found industrial applications.

### 6.2.5 Toroidal CVT and NuVinci transmission

These transmissions are particular mechanical CVT where the drive and the driven pulleys are collapsed in a single assembly with an intermediate element, which transmits the torque. The transmission ratio is continuously changed varying the radius of the contact forces between the intermediate element and the input and output elements.

In the automotive industry, an application of this concept is represented by the Nissan Extroid CVT. Its scheme is shown in Figure 6.8 (left side). The input and output elements are half toroids with rollers between them. The rollers rotate around their axes to transmit the motion from the input half toroid to the output one. In order to change the transmission ratio, the orientation of the rollers is changed, so that the contact points between the half toroids moves to a higher radius, on one side, and to a lower radius, on the opposite side.

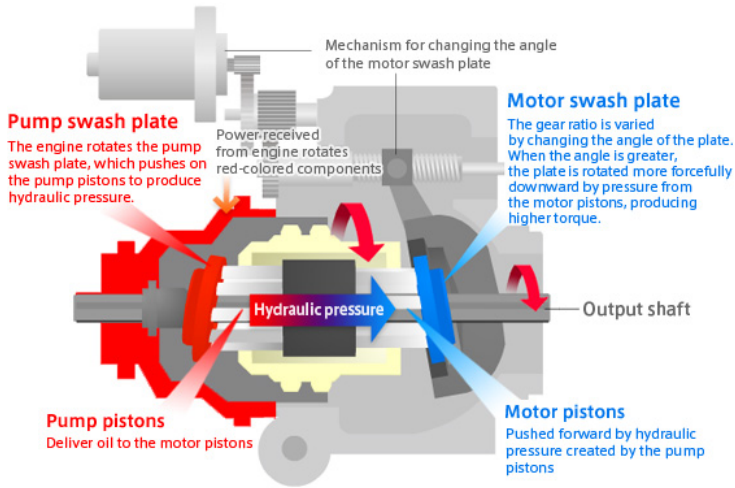


Figure 6.9: Honda Human Friendly Transmission (HFT) [28].

A similar system has also been developed, called NuVinci [14]. As shown in Figure 6.8, the concept is analogue to the half toroidal transmissions, with some differences. This system makes use of balls instead of rollers and input and output discs differently shaped. In this case, by moving the rolling axis of the balls, the radii of the contact points from the ball axis change, varying the transmission ratio. This system is also known as Continuously Variable Planetary (CVP).

In general, for both systems, high pressure (preloading the inputs and output discs or half toroids) is needed because of the very small contact area, which has to be lubricated with specific traction fluids. In order to accurately set the orientation of the axes of the rolling intermediate elements, a controlled system is also needed.

The advantages of these systems are the light weight and simplicity with respect to a gear transmission, together with low manufacturing and maintaining costs.

### 6.2.6 Hydraulic transmission: Honda HFT

This transmission differs from the others presented, being the unique with an other type of power involved in the powertrain. This system is, in fact, a hydraulic transmission which has been recently introduced into the motorcycle market by Honda [28].



The Human Friendly Transmission (HFT), shown in Figure 6.9 is based on a hydraulic pump – motor system with continuously variable transmission ratio. The engine is connected to the pump swash plate, which alternately pushes the pump pistons generating hydraulic pressure in the cylinders. On the other side of the cylinders, the motor pistons are pushed by the pressure. They transfer the torque on the motor swash plate, rotating it. The inclination of this plate can be changed with a simple mechanism connected to an electric motor, thus changing the torque transmitted (the transmission ratio).

Even if the transmission requires the hydraulic system, the HFT results very compact, fitting near the engine in the Honda motorbike. Moreover, despite the double power types involved, the transmission itself and the control system result quite simple. However, with respect to pure mechanically controlled CVT, the system is expected to have higher cost. Finally, from the energy efficiency point of view, the system has a higher efficiency (with respect to the CVT).

### 6.2.7 Considerations about the systems presented

The transmission systems presented have advantages and disadvantages, which make them being competitive to each other. The choice of a system depends on the objective of the specific application. In the case of the present work, i.e motor-scooters or small sized vehicles (endowed with combustion engines or electric motors), high efficiency and low manufacturing costs were considered the main features of the powertrain, keeping also the comfort as a fundamental aspect.

Among the solutions presented, transmissions based on gears have typically the best mechanical efficiency, but require specific mechanisms (usually based on friction) to change between the discrete gear ratios and to carry out the power-shift. Their cost is in general higher than that of CVT, but among the other high efficiency automatic transmissions, they are absolutely competitive from this point of view.

In the present work, the solution of automated manual transmission with centrifugal clutches was chosen for further analyses and it is described in more details in the next section. Such system was selected to obtain a higher overall efficiency with respect to the conventional CVT belt transmission, maintaining, at the same time, a sufficient level of comfort with the power-shift. With respect to the other systems derived from manual transmissions, this solution has a low manufacturing cost mainly

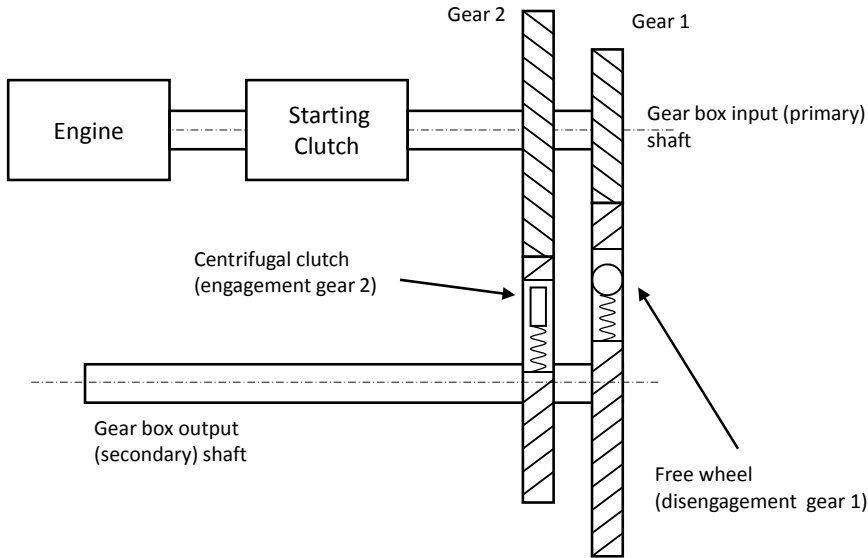


Figure 6.10: Scheme of the two-speed transmission.

due to the simple mechanical actuation and control of the gear shift. The limits of comfort and performance highlighted in Section 6.2.4 can be nowadays overcome using multi-speed systems and technologies, at low costs, which were not available in the seventies.

### 6.3 Layout and characteristics of the studied system

Automated manual transmissions with centrifugal clutches have been already introduced in Section 6.2.4. In the following, their working principle is deeply analysed and their architectures are presented.

#### 6.3.1 System working principle

The working principle of the analysed powertrain can be easily understood with reference to the simple case of the two-speed transmission, such as that of the Kreidler Flory shown in Figure 6.7. In the scheme shown in Figure 6.10 there is a centrifugal clutch (called starting clutch) prior to the gearbox, necessary for starting the vehicle from zero speed. Then, two

gears are fixed to the primary shaft of the gearbox, while the corresponding gears are connected to the secondary shaft through a free wheel (for the first speed) and a centrifugal clutch (for the second speed).

Considering a simple acceleration manoeuvre, after the engagement of the first centrifugal clutch, the first gear is engaged and the drive torque is transmitted to the output shaft by the free wheel. At a given vehicle speed, the centrifugal clutch mounted on the second gear begins transmitting torque to the output shaft. The torque transmitted by friction increases with the vehicle speed until all the drive torque is transmitted by the centrifugal clutch, and the free wheel opens. From this point, the centrifugal clutch acts as a synchronizer, but continuing transmitting torque to the drive wheel. When it engages, the vehicle is finally in second gear and the gear shift is completed.

This concept can be generalized to a system with  $n$  (more than two) gears. The main elements required are the centrifugal clutches to engage the new gears at given vehicle speeds and the free-wheels to disengage the previous gear disconnecting the primary and the secondary shaft. As shown in the next section, these elements can be arranged in different ways keeping the same working principle, which can be summarized in the following phases:

1. gear  $i$  is engaged and transmit the drive torque;
2. the centrifugal clutch of gear  $i + 1$  begins to transmit torque (in this phase both gears transmit the drive torque);
3. the free wheel of gear  $i$  opens when the whole torque is transmitted by the centrifugal clutch of gear  $i + 1$ ;
4. synchronization phase: the drive torque is transmitted by the gear  $i + 1$  with a variable transmission ratio between  $\tau_i$  and  $\tau_{i+1}$ ;
5. engagement of the centrifugal clutch of gear  $i + 1$  (engagement of gear  $i + 1$ ).

It is worth noting once more that, thanks to the centrifugal clutches, this transmission performs the power-shift. An other important aspect to point out is that, because of to presence of the free wheels, this system lacks of any engine braking, with the only exception of the last gear; this, in fact, does not need the free wheel for disengagement. In order to allow the engine braking torque to be transmitted, a locking system of the free

wheels should be provided, which has of course to be disconnected when the gear shift occurs.

### 6.3.2 System architectures

In a first part of this work, different system architectures of the studied transmission were analysed. In fact, this transmission can be designed following different architectures, changing the number of the gears and the position of the free wheels and centrifugal clutches on the primary or secondary shaft. Before going into details about the modelling and simulation, this analysis is briefly presented.

A generic  $n$ -gears system, based on the working principle described in Section 6.3.1, is shown in Figure 6.11 and, with a different architecture, in Figure 6.12.

The source of power can be an internal combustion engine or an electric motor, which generally requires just a two-speed system.

In order to keep an acceptable mechanical complexity, the transmission should be made of two shafts (primary and secondary) with optional primary and final ratio. A primary ratio can be needed for layout issues, to have room for the assemble of the engine (or motor). On the other side, the final ratio is generally required for reducing the torque, and hence the dimensions, of the centrifugal clutches on the gearbox shafts.

Among the centrifugal clutches, the 1<sup>st</sup> gear clutch has a different task, being the starting clutch. This, in fact, has to rotate responding to the engine speed (for starting the vehicle from zero speed), whereas the other clutches must respond to the vehicle speed, shifting gears at given and different vehicle speeds.

The starting clutch can be positioned in these ways:

- before the gearbox;
- as 1<sup>st</sup> gear clutch on the primary shaft;
- as 1<sup>st</sup> gear clutch on the secondary shaft.

If it is before the gearbox, as in Figure 6.10, it is always subjected to the drive torque. On the contrary, if it is inside the gearbox as 1<sup>st</sup> gear clutch, when a different gear is engaged, it is unloaded. Assembling the starting clutch in the gearbox, if there are no dimensional issues, allows also to reduce the system complexity and the number of components.

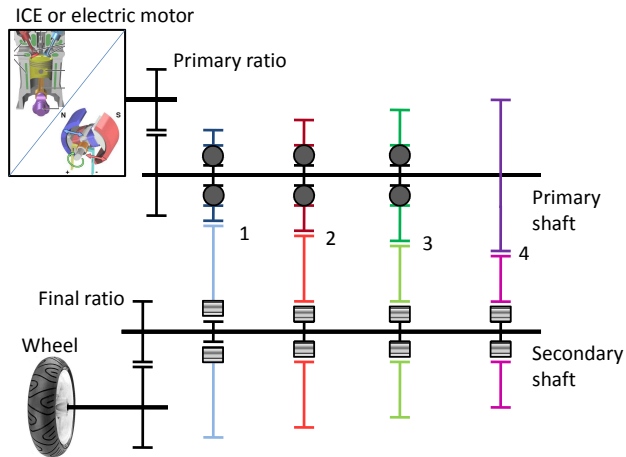


Figure 6.11: Architecture of a four speed transmission with free wheels on the primary shaft and centrifugal clutches on the secondary shaft. Free wheels are represented with circles, whereas centrifugal clutches with symbols for the friction pads, connected to the right element (shaft or gear).

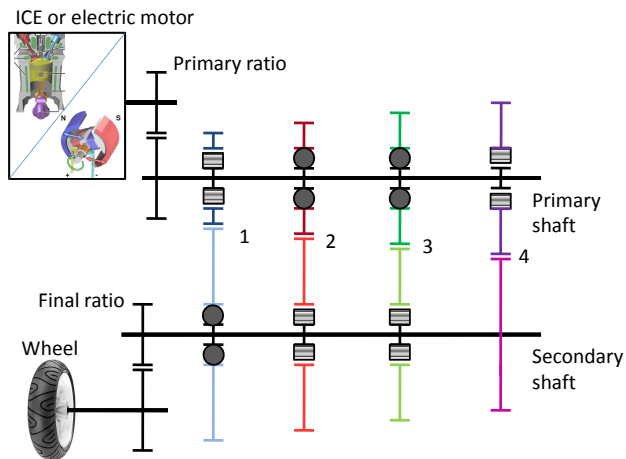


Figure 6.12: Architecture of a four speed transmission with starting (first gear) clutch on the primary shaft, as well as the last gear clutch. Other clutches are on the secondary shaft. See Figure 6.11 for symbol legend.

The two solutions of having the starting clutch as 1<sup>st</sup> gear clutch on the primary or secondary shaft have pro and con. If the starting clutch is on the primary shaft (Figure 6.12), it can be easily assembled with the friction pads rotating with the primary shaft itself, so that the clutch responds to the engine speed. Moreover, the torque to be transmitted is reduced by the 1<sup>st</sup> gear ratio, thus having smaller dimensions. On the other side, when the primary shaft and, therefore, the engine speed, goes below the engagement speed, for instance for the lack of engine braking, the clutch opens. This means that when drive torque is once more applied, slipping occurs for a new clutch engagement with energy loss and friction pads consumption. This can be avoided assembling the 1<sup>st</sup> gear clutch on the secondary shaft (Figure 6.11). In this case, it must be fixed to the gear, so that it responds to the engine (and not the vehicle) speed. However, when a different gear is engaged, its velocity is related to secondary shaft and, therefore, it opens just when the vehicle speed goes below the engagement speed limit. From the design point of view, this solution is a little bit more complex, assembling the clutch friction pads on the gear (and not on the shaft) and requiring the transmission of higher torques.

For what concerns the position of the other centrifugal clutches, which must respond to the vehicle speed, the most simple solution is assembling them on the secondary shaft, fixed with the shaft itself. Moreover, if they were on the primary shaft (fixed to the gears), they could not be drag by the secondary shaft because of the presence of the free wheels, which avoid any torque back flow. Only if a mechanical block of the free wheels (when they are not needed) is provided, the centrifugal clutches can be placed on the primary shaft. The last gear centrifugal clutch, being no free wheel in last gear, can be assembled on either shafts: on the primary, fixed to the gear (Figure 6.11) or on the secondary, fixed to the shaft (6.12).

The position of the free wheels depends on that of the centrifugal clutches and they are assembled on the other shaft with respect to that of the centrifugal clutch of each gear.

It is worth noting that the basic mechanical transmission can be endowed also with active systems to modify its behaviour. The centrifugal clutches could be partially controlled to modify their mechanical characteristics, e.g. changing the engagement speed. The free-wheels, as already pointed out, could be blocked when they are not needed for the gear shifting, so that the engine braking torque, or the electrical braking

torque, can be transmitted also in other than last gear.

In the next chapter, a generic simulation model for the transmission system is presented. The model allows the simulation of all possible architectures discussed. Some of them are analysed by simulation results in Chapter 8, with reference to applications on an internal combustion engine and an electric motor.





# Chapter 7

## Powertrain simulation model

### 7.1 Equations of the system

In this work, a generic dynamic mono-dimensional model of the powertrain with the studied transmission presented in Section 6.3 was developed. This model is shown in Figure 7.1 with all main quantities involved. In the picture a four-speed gearbox is represented as example with a specific layout of free wheels and centrifugal clutches. A two-wheeler with rear drive wheel is considered, but in general also four wheel vehicles can be analysed with the same model just doubling the wheel inertial terms and considering the wheel torques to be split between two drive wheels. It is worth noting that no tire slip model was implemented, being the focus of the work on the powertrain behaviour.

The model of a generic  $n$ -speed system is made of rotational inertias connected by rigid shafts, i.e. damping and stiffness are considered infinite. Referring to the picture, the bodies involved in the model are (with their inertia):

- engine (or electric motor) with driving gear of the primary ratio ( $J_e$ );
- primary shaft with driven gear of the primary ratio ( $J_p$ );
- $n$  gears on the primary shaft ( $J_{g,i}$ );
- $n$  gears on the secondary shaft ( $J_{G,i}$ );
- secondary shaft with driving gear of the final ratio ( $J_s$ );

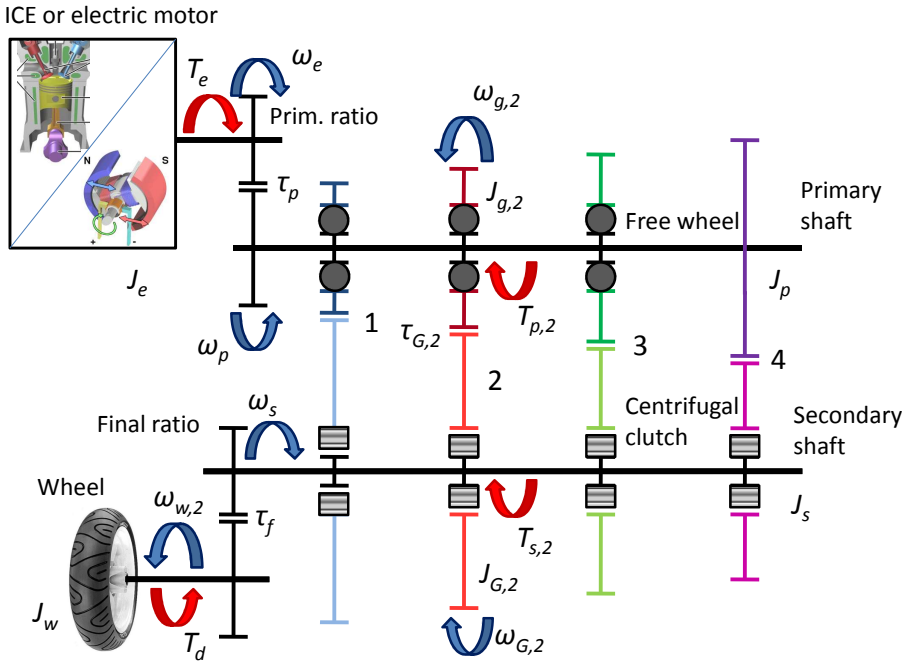


Figure 7.1: Simulation model of the transmission studied (case with four gears and a specific configuration of free wheels and centrifugal clutches). The quantities related to the gears are represented just for the second gear.

- drive wheel(s) with vehicle and driven gear of the final ratio ( $J_w$ ).

The system is subjected to external torques which are:

- engine (or electric motor) torque (either drive or braking torque) ( $T_e$ );
- drag torque at the wheel ( $T_d$ );

whose expressions are presented in the following. In addition to these, internal torques between the gears and the primary and secondary shafts are introduced by these friction elements:

- free wheel ( $T_{f,i}$ );
- centrifugal clutch ( $T_{c,i}$ )

These last torque terms depend on the constitutive equations of free wheels and centrifugal clutches, also shown in the following.

Being all gear ratios constant, the model equations can be written considering just these degrees of freedom:

- primary shaft angular velocity  $\omega_p$ ;
- secondary shaft angular velocity  $\omega_s$ ;
- $n$  angular velocities of the gears on the primary shaft  $\omega_{g,i}$ .

This can be done using the following relationships to obtain the angular velocities of the engine  $\omega_e$ , of the wheel  $\omega_w$  and of the gears on the secondary shaft  $\omega_{G,i}$ :

$$\begin{aligned}\omega_p &= \omega_e \tau_p \\ \omega_w &= \omega_s \tau_f \\ \omega_{G,i} &= \omega_{g,i} \tau_{g,i},\end{aligned}\tag{7.1}$$

where  $\tau_p$  is the primary ratio,  $\tau_f$  the final ratio and  $\tau_{g,i}$  the ratio of the generic gear pair.

The equilibrium equations of the powertrain model can be written, using the degrees of freedom just introduced, as:

$$\begin{aligned}\left(\frac{J_e \tilde{\eta}_p}{\tau_p^2} + J_p\right) \dot{\omega}_p &= \frac{T_e \tilde{\eta}_p}{\tau_p^2} - \sum_{i=1}^n T_{p,i} - S_p(\omega_p) \\ \left(J_s + \frac{J_w \tau_f^2}{\tilde{\eta}_f}\right) \dot{\omega}_s &= \sum_{i=1}^n T_{s,i} - \frac{T_d \tau_f}{\tilde{\eta}_f} - S_s(\omega_s) \\ \left(J_{g,i} + \frac{J_{G,i} \tau_{g,i}^2}{\tilde{\eta}_{g,i}}\right) \dot{\omega}_{g,i} &= T_{p,i} - \frac{T_{s,i} \tau_{g,i}}{\tilde{\eta}_{g,i}} - S_{g,i}(\omega_{g,i}),\end{aligned}\tag{7.2}$$

computing the inertial and torque terms on the primary and secondary shafts and those of the gear couples on the gears on the primary shaft. In the equations  $T_{p,i}$  is the generic torque of a free wheel or a centrifugal clutch on the primary shaft and  $T_{s,i}$  on the secondary shaft. Substituting to these terms,  $T_{f,i}$  or  $T_{c,i}$  depending on the specific case, every possible architecture of the transmission can be modelled with this equation system.

The inertial term of the wheel  $J_w$  of the model takes into account the inertia of the complete vehicle and that of the front non-drive wheel with

this relationship:

$$J_w = mr_w^2 + J_{w,2} \frac{J_{w,1} r_w^2}{r_{w,1}^2}, \quad (7.3)$$

where  $m$  is the vehicle mass,  $r_w$  the rear wheel radius (also called  $r_{w,2}$  in the following),  $r_{w,1}$  the front wheel radius,  $J_{w,1}$  and  $J_{w,2}$  the front and rear inertias of the wheels.

In the equations 7.2 the terms  $\tilde{\eta}$  represent the gear efficiency for each gear couple (using the same index of the gear ratio). When the torque flow changes sign, i.e. when the driving torque comes from the wheel (coast drive), the gear efficiency terms should be the reciprocal. This is implemented in the equations having:

$$\tilde{\eta} = \eta^{(3-2s_\eta)} \quad s_\eta = 1, 2, \quad (7.4)$$

where  $s_\eta$  is 1 when the drive torque comes from the engine and 2 when it goes in the opposite direction.

The final terms of all equations represent resistance torques due to friction and fluid dynamics effects. These are obtained, for each body, as function of its speed as  $s(\omega)$ , using the same index already in use. Computing the equilibrium using the three degrees of freedom already known, these terms become:

$$\begin{aligned} S_p(\omega_p) &= \frac{s_e(\frac{\omega_p}{\tau_p})\tilde{\eta}_p}{\tau_p^2} + s_p(\omega_p) \\ S_s(\omega_s) &= s_s(\omega_s) + \frac{s_w(\omega_s\tau_f)\tau_f^2}{\tilde{\eta}_f} \\ S_{g,i}(\omega_{g,i}) &= s_{g,i}(\omega_{g,i}) + \frac{s_{G,i}(\omega_{g,i}\tau_{g,i})\tau_{g,i}^2}{\tilde{\eta}_{g,i}} \end{aligned} \quad (7.5)$$

Finally, from the main equations of the system, the vehicle speed  $u$  can be easily obtained, having implemented no tire slip in the model:

$$u = \omega_w r_w = \omega_s \tau_f r_w. \quad (7.6)$$

The main terms of the model equations are described in more detail in the following sections.

### 7.1.1 Drive torque

The engine or the electric motor drive torque represents the input torque of the powertrain. This is function of  $\omega_e$  and depends also on the throttle input of the driver  $a$ , which can be between 0 and 1. Its expression is therefore:

$$T_e = T_e(a, \omega_e) \quad (7.7)$$

and can be implemented in the model as a look up table.

In both cases of internal combustion engine and electric motor,  $T_e$  can be a resistance torque. This occurs with engines, when the throttle signal is zero (engine drag torque), and in electric motors, when regenerative brake is implemented. In the first case, the engine drag torque is directly implemented in eq. (7.7); in the last case, the regenerative braking torque is implemented as shown in Section 7.1.3.

### 7.1.2 Drag torque

The vehicle drag force depends on three causes:

- rolling resistance;
- aerodynamic drag;
- road slope  $\alpha$ .

This is applied to the powertrain as a drag torque  $T_d$ , which is given by:

$$T_d = \left( mgf_r (\cos \alpha + \sin \alpha) + \frac{1}{2} \rho S C_x (\omega_w r_w)^2 \right) r_w, \quad (7.8)$$

where  $f_r$  is the rolling resistance friction coefficient,  $S$  the vehicle frontal surface,  $C_x$  the aerodynamic drag coefficient and  $\rho$  the air density. Additional drag torque is given by the braking torque, as described in the following section.

### 7.1.3 Braking torque

The braking torques do not appear directly in equations 7.2; they are, in fact, included in the drag and in the drive torques.

The braking is easily modelled considering that the braking torque of each wheel is an amount of the maximum allowable braking torque given by the tire–road friction coefficient  $\mu$ . This amount is set by the driver's

braking input signal  $b$ . The front  $T_{b,1}$  and the rear  $T_{b,2}$  braking torques are then obtained with the following equations [22]:

$$\begin{aligned} T_{b,1} &= br_{w,1}\mu \left( \frac{mga_2}{l} + \frac{mg\mu h}{l} \right) \\ T_{b,2} &= br_{w,2}\mu \left( \frac{mga_1}{l} - \frac{mg\mu h}{l} \right), \end{aligned} \quad (7.9)$$

where  $a_1$  and  $a_2$  are the distance between the centre of mass and the front and the rear axles,  $l$  is the vehicle wheelbase (given by  $a_1 + a_2$ ) and  $h$  is the centre of mass height from ground. From these equations, the following relationship of the brake bias can be obtained:

$$T_{b,1} = T_{b,2} \frac{a_2 + \mu h}{a_1 - \mu h} \frac{r_{w,1}}{r_{w,2}}. \quad (7.10)$$

The front braking torque influences the powertrain dynamics by adding a drag torque to that already computed in Section 7.1.2. This additional drag torque is obtained by the following equation:

$$T_{d,b1} = T_{b,1} \frac{r_{w,2}}{r_{w,1}} = T_{b,2} \frac{b + \mu h}{a - \mu h} \quad (7.11)$$

The rear braking torque can be considered split in two parts. The first one is the regenerative braking torque, which can be applied by the electric motor (if present). This torque is considered to be at maximum  $2T_e(1, \omega_e)$ , i.e. twice the maximum drive torque ( $a = 1$ ) at the current motor speed (see eq. (7.7)). This part is implemented in the model as a negative drive torque  $T_{e,b2}$ , given by:

$$T_{e,b2} = -\min(2T_e(1, \omega_e); T_{b,2}\tau_f\bar{\tau}_{g,i}\tau_p), \quad (7.12)$$

considering the current gear ratio  $\bar{\tau}_{g,i}$  and neglecting the inertial effects and the gear efficiencies when computing the torque from the wheel to the engine shaft.

The second part of the rear braking torque is applied on the wheel brake and it is therefore treated, like the front braking torque, as an additional drag term:

$$T_{d,b2} = T_{b,2} - \left| \frac{T_{e,b2}}{\tau_f\bar{\tau}_{g,i}\tau_p} \right|. \quad (7.13)$$

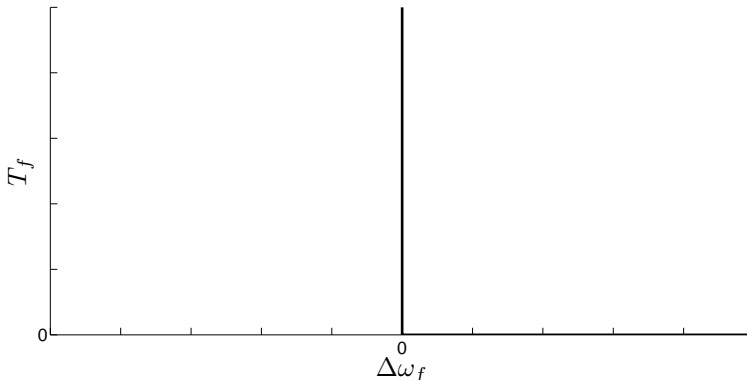


Figure 7.2: Free wheel characteristic.

#### 7.1.4 Free wheels

Free wheels have a torque–speed characteristic, shown in Figure 7.2, which allows the torque flow with equal input and output element velocities (free wheel is engaged). On the other side, no torque can be applied in the other direction and the two elements can freely rotate at different speeds. It is worth noting that, when the free wheel is engaged, the torque  $T_f$  can not be computed from the angular velocities of the input and output elements, being a static friction torque and hence depending on the other torques applied in the system.

The input and output elements are, in this application, the gear where the free wheel is mounted and the corresponding primary or secondary shaft. Even if in the last gear, where it is not necessary, there is no free wheel (like in Figure 7.1), it is nevertheless implemented in the model. This allows, as it will be shown in the next section, to keep a fixed model architecture. When not present, the free wheel is therefore modelled with a different constitutive equation which allows no speed difference and torque flow in both directions.

#### 7.1.5 Centrifugal clutches

As free wheels, centrifugal clutches generate an internal torque between the two elements to which they are connected. If the speed of the input and output elements are the same, the clutch is engaged and a static friction torque is transmitted. If this torque goes above the limit of

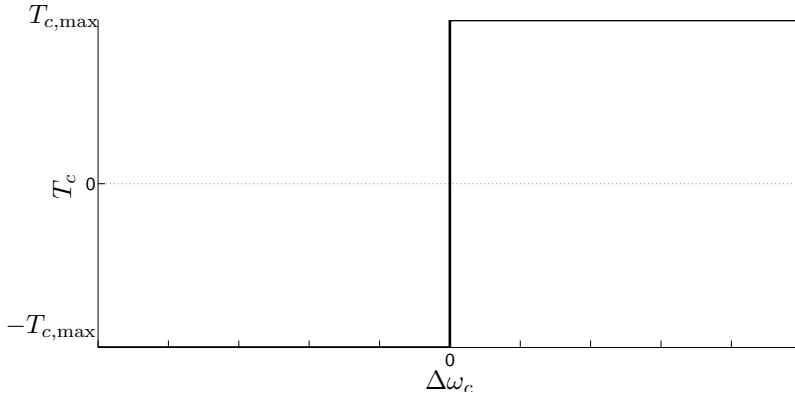


Figure 7.3: Centrifugal clutch (ideal) friction function characteristic.

the maximum static allowable torque  $T_{c,\max}$  (function on the clutch speed), the clutch is disengaged and the input and output element speeds becomes different. In this condition, the dynamic (maximum) friction torque of the clutch is transmitted. Considering no difference between the static and dynamic friction coefficients, this is once more  $T_{c,\max}$ . The described behaviour is represented in Figure 7.3 by the friction function characteristic.

The maximum transmissible torque of centrifugal clutches, which is the actual torque in dynamic friction (slipping) conditions, is, as well known, a quadratic function of the angular velocity of the element on which the friction pads are fixed. This is shown in Figure 7.4 and can be written, for a generic clutch of the  $i$  gear, as:

$$T_{c,i,\max} = k_{1,i} + k_{2,i}\omega_{c,i}^2, \quad (7.14)$$

where  $k_{1,i}$  and  $k_{2,i}$  are clutch design constants and  $\omega_{c,i}$  can be:

- $\omega_s$  (gear shifting clutch on the secondary shaft);
- $\omega_{g,i} = \frac{\omega_s}{\tau_{g,i}}$  (gear shifting clutch on the gear on the primary shaft);
- $\omega_p$  (starting clutch on the primary shaft);
- $\omega_{G,i} = \omega_p \tau_{g,i}$  (starting clutch on gear on the secondary shaft);

The clutch constants, which depend on the clutch dimensions, masses and spring preloads (see Section 8.1.1 and Section 8.2.2), can be determined from two specifications on the powertrain dynamic behaviour.



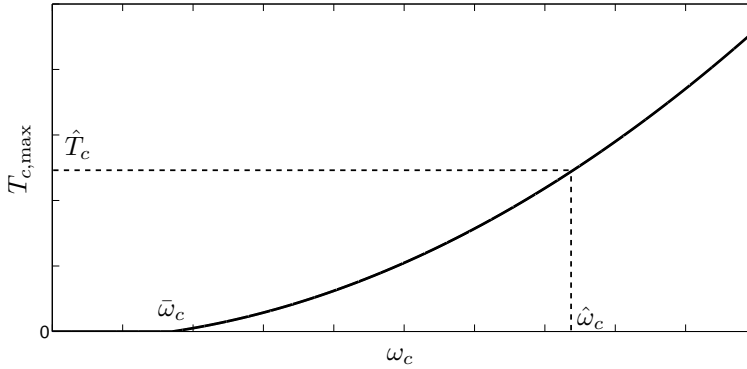


Figure 7.4: Centrifugal clutch characteristic.

Setting, in fact, the points of the clutch characteristic corresponding to the speeds  $\bar{\omega}_{c,i}$  and  $\hat{\omega}_{c,i}$ , eq. (7.14) can be written two times obtaining the constants.  $\bar{\omega}_{c,i}$  represents the speed at which the clutch begins to transmit torque;  $\hat{\omega}_{c,i}$  is the speed at which the clutch transmits the objective torque  $\hat{T}_c$ . This value can be set to the torque which causes the opening of the free wheel of the previous gear during a gear shift.

The clutch constants can then be obtained from:

$$\begin{aligned} 0 &= k_{1,i} + k_{2,i}\bar{\omega}_{c,i}^2 \\ \hat{T}_{c,i} &= k_{1,i} + k_{2,i}\hat{\omega}_{c,i}^2, \end{aligned} \quad (7.15)$$

as:

$$\begin{aligned} k_{1,i} &= -k_{2,i}\bar{\omega}_{c,i}^2 \\ k_{2,i} &= \frac{T_{c,i,\max}(\hat{\omega}_{c,i})}{\hat{\omega}_{c,i}^2 - \bar{\omega}_{c,i}^2}. \end{aligned} \quad (7.16)$$

## 7.2 Model implementation in Simulink

The dynamic model of the complete powertrain, described in the previous chapter, was implemented in Matlab/Simulink. This model receives, as input, the driver's throttle (accelerator) and the brake input signals and computes, as output, all kinematic and dynamic quantities of the powertrain (such as the shafts velocities, the vehicle speed, the engine torque, the clutches and free wheels torques and status, etc.).

The simulation model is completely parametric and, as already pointed out, all possible transmission architectures can be simulated. With a parameters Matlab file, all vehicle and transmission parameters are supplied to the Simulink model. After the simulation, a post-processing Matlab file generates automatically the output plots to analyse the powertrain behaviour.

Different architectures can be simulated, setting in the parameters file the position of the free wheels and the centrifugal clutches with the vector  $p$ . Each component of  $p$  can be 1 or 2, indicating that the centrifugal clutch of the gear  $i$  is on the primary or secondary shaft. The free wheel is then assembled, of course, on the opposite shaft. With electric motors, the starting clutch is often not required; in this case it is possible to set the first component  $p$  to 0.1 or 0.2, indicating that there is no starting clutch, but the free wheel (which is needed) is on the secondary or on primary shaft respectively. In general, the system is modelled considering centrifugal clutches and free wheels for all other gears. When, in the last gear, the free wheel is not present, a specific parameter which gives the maximum reverse torque of the free wheels, can be set to a very high torque value.

A typical issue when modelling static–dynamic friction elements, is correctly reproducing the behaviour of this phenomenon, building, at the same time, simple models. When free wheels are disengaged and centrifugal clutches are open or in slipping conditions, dynamic friction occurs and all angular velocities of eq. (7.2) are actual degrees of freedom of the system. On the other side, when one or more elements are engaged, some equations of the model result coupled because the respective angular velocities are no longer independent. In this case, the transmitted torque by these elements is unknown until the system dynamics is solved.

When building the model, this issue can be solved in several ways, such as implementing continuous friction functions or using switches between the two different conditions. Friction functions, such as those implemented in the driving simulator model (see Figure 3.10 at page 62), allow to keep all model degrees of freedom independent, computing the transmitted torque as function of the angular velocities even when the clutch, or the free wheel, is engaged. This leads to a simple model implementation, but, on the other side, the angular velocities are always different. The amount of this difference depends on the slope of the friction function, which, if too high, leads to numerical problems or require a very short sample time of the solver.

Being this activity focused on the powertrain (and not on the complete vehicle, such as in the driving simulator), the solution of the friction functions was discarded for the reasons just explained. It was chosen instead to use a switch signal  $s$  which is based, as shown in Section 7.2.2, on different status signals indicating the conditions of the clutches and the free wheels. This switch signal is used to alternately activate two different sub-models of the transmission:

- open system: there is no gear pair engaged, the primary and secondary shafts have independent velocities;
- closed system: a gear pair is engaged, the primary and secondary shaft have dependent angular velocities (gear ratio) and represent just one degree of freedom.

The model continuously monitors the conditions of all free wheels and centrifugal clutches and switches between the two systems stopping the previously active, giving the last state of the previous activated as initial condition of the other system, and activating it. The status signals of the free wheels and the centrifugal clutches are used, in both open and closed system, to select which inertias are rotating with the primary shaft and with the secondary shaft. They are used also to correctly compute the drive, the drag and the friction torques on the right shaft.

The Simulink model is shown in Figure 7.5, where the main blocks and their connection signals can be observed. The blocks are listed in the following, with their main functions.

- **Driver's inputs block:** it outputs the throttle and brake input signals. These can be implemented with simple functions, such as steps or ramps, or modelling a controller (virtual driver) based on the vehicle and/or the engine speed.
- **Input torques block:** the drive torque  $T_e$  and the drag torque  $T_d$  are computed, using the model equations presented in Section 7.1, from the throttle and the brake input signals and the angular velocities of the engine and the wheel.
- **Open system block:** the equations of the powertrain dynamics are integrated here when the model is in the open condition. More details about this block are given in Section 7.2.1.

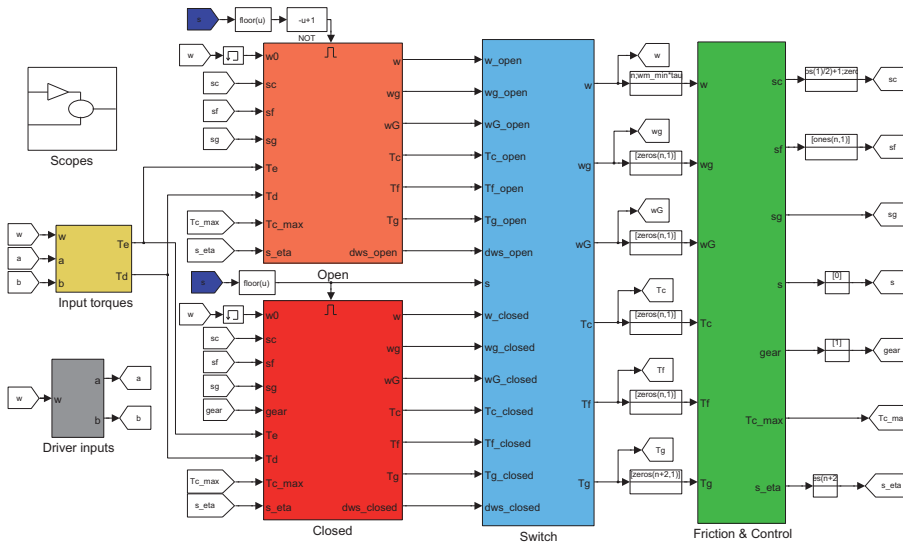


Figure 7.5: Main Simulink window of the dynamic simulation model of the powertrain.

- Closed system block:** the equations of the powertrain dynamics are integrated here when the model is in the closed condition. Also for this block, more details are given in Section 7.2.1.
- Switch block:** it selects the outputs of the open or the closed system, depending on which of them is currently active.
- Friction and control block:** it computes the maximum transmissible torques of the centrifugal clutches as function of their velocities. It also controls the free wheels and the centrifugal clutch status, monitoring the transmitted torques and the angular velocities; this block produces also all status signals and the switch signal, which controls the switching between the open and the closed system.
- Scopes block:** the main output quantities can be seen in graphs in this block for quick post-processing.

### 7.2.1 Open and closed system block

These blocks represent the core part of the model, solving the dynamics of the powertrain. Both the open and the closed systems carry out the

following operations:

- computation of the equivalent inertia terms on the primary and on secondary shaft depending on the status signals of the free wheels and the centrifugal clutches, associating each gear pair inertia to the shaft with which it is rotating fixed.
- computation of the torques on the primary and secondary shaft using the status signals of the free wheels and the centrifugal clutches;
- integration of the motion equations: two equation for the open system ( $\omega_p$  and  $\omega_s$ ), one equation for the closed ( $\omega_p = \omega_s$ ). The dynamics of the gear pairs which are free from any shaft are also computed;
- computation of all angular velocities of the system ( $\omega_e$ ,  $\omega_p$ ,  $\omega_s$ ,  $\omega_{g,i}$ ,  $\omega_{G,i}$  and  $\omega_w$ );
- computation of all static friction torques (of engaged free wheels and centrifugal clutches) from the dynamic equilibrium of the system.
- computation of the torque flow in each gear pair, which is needed to obtain the gear efficiency terms.

### 7.2.2 Friction and control block

This block, using the signals coming from the previous blocks, firstly computes the dynamic friction torques of the centrifugal clutches, by implementing the equations presented in Section 7.1.5.

Its main function is, however, to monitor the system condition and evaluate all status signals needed by the open and closed system blocks to write the equilibrium equations. To do so, this block observes the model output quantities at the previous time step (to avoid algebraic loops) and computes the following status signals:

- free wheel status  $s_{f,i}$  (0: disengaged, 1: engaged);
- centrifugal clutch status  $s_{c,i}$  (0: disengaged, 0.5: slipping, 1: engaged);
- gear pair status  $s_{g,i}$  (0: free from any shaft, 1: fixed on primary shaft, 2: fixed on secondary shaft);

- gear efficiency status  $s_{\eta_i}$  (1: torque flow from the engine to wheel, 2: opposite torque flow).

The status signal of the system, used to switch between the open and closed systems, is obtained from the status of the free wheels and centrifugal clutches, with this relationship:

$$s = \sum_{i=1}^n s_{c,i} s_{c,f}. \quad (7.17)$$

This signal can be 0 (open system), 0.5 (open system with a centrifugal clutch slipping), 1 (closed system) or 1.5 (closed system with a centrifugal clutch slipping).

Free wheels status signals are switched from engaged to disengaged if the torque goes below the maximum allowable reverse torque (which is zero in the conventional free wheels). On the other side, they are switched from disengaged to engaged when the difference of the angular velocities between the input and output elements goes below a threshold value, which is very close to zero.

Similarly, centrifugal clutches change their status from engaged to disengaged (in slipping condition, i.e.  $s_{f,i} = 0.5$ ) when the transmitted torque overtakes the maximum allowable torque previously computed. From the slipping condition, the clutch can become completely open when the dynamic friction torque goes to zero, i.e when its speed goes below  $\bar{\omega}_{c,i}$  (see Section 7.1.5). Finally, from the slipping status, the centrifugal clutches can go into the engaged status, if the difference of the angular velocities between the input and output elements goes below a threshold value.

The gear pair status signals  $s_{g,i}$  are easily obtained from  $s_{f,i}$  and  $s_{c,i}$ , knowing the positions  $p$  of the centrifugal clutches and the free wheels in each gear.

Finally, the gear efficiency status signals are simply obtained by the sign of the torque transmitted by each gear pair, which is positive when directed from the engine to wheel and negative vice versa.

# Chapter 8

## Applications of the studied transmission

### 8.1 Multi-speed with ICE

The powertrain simulation model (presented in Chapter 7) of the studied transmission was firstly applied to a specific case of a motor-scooter endowed with classic internal combustion engine (ICE) of 125 cm<sup>3</sup>. This represented a preliminary study, carried out to investigate all aspects of the transmission dynamic behaviour and especially the influence of the parameters of the centrifugal clutches.

In order to simulate the transmission, a first stage of design was also carried out, determining the main transmission parameters from the

Table 8.1: Vehicle basic parameters of the scooter with ICE.

Parameter	Value
Vehicle mass	200 kg
Driver mass	75 kg
Engine maximum torque	11.1 N m (at 6000 rpm)
Engine maximum power	10.3 kW (at 9500 rpm)
Wheel radius	253 mm
Frontal <i>corrected</i> surface ( $SC_x$ )	0.48 m <sup>2</sup>

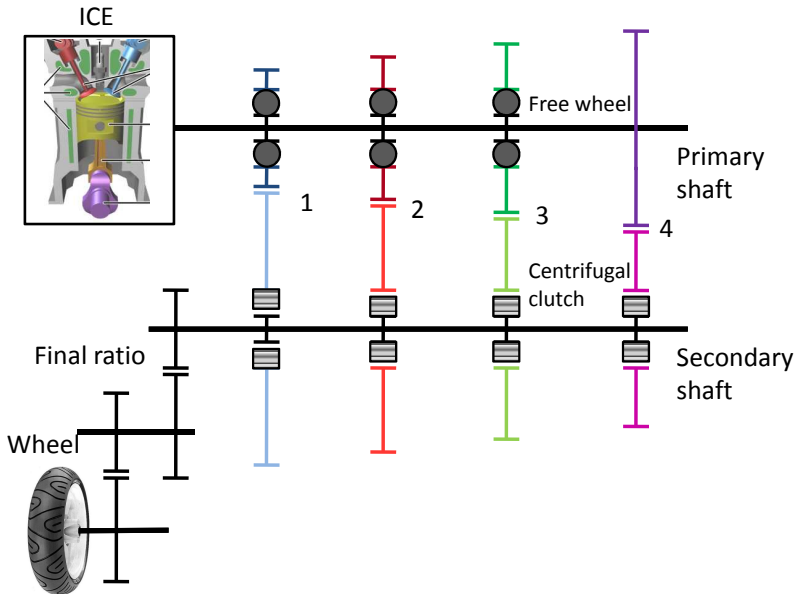


Figure 8.1: Studied case: four-speed transmission with free wheels on the primary shaft and centrifugal clutches on the secondary shaft. There is no primary ratio and the final ratio is made with two gear couples.

vehicle basic parameters, which are shown in Table 8.1. These were taken from a medium-size commercial motor-scooter. Other parameters needed by the simulation model, such as the gear efficiency, were estimated.

The transmission layout chosen for this application is shown in Figure 8.1. This was already presented, in a very similar form, in Section 6.3.2. In this case, no primary ratio is implemented, but there is a final ratio in two steps, as usually in motor-scooter endowed with CVT. The number of gears, which is four, is topic of the next section, being a design parameter dependent on the vehicle characteristics. The present system architecture was selected for the reasons explained in Section 6.3.2, being the best compromise between practical issues and transmission dynamic behaviour.

In the next section the design parameters of the transmission, i.e. the gear ratios and the centrifugal clutch parameters, are determined, whereas in Section 8.1.2 simulation results of the powertrain are shown and discussed.



### 8.1.1 Gear ratios and centrifugal clutch parameters

From the vehicle parameters represented in Table 8.1 and the available engine torque curve, the gear ratios and the centrifugal clutch parameters could be defined by implementing some design criteria. In particular, as it will be further shown, the parameters of the centrifugal clutches are set in reference to the transmission behaviour during the gear shifts. In the following this first step of the transmission design is shown for the case studied. It is worth noting that the following procedure is general for each architecture of this kind of transmission and represents a tool for the first step of the design process.

#### Gear ratios

Gear ratios were defined from the classic design criteria of the maximum slope and the maximum speed. In details, this means to obtain the first and the last gear ratio as follows:

- first gear ratio: the vehicle (with just the driver) must be able to climb a road which has a 30% slope;
- last gear ratio: the vehicle (with just the driver) must reach the maximum speed using all available power.

Once the first and the last gear ratios were determined, the other gear ratios were obtained supposing to use the engine speed range, at maximum, between the maximum torque and the maximum power speeds. The ratios result therefore in geometrical progression and the gear shifts occur with the same engine speed.

With these criteria, the a four speed transmission was obtained, whose gear ratios are shown in Table 8.2. A final ratio of 0.1, made with two gear couples, was considered. In Figure 8.2 it is shown how the obtained gear ratios respect the design criteria: the vehicle reaches its maximum possible speed with the fourth gear, and is able to climb a road with 30% slope.

The vehicle speeds of the gear shifts were also obtained, by considering that these occur when the engine is at the maximum power speed. The so obtained gear shift speeds are listed in Table 8.2 and visually represented in a vehicle speed – engine speed graph in Figure 8.3.

Table 8.2: Gear ratios and gear shift speeds of the four-speed application with ICE (for gear the fourth gear the maximum vehicle speed is indicated). A final ratio of 0.1 is employed.

Gear	Ratio	Max. speed (km/h)
1	0.46	42.0
2	0.64	57.8
3	0.88	79.4
4	1.21	109.2

### Centrifugal clutch parameters

As described in detail in Section 7.1.5, centrifugal clutches have a quadratic torque – angular velocity characteristic, which can be therefore fully determined by setting two constants  $k_1$  and  $k_2$  (gear index  $i$  is here suppressed for clarity). In order to set these clutch constants, as already shown in Section 7.1.5, two conditions on the clutch speed  $\omega_c$  were used, the first based on the initial torque transmission (at  $\bar{\omega}_c$ ) and the second based on a specific value of the transmitted torque  $\hat{T}_c$  (at  $\hat{\omega}_c$ ).

These criteria were applied to the case studied in the following ways for the starting clutch and the gear shift clutches.

- **Starting clutch:**  $\bar{\omega}_c$  was fixed setting the engine speed at which the clutch should begin to transmit torque (3000 rpm). On the other side,  $\hat{\omega}_c$  was set as the speed at which the engine torque (with full throttle) is equal to the clutch torque, so that the synchronization occurs at the corresponding engine speed (4000 rpm).
- **Gear shift clutches:**  $\hat{\omega}_c$  were set, for each gear ratio, from the vehicle speed at which the centrifugal clutch torque transmits entirely the drive torque, thus disengaging the free wheel of the previously engaged gear. This speed corresponds to the gear shift speed computed in the previous section. It is worth remembering that, at this speed, the previous gear is disengaged and the synchronization phase carried out by the centrifugal clutch begins. The new gear is therefore engaged at a higher speed value.

For each gear, the speed  $\bar{\omega}_c$  at which the centrifugal clutch begins

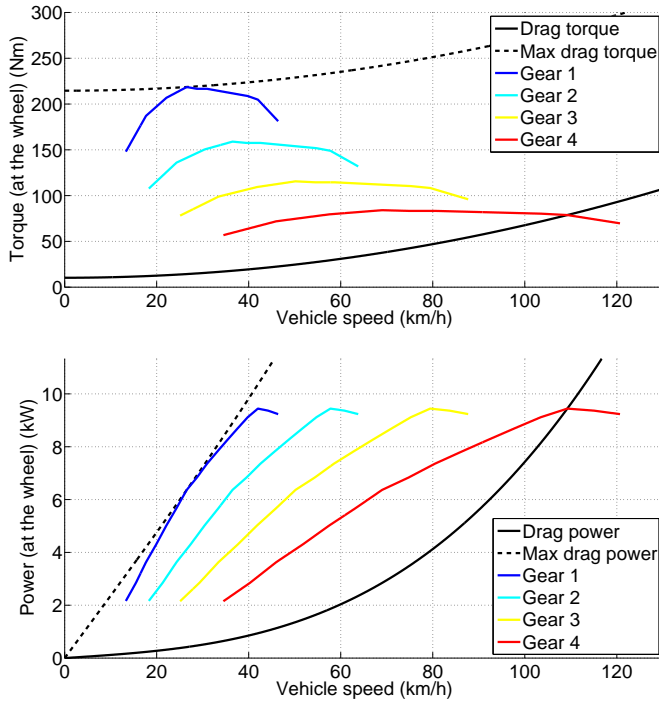


Figure 8.2: Drive and drag torques (top) and powers (bottom) at the wheel.

to transmit torque was set with respect to  $\hat{\omega}_c$ , choosing a speed value difference. This parameter has a fundamental influence on the transmission behaviour, especially in its comfort and efficiency performances. The effects of this are analysed in Section 8.1.2. At this point, a difference of 4 km/h between the gear shift speed and the initial torque transmission speed was set for all gear shifts.

From the  $\omega_c$  values just defined, the clutch constants  $k_1$  and  $k_2$  could be obtained, for each gear, using eq. (7.16), hence defining the characteristics of all centrifugal clutches. These are shown in Figure 8.4 together with the engine torque curves in order to highlight the gear shift speeds, given by the intersection of the engine and the clutch torque curves.

In this first design step, it was also investigated if and how the desired centrifugal clutch characteristics could be physically obtained. To do so,

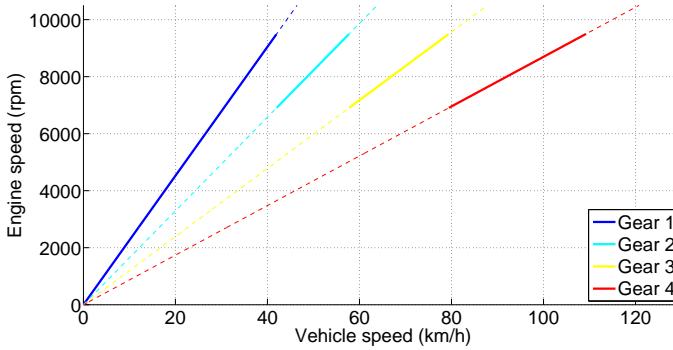


Figure 8.3: Vehicle and engine speed with the different gears. The used range in each gear is represented, highlighting the gear shift points.

a centrifugal clutch physical model, available from the project partner, was employed, writing the following relationships:

$$\begin{aligned} k_1 &= k_1(\mathbf{d}, m_c, p_c) \\ k_2 &= k_2(\mathbf{d}, m_c, p_c) \end{aligned} \quad (8.1)$$

where  $\mathbf{d}$  is a vector containing all geometrical parameters of the clutch,  $m_c$  is the value of the single centrifugal mass and  $p_c$  is the preload of the springs (for details on theory and design of centrifugal clutches see [37]). In order to analyse the different sizes of clutches, all geometrical parameters were considered proportional to the clutch radius  $r_c$ , keeping the angular parameters constant. The relationships  $\mathbf{d} = \mathbf{d}(r_c)$  were obtained from an available centrifugal clutch.

The previous equations can now be written as:

$$\begin{aligned} k_1 &= k_1(r_c, m_c, p_c) \\ k_2 &= k_2(r_c, m_c, p_c) \end{aligned} \quad (8.2)$$

and, having already determined the clutch constants  $k_1$  and  $k_2$ , the masses  $m_c$  and the spring preloads  $p_c$  can be obtained as function of the clutch radius, as shown in Figure 8.5. This showed the manufacturing possibility of the so designed clutches, having, in the range of reasonable radius values (40 mm-70 mm), masses of a few hundreds of grams and preload values of about 100 N–300 N.

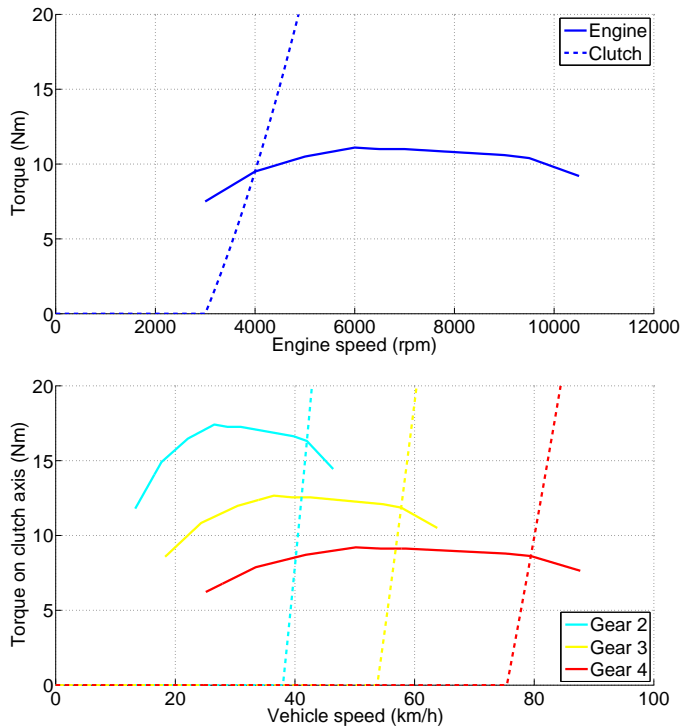


Figure 8.4: Starting clutch (top) and gear shift clutches (bottom) characteristics related to the engine characteristics. The intersections between the curves give the speeds at which the synchronizations occur. In the second graph, solid lines are for the engine torque curves and dotted lines for the centrifugal clutches.

### 8.1.2 Simulation results

Once the transmission was completely defined in terms of all its parameters, the system was simulated with the powertrain simulation model described in Chapter 7. In order to analyse its dynamic behaviour, a manoeuvre of acceleration, coast and then braking was carried out. In details, this is made of the following steps:

- no driver's input for 1 s;
- full throttle from 1 s to 40 s;
- no driver's input from 40 s to 60 s (coast down);

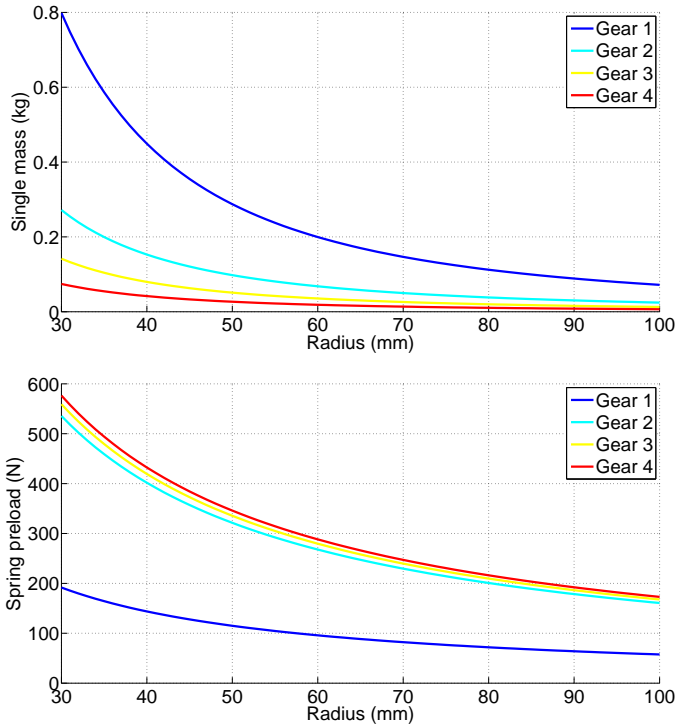


Figure 8.5: Centrifugal clutch masses (top) and springs preload (bottom).

- full braking from 60 s until the vehicle is stopped.

An overview of the behaviour of the transmission is given by the graphs in Figure 8.6. In the first graph the engine speed and the vehicle speed (or the secondary shaft velocity) computed on the engine shaft by all four gear ratio, are shown. The vehicle starts stopped, whereas the engine is rotating at its idle speed (1700 rpm). When the throttle signals goes to 1 (at 1 second) the engine accelerates very quickly, until it reaches the speed at which its torque is equilibrated by the starting (first gear) clutch. Then, the engine speed is almost constant (4000 rpm) during the first gear clutch engagement, whereas the vehicle (secondary shaft) accelerates. After the engagement, the engine and the first gear curves are overlapped until the first gear free wheel opens because the torque is all transmitted by the second gear centrifugal clutch. At this point, the second gear centrifugal clutch decelerates the engine and accelerates

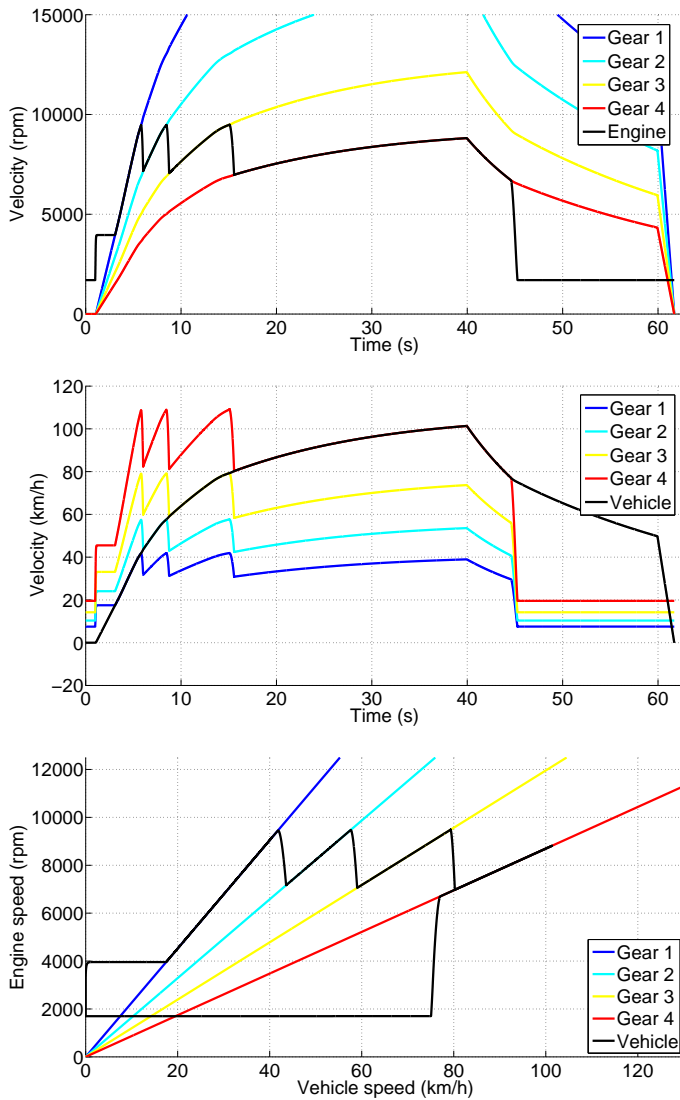


Figure 8.6: Engine speed and vehicle speed computed on the engine shaft by the four gear ratios (top). Vehicle speed and engine speed computed on the wheel shaft by the four gear ratios (centre). Vehicle and engine speed (bottom).

the vehicle until their speed are synchronized on the second gear ratio: the clutch is then engaged and the engine speed curve is overlapped on the second gear curve. The same occurs during the following gear shifts and can be observed also in the second graph (velocities computed on the secondary shaft in terms of vehicle speed) and in the last one (engine and vehicle speeds).

When the throttle signal goes to zero (at 40 s) the vehicle is in coast down and engine braking occurs, having no free wheel on the fourth (last) gear, thus allowing reverse torque. But when the vehicle speed goes below the engagement speed of the centrifugal clutch of the fourth gear, this clutch opens disconnecting the fourth gear and hence the engine from the wheel. From this point there is no more engine braking because of the free wheels on the other gears. The engine is therefore rapidly braked whereas the vehicle becomes slowed just by the aerodynamic drag and the rolling resistance. The other centrifugal clutches open when the vehicle speed goes below their threshold speeds. It is worth noting that in this phase, if the throttle input was once more activated, the engine would quickly accelerate (almost without resistance) and the free wheel, corresponding to the highest gear with still closed centrifugal clutch, would be engaged, transmitting the torque to the wheel. Finally, when the brakes are activated, the vehicle brakes decelerating using the maximum allowable road–tire friction coefficient (0.8).

In Figure 8.7 the status signals of the transmission elements are shown during the manoeuvre. These signals, whose meaning has been already introduced in Section 7.2.2, describe completely the behaviour of the transmission. In specific, it can be seen how, during a gear shift, the centrifugal clutch of the upcoming gear begins to transmit torque (its status goes from 0 to 0.5). During this slipping phase, when the torque flow is all transmitted through the clutch, the free wheel of the current gear opens (status from 1 to 0) and then the clutch, after the synchronization phase, becomes engaged (status from 0.5 to 1). In coast down, when the centrifugal clutches open, the gear pair quickly decreases its speed and the corresponding free wheels are once more engaged.

The gear shift phases can be analysed focusing also on the torques on both the primary and secondary shafts, as shown in Figure 8.8. During the whole acceleration part of the manoeuvre the drive torque (i.e. the torque sum of all gear torques) is always positive, thus carrying out the power-shift. In each gear shift, the torque is in fact transmitted by the two consecutive gear pairs; when the centrifugal clutch of the upcoming



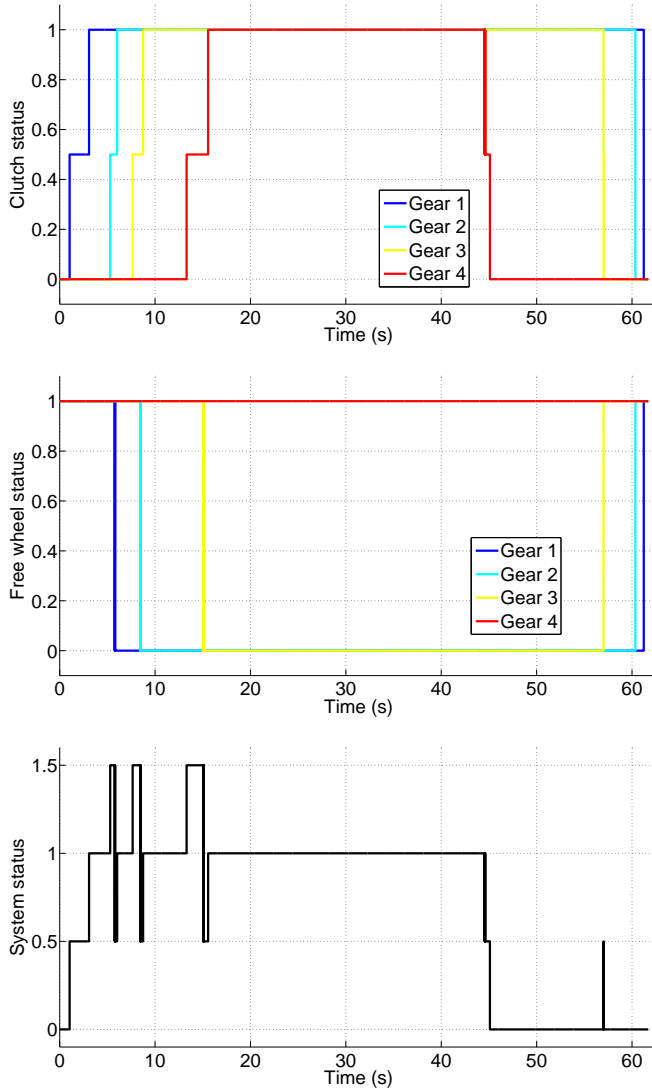


Figure 8.7: Status signals of centrifugal clutches (top), free wheels (centre) and of the complete system (bottom).

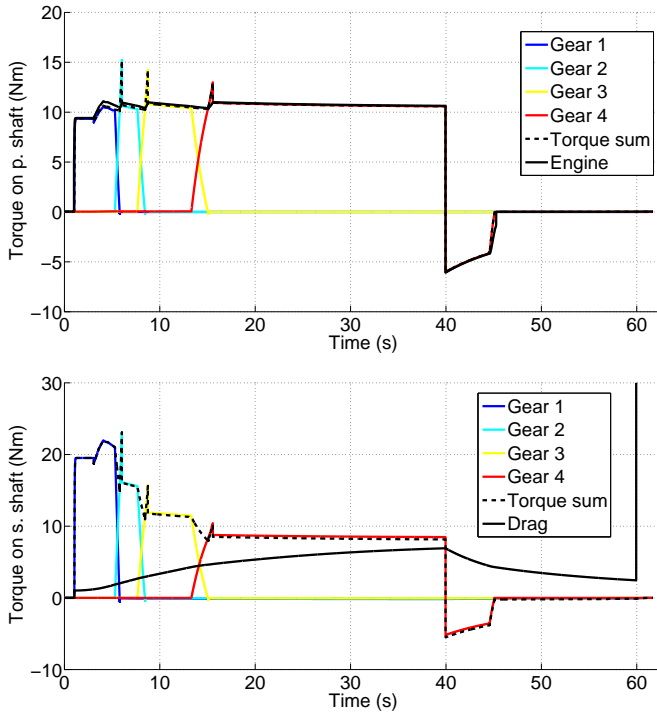


Figure 8.8: Torques on the primary and secondary shaft of the transmission.

gear begins to transmit torque, the torque of the other gear decreases reaching zero when the free wheel opens. As it is clear in the picture, from this point the torque transmitted by the centrifugal clutch increases because the vehicle speed increases too. Finally, when the speeds are synchronized on the new gear ratio, the transmitted torque falls rapidly to the static friction torque value.

This torque variation influences of course the vehicle acceleration during gear shifting, which is represented with the black solid line in the top graph in Figure 8.9. The signal, which is as expected always positive (power-shift), has some peaks when gear shifts occur. These peaks, as well as those in the torque sum signal, are due to the gear shift mechanism, which includes the initial slip of the centrifugal clutch (decrease of acceleration), the disengagement of the free wheel (increase of acceleration) and finally the clutch engagement (decrease of acceleration),

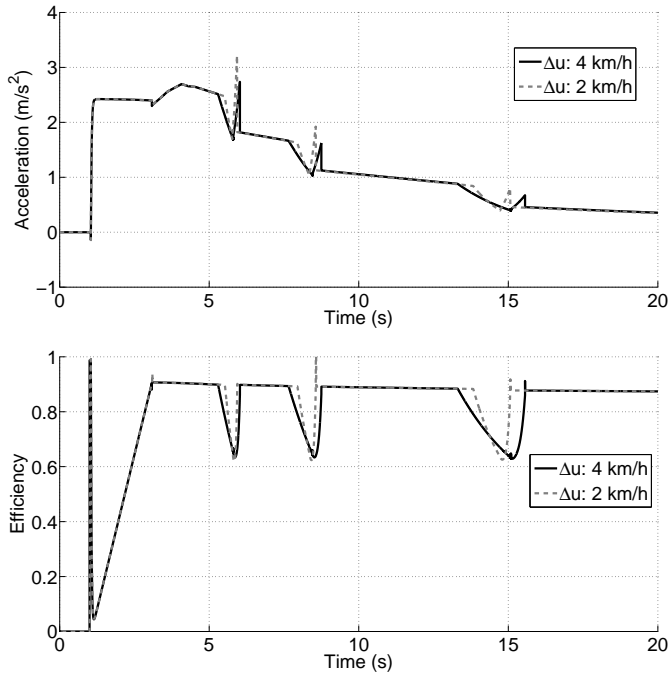


Figure 8.9: Vehicle longitudinal acceleration (top) and energy efficiency of the transmission (bottom) for two different different centrifugal clutch parameters ( $\Delta u$  is the speed difference between the point of initial torque transmission of the clutches and the gear shift speed).

setting the new gear ratio which leads to lower acceleration.

These peaks influence the comfort of the powertrain leading to higher jerk. They result higher if the gear shifting time is shorter (e.g. from first to second gear), whereas they are smoother when the gear shift takes more time, such as in the last one. Having the same value of  $\hat{\omega}_c - \bar{\omega}_c$  for all centrifugal clutches (corresponding to 4 km/h), the last gear shift needs, in fact, more time, having the vehicle less acceleration.

In Figure 8.9 a comparison with the same powertrain but with different centrifugal clutches is shown. In this case, the same gear shift speeds were kept, but  $\hat{\omega}_c - \bar{\omega}_c$  was set to 2 km/h, obtaining different clutch constants, following the presented procedure. As expected, the peaks of the acceleration are higher than the previous case (and therefore comfort is lower), but, on the other side, gear shifting times are shorter. This

has an important influence on the energy efficiency of the transmission, as shown in the graph at the bottom of Figure 8.9, where the results of a preliminary study on the system efficiency are shown for the same manoeuvre. When the centrifugal clutches slip, the current efficiency is lowered and, depending on how much time the slipping phases go on, they have more or less weight in the global efficiency in a cycle. Therefore, when designing the system and especially the centrifugal clutches, a trade-off between comfort and efficiency takes place.

The simulation results of Figure 8.9, in terms of comfort and efficiency, lead to some considerations, even if at this point just qualitatively. They show how the studied transmission has more comfort than a typical manual transmission, having always positive acceleration during gear shifting. On the contrary, vehicles endowed with manual transmissions would have negative acceleration phases when the torque flow from the engine to the wheel is interrupted during gear shifting. However, with respect to a CVT belt transmission, because of the acceleration peaks just shown, the system is likely to have a lower comfort performance.

From the efficiency point of view, from the preliminary available data, the system results with a better performance than a CVT. The main advantage is that torque is transmitted by gears when no gear shift occurs. It is worth once more noting that, the comfort and efficiency objectives are in trade-off for studied transmission and, if no tunable feature is implemented, a choice must be made in the design phase.

## 8.2 Two-speed with electric motor in hybrid powertrain

The second case study of the present transmission regarded a hybrid powertrain for an application in a supposed small-sized passenger vehicle. A preliminary study was carried out to investigate the transmission dynamic behaviour when employed in the hybrid powertrain and to obtain the main transmission parameters carrying out a first design stage.

The present powertrain system is made of a classic internal combustion engine with a CVT, which had to be mechanically coupled with an electric motor. The main data of the supposed vehicle are summarized in Table 8.3. Other data, such as the engine and the electric motor torque curves, their inertial properties and other parameters were available; some other were reasonably estimated.

Table 8.3: Basic parameters of the vehicle with hybrid powertrain.

Parameter	Value
Vehicle mass	500 kg
Driver mass	75 kg
Engine maximum torque	20 N m (at 4500 rpm)
Engine maximum power	10.5 kW (at 5500 rpm)
Electric motor maximum torque	15 N m
Electric motor maximum power	2.5 kW
Wheel radius	270 mm
Frontal <i>corrected</i> surface ( $SC_x$ )	1 m <sup>2</sup>

As already pointed out in Section 6.1, the electric motor may need a variable gear ratio with respect to the wheel, in order to limit its torque (and hence its dimensions and weight) and its maximum velocity. In this application the vehicle should be able to start in pure electric (i.e. with the ICE turned off) requiring a low gear ratio to have a sufficient torque. On the other side, the limit on the maximum velocity of the motor suggested the use of a second higher gear ratio. For the specifications of this vehicle, the gear shifting should be automatic and, therefore, the studied transmission was considered suitable for the present application.

The complete system which was studied is shown in Figure 8.10. The power flows of the ICE and the electric motor are summed on the secondary shaft of the gearbox, before a common final ratio and the wheels. The ICE powertrain part is made of the CVT, endowed, as commonly in motor-scooter applications, with a centrifugal (starting) clutch after the secondary shaft of the CVT. The electric powertrain part is made of the electric motor and a two-speed transmission, belonging to type studied. In this case, no starting clutch (1<sup>st</sup> gear clutch) is implemented, having an electric motor which has, of course, no minimum speed. The first gear has therefore just the free wheel for disengagement, which is on the secondary shaft. The second gear is endowed with the gear shift clutch on the secondary shaft, whereas it has no free wheel being the last gear. A primary ratio was also considered in order to have a design degree of freedom for layout issues, even if not necessary for the system working.

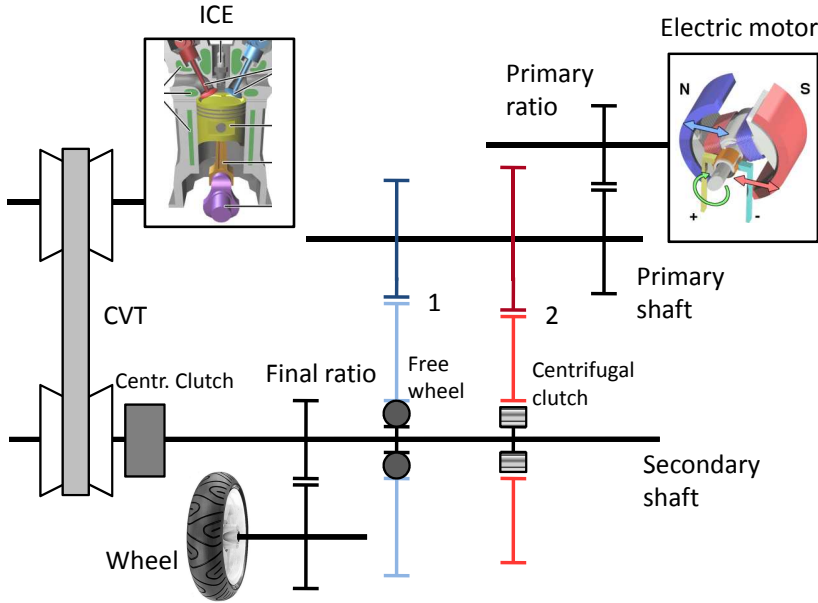


Figure 8.10: Hybrid powertrain made of ICE with classic CVT mechanically coupled on the secondary shaft with an electric motor with the two-speed automatic transmission.

It is worth noting that the electric motor is used also for regenerative braking. With this transmission, because of the free wheel, this is allowed just in the second gear (where the speed and thus the energy is higher). The free wheel could be mechanically blocked when no gear shift occurs in order to have torque back flow also in first gear.

### 8.2.1 Modifications to the powertrain model

From the simulation model point of view, the implementation of the hybrid powertrain just presented required some modifications to the equations of Section 7.1 and hence to the Simulink model of Section 7.2. Without going into details, the main difference is represented by the equilibrium equations of the ICE with CVT. This is written with all terms computed on the engine shaft (primary CVT shaft), as follows:

$$\left( J_{e,1} + \frac{J_{e,2}\tau_{CVT}^2}{\eta_{CVT}} \right) \dot{\omega}_{e,1} = T_e - \frac{T_{c,e}\tau_{CVT}}{\eta_{CVT}} - S_e(\omega_{e,1}), \quad (8.3)$$

where  $\omega_{e,1}$  is the primary CVT shaft speed,  $J_{e,1}$  and  $J_{e,2}$  are the inertias on the primary and secondary shaft of the CVT,  $\tau_{CVT}$  is the current CVT ratio,  $\eta_{CVT}$  is the current CVT mechanical efficiency,  $T_e$  is the ICE torque,  $T_{c,e}$  is the centrifugal clutch torque and  $S_e(\omega_{e,1})$  represents the resistance torque due to friction and fluid dynamics effects.

In CVT, the ratio and the efficiency are complex functions of the working conditions. In the model of this work, these functions were implemented as:

$$\begin{aligned}\tau_{CVT} &= \tau_{CVT}(\omega_{e,1}, T_{CVT}) \\ \eta_{CVT} &= \eta_{CVT}(\omega_{e,1}, T_{CVT}),\end{aligned}\tag{8.4}$$

where  $T_{CVT}$  is the torque transmitted. In the present application these functions were modelled very simply, having a constant efficiency of 0.8 and an ideal CVT ratio function with the variation between the maximum and the minimum ratios at a defined engine speed, different for drive and coast down conditions<sup>1</sup>.

An other important modification of the simulation model regards the equilibrium equation of the secondary shaft (second equation in eq. (7.2)), where the torque  $T_{c,e}$  transmitted by the centrifugal clutch of the ICE powertrain was added.

The model in Simulink was modified implementing the new equations and keeping the same modelling principle described in Section 7.2. In this case, there are two switches for the two powertrain parts which define the open or closed conditions. The switch of the ICE powertrain part depends only on the centrifugal clutch status signal, whereas the switch of the electric powertrain part is still computed with eq. (7.17).

## 8.2.2 Gear ratios and centrifugal clutch parameters

The transmission parameters of the electric powertrain part were obtained following a similar procedure of that described in Section 8.1.1 for the other studied application. In this case, the criteria for determining the first and second (last) gear ratio were supposed as follows:

- first gear ratio: the vehicle (fully loaded) must be able to climb a road which has a 15% slope in pure electric conditions;
- second gear ratio: the electric motor speed should not be higher than a maximum value (12 000 rpm) at a reference high vehicle

---

<sup>1</sup>For details on CVT see [18].

Table 8.4: Gear ratios the two-speed application in hybrid powertrain. A final ratio of 0.1 is employed.

Gear	Ratio
1	0.51
2	0.67

speed (80 km/h).

These criteria lead to the gear ratios shown in Table 8.4, considering a final ratio of 0.1. The torque and power curves in pure electric conditions are shown in Figure 8.11 where it can be seen how the vehicle does not reach the maximum speed, having fixed the second ratio with an other criterion.

The gear change speed can be arbitrarily determined and was set over 30 km/h, so that the vehicle could be driven within this speed limit in pure electric without gear shifting. In Figure 8.12 the ranges of motor and vehicle speed in both gears are shown, highlighting the gear shift point.

The centrifugal clutch which carries out the gear shift was selected among physically available clutches or possible manufacturable clutches. After a parametric study, such as that presented in Figure 8.5, a clutch was selected for the application. Its characteristic is shown in Figure 8.13 compared to the electric motor drive torque. In the picture the vehicle speed, at which the clutch begins to slip, can be individuated (31.2 km/h) together with the speed at which the free wheel opens (33.1 km/h), given by intersection between the curves).

In this studied application, the following design step was also carried out determining the dimensions of the gears and their parameters, such as number of teeth, modulus, etc.

### 8.2.3 Simulation results

The dynamic behaviour of the studied transmission has been already investigated in detail in Section 8.1.2 with reference to the multi-speed powertrain with internal combustion engine. For the present application of the hybrid powertrain, analogue manoeuvres were simulated using the



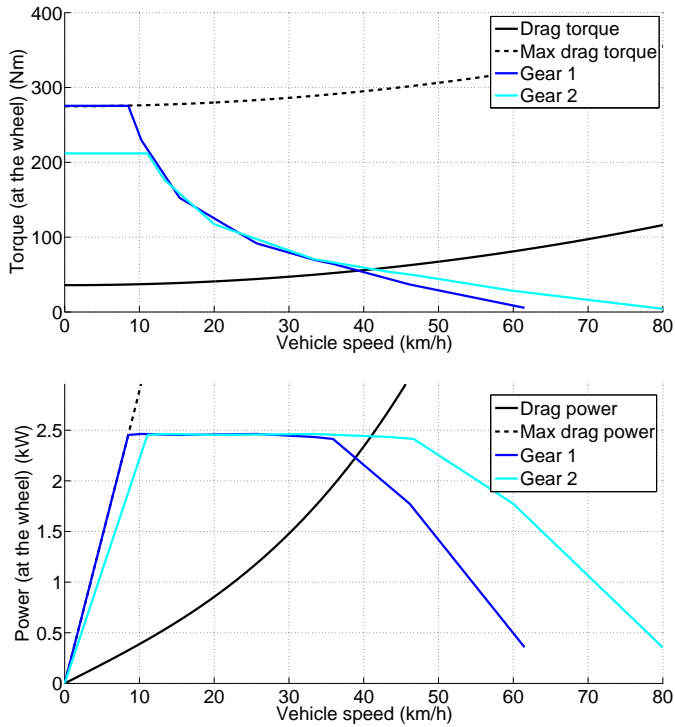


Figure 8.11: Drive and drag torques (top) and powers (bottom) at the wheel.

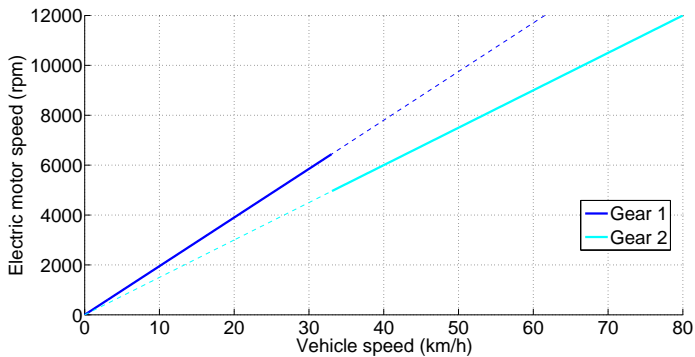


Figure 8.12: Vehicle and engine speed with the different gears. The used range in each gear is represented, highlighting the gear shift points.

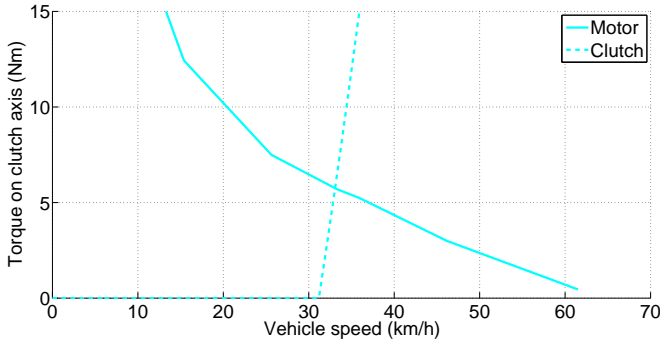


Figure 8.13: Gear shift clutch characteristic related to the electric motor characteristic. The intersection between the curves gives the speed at which the synchronization occurs for the second gear ratio.

simulation model with the modifications previously introduced. For the sake of completeness, simulation results are shown also for the present application. In this case, results of a 30s full throttle acceleration manoeuvre are shown in order to focus on the gear shifting mechanism and on the interaction with the CVT.

Being all engagement mechanisms of both the ICE and the electric powertrain parts on the secondary shaft, the velocity of the elements on this shaft, shown in Figure 8.14, are representative of the system behaviour. It can be observed how the CVT secondary shaft starts from a minimum speed, related to the engine idle speed, whereas the gears, and hence the electric motor, start with zero speed. Giving full throttle (at 1 s), the engine speed increases quickly until the CVT clutch begins to slip and the synchronization of the CVT secondary shaft with the gearbox secondary shaft occurs.

The gears of the electric motor transmission on the secondary shaft rotate both with a fixed ratio with respect to the motor, being the correspondent gears on the primary shaft fixed to the shaft itself. As can be seen in the figure, at the beginning of the simulation the first gear is engaged. As already described in Section 8.1.2, when the secondary shaft velocity reaches the value at which the centrifugal clutch transmits all the drive torque, the free wheel opens disengaging the first gear. From this point the secondary shaft curve is different from both curves of the gears: in fact the synchronization phase of the second gear occurs. The

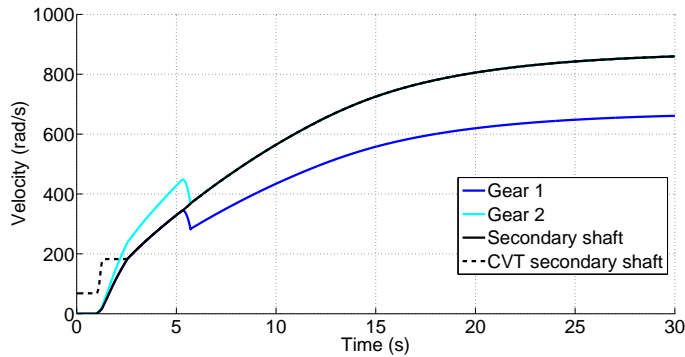


Figure 8.14: Velocities on the secondary shaft.

second gear velocity is decreased (and thus the motor velocity) whereas the secondary shaft velocity (and thus the vehicle speed) is increased until these curves are overlapped and the second gear is therefore engaged.

The described transmission behaviour can be observed also in Figure 8.15, where, in the first graph, the electric motor velocity is compared to the vehicle speed computed on the motor shaft by means of the two gear ratios. The same is shown in the second graph for the engine using the maximum and minimum CVT ratios. In this graph, the CVT characteristic can be easily observed. After the CVT clutch engagement, the engine curve is overlapped to the minimum CVT ratio curve until it reaches the value at which the ratio variation is carried out (5000 rpm). In the last graph of the picture the behaviour of both the powertrain parts can be observed in terms of vehicle speed. It can be seen here that the gear shift of the gear transmission occurs when the CVT is between the extreme ratios.

Finally, in Figure 8.16 the transmission behaviour is summarized by means of the status signals of the centrifugal clutches and the free wheel. The signals have the same meaning already described, i.e. disengaged (0), engaged (1) and in slipping condition (0.5, just for clutches).

For what concerns coast down and braking, analogue considerations of those in Section 8.1.2 can be made. It is just worth remembering that the lack of opposite torque flow in first gear does not allow regenerative braking with the electric motor, which can be carried out just in second gear. This issue can be solved just blocking the free wheel, living it free just before the gear shift. However, having set the gear shift at about

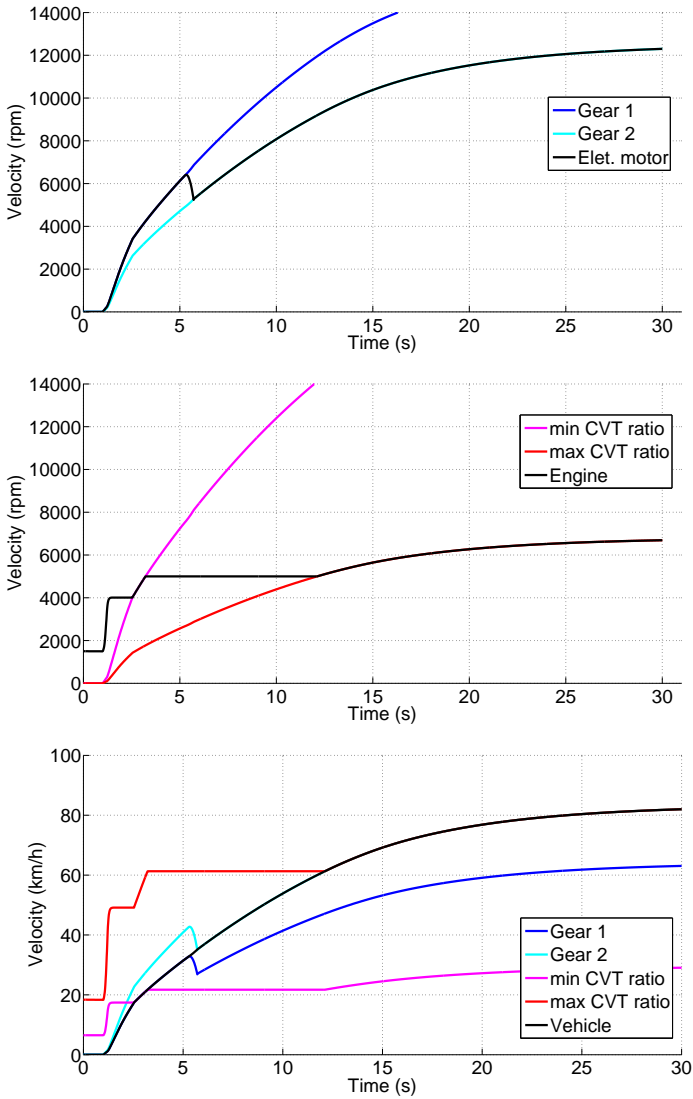


Figure 8.15: Electric motor speed and vehicle speed computed on the motor shaft by the two gear ratios (top). Engine speed and vehicle speed computed on the engine shaft by the minimum and maximum CVT ratios (centre). Vehicle speed, electric motor speed computed on the wheel shaft by the two gear ratios and engine speed computed on the wheel shaft by the minimum and maximum CVT ratios (bottom).

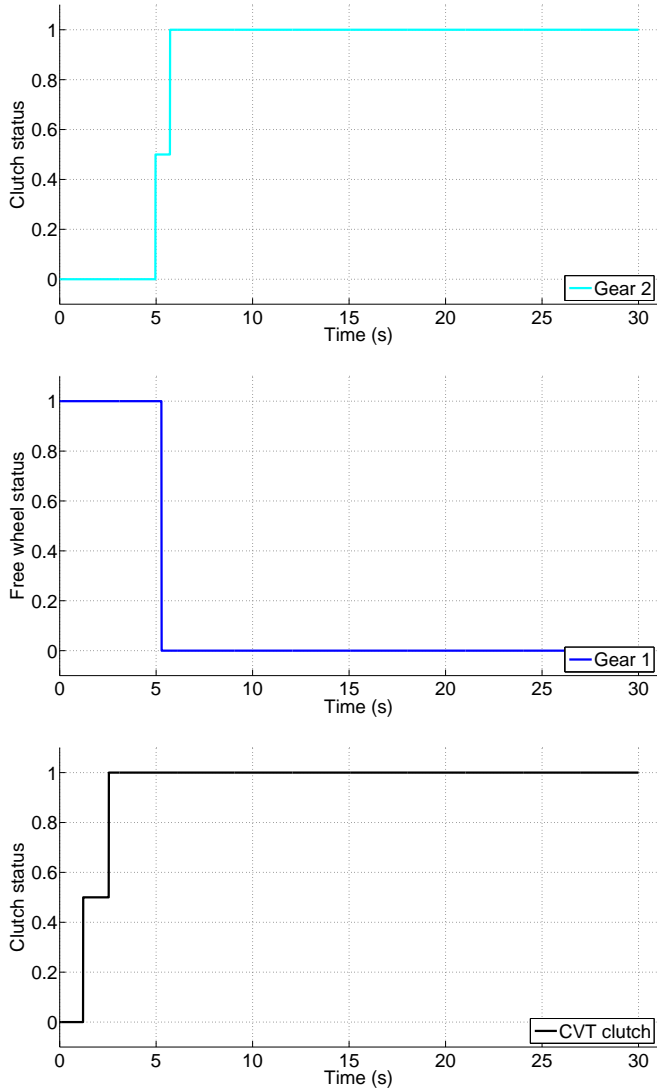


Figure 8.16: Status signals of gear shift centrifugal clutch (top), free wheel (centre) and centrifugal clutch of the ICE powertrain part (bottom).

30 km/h, the energy that can not be recovered represents a little amount, thus justifying the solution presented.

# Conclusions

In the present work, the development of a driving simulator for road safety purposes and the Analysis and design of an automatic transmission for motor-scooters have been presented and discussed. In both activities, dynamic simulation models were developed and used for the applications. In the following, conclusions are given for both the researches presented.

## **Development of a driving simulator**

A driving simulator was developed with the aim of achieving, during simulated driving tests, data related to both driver actions and vehicle motion conditions. This system was fundamental to carry out safe and monitored test drives in laboratory investigating the human factor with respect to the simulated vehicle and environment. The main aim was to study the driving style to develop a diagnostic tool in the preventive safety area, which should be able to detect dangerous situations, coming from a non proper relationship between the driver's actions, the vehicle motion conditions and the environment conditions.

A driving simulator with a fixed driving platform and a single channel frontal view was developed, which was suitable for the simulations at low accelerations, such as those necessary to investigate the driving style when driver's attention level is low. The human-machine interface was correctly reproduced, implementing also an active torque feedback on the steering wheel and passive force feedbacks on the pedals. The simulator was endowed with a parametric vehicle simulation model with 14 degrees of freedom. This model reproduces correctly the dynamic behaviour of the vehicle and its main subsystems, such as the engine, the suspensions, the braking system, the transmission, etc., allowing also, as shown in the present thesis, extreme manoeuvres with loss of grip.

The simulator was built, installed in the DIMNP laboratories and used

in some experimental campaigns, carrying out several hours of simulated drives. The performance of the system appears to be fully satisfactory; indeed, the total time for data acquisition, running the model (one time step) and obtaining the results to be sent on the network is about 0.4 ms, fulfilling the general requirements for real-time applications.

A first experimental campaign showed a good correlation between the simulation environment and real drives on the same roads which are reproduced in the graphical scenario. With the second campaign, drivers in rested and tired conditions followed a test protocol with the driving simulator; the data acquired were successfully used by the project partners to develop an algorithm which recognizes different driving styles and driving conditions.

Beyond the experimental campaigns described in this work, the developed driving simulator offers the possibility of carrying out many other tests on the interaction between driver, vehicle and environment, focusing on the human factor. Some collaborations with other university departments have been already started and tests have been planned in order to study, for instance, the effects of alcohol on the driving style.

In order to enlarge the field of possible applications of the driving simulator, some improvements can be thought as future developments. A visual system with a wider frontal view, employing three flat screens or a cylindrical screen, seems to be necessary to carry out simulated drives in the urban environment with a higher level of realism. Another important step forward is represented by the moving driving platform. By means of this, the driver feels the inertial effects and the realism of the simulated drives can be dramatically increased, especially when the vehicle is subjected to high longitudinal and lateral accelerations. This could extend the study possibilities to the drivers' behaviour in extreme driving conditions and the interaction of drivers with the vehicle active safety systems.

### **Analysis and design of an automatic transmission for motor-scooters**

With the aim of studying and developing an automatic transmission with high efficiency for small powertrains (especially for motor-scooters), a system based on gears with centrifugal clutches and free wheels was analysed in this work. Different system architectures and their functioning were presented. A parametric powertrain dynamic model was built to simulate



the behaviour of different configurations of the studied transmission.

Acceleration, coast down and braking manoeuvres were simulated with a four-speed configuration of the system with an internal combustion engine. The system showed the possibility of automatic gear shifting with no interruption of the drive torque and the effects of the centrifugal clutch parameters on comfort and energy efficiency were also analysed with the simulation model.

A second application study regarded a two-speed configuration of the transmission for an electric motor coupled with a classic ICE in a hybrid powertrain. The system was analysed and a preliminary design phase was carried out obtaining the values of the main transmission parameters.

The project in which this activity was included is currently still ongoing and further work is therefore foreseen. Developments of the work could be focused on more detailed analyses on the system efficiency, on the friction losses and on the comfort during gear shifting in a typical driving cycle, comparing the results with other conventional powertrains. Experimental tests with physical prototypes should be also considered to validate the simulation model and to investigate further aspects which are not taken into account by the model.

The studied transmission could also be improved by active elements to overcome some problems of the completely mechanical solution. Free wheels could be mechanically blocked in order to avoid the lack of torque back flow (for engine braking and regenerative braking) in gears other than the last one. Controlled centrifugal clutches could be implemented to adjust the transmission dynamic behaviour to the current comfort or efficiency requirements. Finally, it is worth noting that these modifications to the basic passive mechanical system should be considered in relation with the application and its expected cost.



## Appendix A

# Tire constitutive equations of the driving simulator vehicle model

In this section the constitutive equations of the tire model are presented. The tire model is treated in Section 3.6, where the following equations have been already introduced:

$$\begin{aligned}F_x &= F_x(F_z, \alpha, \gamma, s_x) \\F_y &= F_y(F_z, \alpha, \gamma, s_x) \\M_x &= M_x(F_z, \alpha, \gamma, s_x) \\M_y &= M_y(F_z, \alpha, \gamma, s_x) \\M_z &= M_z(F_z, \alpha, \gamma, s_x).\end{aligned}$$

These are implemented in the model using the Pacejka 2002 tire model (PAC2002) [47, 51], whose relationships are shown in the following. The coefficient  $p$ ,  $q$ ,  $r$  and  $s$  which appear in the equations are obtained by experimental tests carried out in a tire test rig. If the tire has not been tested in all conditions, some coefficient may not be available (in this case some modifications are made as shown in Section 3.6.4).

In the equations  $u_{t,0}$  represents the longitudinal speed at which the test was performed (available as a tire parameter) and  $dF_z$  is defined as:

$$dF_z = \frac{F_z}{F_z - F_{z,0}},$$

where  $F_{z,0}$  is a reference value of the vertical load.

In the equations there are also some parameters  $\lambda$ , which are used to adapt the equations when the tire is used in different working conditions with respect to the test (e.g. with different road friction coefficient).

The relationships presented in the following are for pure slip and combined slip conditions. The tire dynamic behaviour was already modelled in the tire slips, implementing the relaxation lengths in the equations presented in Section 3.6.3.

### Longitudinal force – pure longitudinal slip

$$F_{x0} = D_x \sin\left(C_x \arctan\left(B_x \bar{s}_x - E_x (B_x \bar{s}_x - \arctan(B_x \bar{s}_x))\right)\right) + S_{V_x}$$

$$\bar{s}_x = s_x + S_{H_x}$$

$$\gamma_x = \gamma \lambda_{\gamma_x}$$

$$C_x = p_{C_{x1}} \lambda_{C_x}$$

$$D_x = \mu_x F_z$$

$$\mu_x = (p_{D_{x1}} + p_{D_{x2}} dF_z) (1 - p_{D_{x3}} \gamma_x^2) \lambda_{\mu_x}$$

$$E_x = (p_{E_{x1}} + p_{E_{x2}} dF_z + p_{E_{x3}} dF_z^2) (1 - p_{E_{x4}} \text{sign}(\bar{s}_x)) \lambda_{E_x}$$

$$K_x = (p_{K_{x1}} + p_{K_{x2}} dF_z) \exp(p_{K_{x3}} dF_z) \lambda_{K_x}$$

$$B_x = \frac{K_x}{C_x D_x}$$

$$S_{H_x} = (p_{H_{x1}} + p_{H_{x2}} dF_z) \lambda_{H_x}$$

$$S_{V_x} = F_z (p_{V_{x1}} + p_{V_{x2}} dF_z) \lambda_{V_x} \lambda_{\mu_x}$$

### Lateral force – pure lateral slip

$$F_{y0} = D_y \sin\left(C_y \arctan\left(B_y \bar{\alpha} - E_y (B_y \bar{\alpha} - \arctan(B_y \bar{\alpha}))\right)\right) + S_{V_y}$$

$$\bar{\alpha} = \alpha + S_{H_y}$$

$$\gamma_y = \gamma \lambda_{\gamma_y}$$

$$C_y = p_{C_{y1}} \lambda_{C_y}$$

$$D_y = \mu_y F_z$$

$$\mu_y = (p_{D_{y1}} + p_{D_{y2}} dF_z) (1 - p_{D_{y3}} \gamma_y^2) \lambda_{\mu_y}$$

$$\begin{aligned}
E_y &= (p_{E_{y1}} + p_{E_{y2}} dF_z) (1 - (p_{E_{y3}} + p_{E_{y4}} \gamma_y) \text{sign}(\alpha_y)) \lambda_{E_y} \\
K_y &= p_{K_{y1}} F_{z,0} \sin \left( 2 \arctan \left( \frac{F_z}{p_{K_{y2}} F_{z,0} \lambda_{F_{z0}}} \right) \right) (1 - p_{K_{y3}} |\gamma_y|) \lambda_{F_{z0}} \lambda_{K_y} \\
B_y &= \frac{K_y}{C_y D_y} \\
S_{H_y} &= (p_{H_{y1}} + p_{H_{y2}} dF_z) \lambda_{H_y} + p_{H_{y3}} \gamma_y \\
S_{V_y} &= F_z ((p_{V_{y1}} + p_{V_{y2}} dF_z) \lambda_{V_y} + (p_{V_{y3}} + p_{V_{y4}} dF_z) \gamma_y) \lambda_{\mu_y}
\end{aligned}$$

### Self-aligning moment – pure lateral slip

$$\begin{aligned}
M_{z,0} &= -t F_{y,0} + M_{z,r} \\
t(\alpha_t) &= D_t \sin \left( C_t \arctan \left( B_t \alpha_t - E_t (B_t \alpha_t - \arctan(B_t \alpha_t)) \right) \right) \\
&\quad \cos(\alpha) \\
\alpha_t &= \alpha + S_{H_t} \\
M_{z,r}(\alpha_r) &= D_r \cos(C_r \arctan(B_r \alpha_r)) \cos(\alpha) \\
\alpha_r &= \alpha + S_{H_f} \\
\gamma_z &= \gamma \lambda_{\gamma_z} \\
B_t &= (q_{B_{z1}} + q_{B_{z2}} dF_z + q_{B_{z3}} dF_z^2) (1 + q_{B_{z4}} \gamma_z + q_{B_{z5}} |\gamma_z|) \frac{\lambda_{K_y}}{\lambda_{\mu_y}} \\
C_t &= q_{C_{z1}} \\
D_y &= (q_{D_{z1}} + q_{D_{z2}} dF_z) (1 + q_{B_{z3}} \gamma_z + q_{B_{z4}} \gamma_z^2) \frac{R_0}{F_{z,0}} \lambda_t \\
E_t &= (q_{E_{z1}} + q_{E_{z2}} dF_z + q_{E_{z3}} dF_z^2) \\
&\quad \left( 1 + (q_{E_{z4}} + q_{E_{z5}} \gamma_z) \frac{2}{\pi} \arctan(B_t C_t \alpha_t) \right) \\
S_{H_t} &= q_{H_{z1}} + q_{H_{z2}} dF_z + (q_{H_{z3}} + q_{H_{z5}} dF_z) \gamma_z \\
B_r &= \left( q_{B_{z9}} \frac{\lambda_{K_y}}{\lambda_{\mu_y}} + q_{B_{z10}} B_y C_y \right) \\
C_r &= 1 \\
D_r &= F_z ((q_{D_{z6}} + q_{D_{z7}} dF_z) \lambda_r + (q_{D_{z8}} + q_{D_{z9}} dF_z) \gamma_z) R_0 \lambda_{\mu_y}
\end{aligned}$$

## Combined slip: longitudinal and lateral forces and self-aligning moment

### Longitudinal force

$$\begin{aligned}
 F_x &= D_{x\alpha} \cos\left(\arctan\left(B_{x\alpha}\alpha_s - E_{x\alpha}(B_{x\alpha}\alpha_s - \arctan((B_{x\alpha}\alpha_s)))\right)\right) \\
 \alpha_s &= \alpha + S_{H_{x\alpha}} \\
 B_{x\alpha} &= r_{B_{x1}} \cos(\arctan(r_{B_{x2}}s_x))\lambda_{x\alpha} \\
 C_{x\alpha} &= r_{C_{x1}} \\
 D_{x\alpha} &= F_{x,0} \left[ \cos\left( C_{x\alpha} \arctan\left( B_{x\alpha}S_{H_{x\alpha}} - E_{x\alpha}(B_{x\alpha}S_{H_{x\alpha}} \right. \right. \right. \\
 &\quad \left. \left. \left. - \arctan((B_{x\alpha}S_{H_{x\alpha}})))\right) \right) \right]^{-1} \\
 E_{x\alpha} &= r_{E_{x1}} + r_{E_{x2}}dF_z \\
 S_{H_{x\alpha}} &= r_{H_{x1}}
 \end{aligned}$$

### Lateral force

$$\begin{aligned}
 F_y &= D_{ys} \cos\left( C_{ys} \arctan\left( B_{ys}s_{xs} - E_{ys}(B_{ys}s_{xs} - \arctan((B_{ys}s_{xs}))) \right) \right) \\
 &\quad + S_{V_{ys}} \\
 s_{xs} &= s_x + S_{H_{ys}} \\
 B_{ys} &= r_{B_{y1}} \cos(\arctan(r_{B_{y2}}(\alpha - r_{B_{y3}})))\lambda_{ys} \\
 C_{ys} &= r_{C_{y1}} \\
 D_{ys} &= F_{y,0} \left[ \cos\left( C_{ys} \arctan\left( B_{ys}S_{H_{ys}} - E_{ys}(B_{ys}S_{H_{ys}} \right. \right. \right. \\
 &\quad \left. \left. \left. - \arctan((B_{ys}S_{H_{ys}})))\right) \right) \right]^{-1} \\
 E_{ys} &= r_{E_{y1}} + r_{E_{y2}}dF_z \\
 S_{H_{ys}} &= r_{H_{y1}} + r_{H_{y2}}dF_z \\
 D_{V_{ys}} &= \mu_y F_z (r_{V_{y1}} + r_{V_{y2}}dF_z + r_{V_{y3}}\gamma) \cos(\arctan(r_{V_{y4}}\alpha)) \\
 S_{V_{ys}} &= D_{V_{ys}} \cos(r_{V_{y5}} \arctan(r_{V_{y6}}s_x))\lambda_{V_{ys}}
 \end{aligned}$$

### Self-aligning moment

$$\begin{aligned}
 M_z &= -t(F_y - S_{V_{y,s}}) + M_{z,r} + SF_x \\
 t(\alpha_{t,eq}) &= D_t \sin \left( C_t \arctan \left( B_t \alpha_{t,eq} - E_t (B_t \alpha_{t,eq} \right. \right. \\
 &\quad \left. \left. - \arctan(B_t \alpha_{t,eq})) \right) \right) \cos(\alpha) \\
 M_{z,r}(\alpha_{r,eq}) &= D_r \cos(C_r \arctan(B_r \alpha_{r,eq})) \cos(\alpha) \\
 \alpha_{t,eq} &= \arctan \left( \sqrt{\tan^2(\alpha_t) + \left( \frac{K_x s_x}{K_y} \right)^2} \right) \text{sign}(\alpha_t) \\
 \alpha_{r,eq} &= \arctan \left( \sqrt{\tan^2(\alpha_r) + \left( \frac{K_x s_x}{K_y} \right)^2} \right) \text{sign}(\alpha_r) \\
 S &= R_0 \left( s_{S_{z1}} + s_{S_{z2}} \frac{F_y}{F_{z0}} + (s_{S_{z3}} + s_{S_{z4}} dF_z) \gamma \right) \lambda_s
 \end{aligned}$$

### Overturning moment

$$M_x = R_0 F_z \left( q_{S_{x1}} \lambda_{V_{M_x}} - q_{S_{x2}} \gamma + q_{S_{x3}} \frac{F_y}{F_{z,0}} \right) \lambda_{M_x}$$

### Rolling resistance moment

$$M_y = R_0 F_z \left( q_{S_{y1}} + q_{S_{y2}} \frac{F_x}{F_{z,0}} + q_{S_{y3}} \left| \frac{\omega_r R_r}{u_{t,0}} \right| + q_{S_{y4}} \left( \frac{\omega_r R_r}{u_{t,0}} \right)^4 \right) \lambda_{M_y}$$





# References

- [1] Audi, Audi Multitronic Transmission, <http://www.audiworld.com/news/99/multitronic/content.shtml>.
- [2] R. Bartolozzi, F. Frendo, Automatic transmission for small displacement motor-scooters, *Proceedings of the 11<sup>th</sup> CONAT International Automotive Congress*, Brasov (Romania), 27-29 October, 2010.
- [3] R. Bartolozzi, F. Frendo, E. Vitale, Sviluppo di un simulatore di guida per studi sulla sicurezza attiva dei veicoli, *Atti del XXXVII Convegno Nazionale dell'Associazione Italiana per l'Analisi delle Sollecitazioni*, Roma (Italy), September 10-13, 2008.
- [4] R. Bartolozzi, F. Frendo, E. Vitale, Driving simulator for the analysis of driving style and vehicle motion conditions, *Proceedings of the 2<sup>nd</sup> IASTED Conference on Modelling and Simulation (AfricaMS 2008)*, Gaborone (Botswana), September 8-10, 2008.
- [5] R. Bartolozzi, F. Frendo, E. Vitale, F. Baronti, F. Lenzi, R. Roncella, D. Vangi, A. Virga, *Strumenti di diagnostica per il riconoscimento del livello di attenzione alla guida*, Tipografia Editrice Pisana, Pisa (Italy), 2009.
- [6] J.E. Bernard, C.L. Clover, Tire modeling for low-speed and high-speed calculations, *SAE paper*, No. 950311, 1995.
- [7] Blanchet et al., Automatic transmission with centrifugal clutches, *United States Patent* No. 3939734, 1976.
- [8] M. Brekke, P. Sherman, Critical evaluation of factors associated with steering wheel data when used for identifying driver drowsiness, *Advanced Transport Telematics*, 223, 1994.

- [9] H. Cai, Y. Lin, An experiment to non-intrusively collect physiological parameters towards driver state detection, *SAE Technical Paper*, 2007-01-0403, 2007.
- [10] T. F. Chen, D. W. Lee, C. K. Sung, An experimental study on transmission efficiency of a rubber V-Belt CVT, *Mechanism and Machine Theory*, 33(4), 351-363, 1998.
- [11] Commission of the European Communities, *White Paper European transport policy for 2010: time to decide*, COM(2001), 370 final, September, 2001.
- [12] M. Ehsani, Y. Gao, A. Emadi, *Modern electric, hybrid electric, and fuel cell vehicles*, 2<sup>nd</sup> Edition, Routledge, 2009.
- [13] M. Eriksson, N.P. Papanikoloupolous, Eye-tracking for detection of driver fatigue, *Proc. IEEE Conference on Intelligent Transportation Systems, ITSC*, Boston, USA, 314-319, 1997.
- [14] Fallbrook Technologies, NuVinci CVP Technology, <http://www.fallbrooktech.com/home.asp>.
- [15] M. Fanfara, S. Garbarino, Dodici mesi sulla strada, *Automobile*, Gennaio 2005.
- [16] F. Frendo, A. Malvasi, N. Novi, E. Vitale, Development of an automotive real-time simulator for preventive safety studies, *Proceedings of the Mathworks Automotive Conference*, Torino, Italy, 2006.
- [17] G. Genta, *Meccanica dell'autoveicolo* (Torino, Levrotto Bella) 1996.
- [18] G. Genta, L. Morello, *The automotive chassis*, Springer, 2009.
- [19] G. Gerbert, Belt Slip – A Unified Approach, *Journal of Mechanical Design*, 118(3), 432-438, 1996.
- [20] G. Gerbert, Force and Slip Behavior in V-belt Drives, *Acta Polytechnica Scandinavica*, Mechanical Engineering Series No. 67, 1972.
- [21] M. Goetz, M. C. Levesley, D. A. Crolla, Dynamics and control of gearshifts on twin-clutch transmissions, *Proceedings of the Institution of Mechanical Engineers, Part D: Journal of Automobile Engineering*, 219(8), 951-963, 2005.

- [22] M. Guiggiani, *Dinamica del veicolo* (Torino, Città Studi Edizioni), 2007.
- [23] D. Guzzo, *Messa a punto di un simulatore di guida per l'analisi del livello di vigilanza del conducente di un autoveicolo*, M. Sc. Thesis, Università di Pisa, 2008.
- [24] Hamane et al., Automatic multispeed transmission for vehicles with manual means for prohibition of engagement of a centrifugal clutch, *United States Patent* No. 4576269, 1986.
- [25] R. P. G. Heath, A. J. Child, Zeroshift Automated Manual Transmission (AMT), *SAE Paper* No. 2007-26-061.
- [26] J. B. Heywood, *Internal Combustion Engine Fundamentals*, McGraw-Hill, 1988.
- [27] Honda, Dual Clutch Transmission, <http://world.honda.com/motorcycle-picturebook/DCT/>.
- [28] Honda, Human-Friendly Transmission, <http://world.honda.com/motorcycle-picturebook/HFT/>.
- [29] Institut National de Recherche sur les Transports et leur Sécurité (INRETS), <http://www.inrets.fr/accueil.html>.
- [30] Istituto Nazionale di Statistica (ISTAT) and Automobile Club d'Italia (ACI), *Incidenti stradali – anno 2008*, <http://www.aci.it>, 2009.
- [31] Istituto Nazionale di Statistica (ISTAT) and Automobile Club d'Italia (ACI), *Incidenti stradali – anno 2009*, <http://www.aci.it>, 2010.
- [32] T. Ito, S. Mita, K. Kozuka, T. Nakano, S. Yamamoto, Driver blink measurement by the motion picture processing and its application to drowsiness detection, *Proceedings of IEEE Conference on Intelligent Transportation Systems*, 168-173, October 3-6, 2002.
- [33] Q. Ji, X. Yang, Eye-tracking for detection of driver fatigue, *Real-Time Imaging*, 8(5), 357-377, 2002.

- [34] J. Krajewski, D. Sommer, U. Trutsche, D. Edwards, M. Golz, Steering wheel behavior based estimating of fatigue, *Proceedings of 5<sup>th</sup> International Driving Symposium on Human Factors in Driver Assessment, Training and Vehicle Design*, 118-124, June 22-25, 2009.
- [35] Kreidlertreff Giessen, <http://www.kreidlertreff-giessen.de>.
- [36] M. Kulkarni, T. Shim, Y. Zhang, Shift dynamics and control of dual-clutch transmissions, *Mechanism and Machine Theory*, 42, 168-182, 2007.
- [37] S. G. Kulkarni, *Machine Desing*, McGraw-Hill, 2008.
- [38] S. K. L. Lal, A. A. Craig, Critical Review of the Psychophysiology of Driver Fatigue, *Biological Psychology*, Elsevier Science, 55, 173-194, 2001.
- [39] W. Lee, J. Kim, J. Cho, 'A driving simulator as a virtual reality tool,' *Proceeding of the 1998 IEEE International Conference on Robotics and Automation*, Leuven (Belgium), May, 0-7803-4300-x-5/98: 71-76, 1998.
- [40] S. F. Liang, C. T. Lin, R. C. Wu, Y. C. Huang, T. P. Jung, Monitoring driver's alertness based on the driving performance estimation and the EEG power spectrum analysis, *IEEE 27<sup>th</sup> Annual Conference on Engineering in Medicine and Biology*, 5738 5741, Shangai (China), September 1-4, 2005.
- [41] C. T. Lin, L. W. Ko, I. F. Chung, T. Y. Huang, Y. C. Chen, T. P. Jung, S. F. Liang, Adaptive EEG-based alertness estimation system by using ICA-based fuzzy neural networks, *IEEE Transactions on Circuits and Systems Part I: Regular Papers*, 53(11), 2469 2476, 2006.
- [42] C. T. Lin, R. C. Wu, S. F. Liang, W. H. Chao, Y. J. Chen e T. P. Jung, EEG-based drowsiness estimation for safety driving using independent component analysis, *IEEE Transactions on Circuits and Systems, Part I: Regular Papers*, 52(12), 2726 2738, 2005.
- [43] A. Malvasi, Sviluppo di un simulatore di guida di autoveicolo per studi di sicurezza preventiva, PhD Thesis, Università di Pisa, 2007.
- [44] Mathworks, Matlab R2010b Documentation, 2010.

- [45] Mercedes-Benz. Attention Assistant. <http://www.mercedes-benz.it>, 2009.
- [46] Ministero Salute, *Fattori che modificano lo stato psico-fisico: la sonnolenza*, [www.ministerosalute.it](http://www.ministerosalute.it), 2004.
- [47] MSC Software, MSC Adams 2005R2 Documentation, 2005.
- [48] The National Advanced Driving Simulator (NADS) at the University of Iowa', <http://www.nads-sc.uiowa.edu/facilities.htm>.
- [49] National Highway Traffic Safety Administration (NHTSA), <http://www.nhtsa.gov/>.
- [50] Ogawa, Kenji, Shimotani, Mitsuo, Drowsiness detection system, *Mitsubishi Electric Advance*, 78, 13-16, 1997.
- [51] H.B. Pacejka, *Tyre and Vehicle Dynamics* (Oxford, Butterworth-Heinemann), 2002.
- [52] I. Park, J. H. Ahn, H. Byun, Efficient measurement of eye blinking under various illumination condition for drowsiness detection system. *Proceedings of International Conference on Pattern Recognition (ICPR06)*, 1, 383-386, Hong Kong (China), August 20-24, 2006.
- [53] E. Pellegrini, *Sviluppo di un modello di simulazione dinamica per vettura Formula SAE*, M. Sc. Thesis, Università di Pisa, 2009.
- [54] T. Pilutti, A.G. Ulsoy, Identification of driver state for lane-keeping tasks, *IEEE Transactions on Systems, Man, and Cybernetics/Part A: Systems and Humans*, 29(5), 486-502, September, 1999.
- [55] J. C. Popieul, P. Simon, P. Loslever, Using driver's head movements evolution as a drowsiness indicator, *Proceedings of IEEE Symposium on Intelligent Vehicles*, 616-621, June 9-11, 2003.
- [56] R. Sayed, A. Eskandarian, Unobtrusive drowsiness detection by neural network learning of driver steering, *Proceedings of the Institution of Mechanical Engineers, Part D: Journal of Automobile Engineering*, 215(9), 969-975, 2001.
- [57] G. P. Siegmund, D. J. King, D. K. Mumford, Correlation of heavy-truck driver fatigue with vehicle-based control measures, *SAE Technical Papers*, 952594, 1995.

- 
- [58] Stisim Drive, <http://www.stisimdrive.com/>.
- [59] Swedish National Road and Transport Research Institute (VTI), 'Driving Simulators, [http://www.vti.se/templates/Page\\_---3257.aspx](http://www.vti.se/templates/Page_---3257.aspx).
- [60] Toyota, Driving simulator, [http://www.toyota.com/esq/articles/2010/Driving\\_Simulator.html](http://www.toyota.com/esq/articles/2010/Driving_Simulator.html).
- [61] University of Michigan, Virtual Reality Laboratory (UM-VRL), 'Virtual Prototyping of Automotive Interiors, [www-vr1.umich.edu/project/automotive/](http://www-vr1.umich.edu/project/automotive/)
- [62] D. Vangi, A. Virga, R. Bartolozzi, F. Frendo, Diagnostica per il riconoscimento del livello di attenzione alla guida di autoveicoli, *Atti del XXXVIII Convegno Nazionale dell'Associazione Italiana per l'Analisi delle Sollecitazioni*, Torino (Italy), September 9-11, 2009.
- [63] World Health Organization, *Global status report on road safety: time for action*, Geneva, WHO, 2009.
- [64] World Health Organization, *The global burden of disease: 2004 update*, Geneva, WHO, 2008.
- [65] World Health Organization, *The top 10 of causes of death*, Fact sheet No 310, 2008.
- [66] T. Yamakoshi, K. Yamakoshi, S. Tanaka, M. Nogawa, Y. Sawada, P. Rolfe, Hemodynamic response during simulated automobile driving in a monotonous situation, *Proc. IEEE 28<sup>th</sup> Annual International Conference on Engineering in Medicine and Biology Society (EMBS06)*, 5129-5132, New York City, August 30 - September 3, 2006.